Tampere University

Mohamed Rohaim

COMPACT FLEXIBLE THREE-BAND PRINTED MONOPOLE ANTENNA

Electronics and
Communications Engineering
Master of Science thesis
January 2020

ABSTRACT

Mohamed Rohaim: Compact Flexible Three-band Printed Monopole Antenna.
Master of science thesis
Tampere University
Electronics and Communications Engineering, High Frequency Techniques
January 2020

A novel compact, flexible three-band printed monopole antenna with letter F–like shape is proposed. It is a three-band antenna to cover the LTE bands (0.8, 1.8, 2.6 GHz) with bandwidths greater than 100 MHz. Screen-printing technology is used to construct the antenna, with highly conductive ink on a thin, flexible, and high permittivity Preperm TP20556 substrate. Antennas on such materials are of interest in printable electronics which reduces the fabrication cost. The proposed antenna has light weight with small volume and planar configuration. The antenna and application circuitry are aimed to be integrated on same substrate.

Advanced Design System ADS, and ANSYS HFSS electromagnetic simulators were both used to design the antenna. CST Microwave Studio was used to do characteristic mode analysis and excitation study of the structure to further understand the working principle. The step-by-step analysis on how various geometrical features affect the antenna characteristics allowed for a better understanding of the working principle of the proposed antenna. We support the ideas with frequency domain, time domain and characteristic mode simulation results. In addition, we discuss challenges that we have faced in modelling and measuring this type of multiband printed monopole antennas.

Antennas have been constructed with copper tape and screen-printing technology. Antennas have been measured with VNA and in the anechoic chamber (Satimo antenna measurement device). Both constructed antennas with ink and copper tape keep the overall characteristics of the simulated ones with triple-band operation at 800 MHz, 1.8 GHz and 2.6 GHz. The copper tape antenna showed a 100 MHz bandwidth with minimum measured total efficiency of 88, 60, and 69 % at the 0.8, 1.8, and 2.6 GHz bands respectively. The ink antenna showed a 100 MHz bandwidth with minimum measured total efficiency of 65, 42, and 46 % at the 0.8, 1.8, and 2.6 GHz bands respectively. The measured maximum gain of the copper tape antenna was 2.54, 2.14, and 4.38 dBi at the 0.8, 1.8, and 2.6 GHz bands respectively. The measured maximum gain of the ink antenna was 1.27, 1.31, and 3.48 dBi at the 0.8, 1.8, and 2.6 GHz bands respectively.

Keywords: Printed antennas, multiband antennas, characteristic mode analysis, bandwidth, efficiency, gain.

PREFACE

The master thesis “Compact Flexible Three-band Printed Monopole Antenna” was done in fulfillment of the requirement for the Master of Science degree in high frequency techniques major, in the department of electronics and communication engineering at Tampere university. This thesis was part of the Towards Digital Paradise TDP project and it was funded by it. The TDP project is a “Research benefit” -project running in Business Finland’s (BF) “Fiiliksestä fyrkkaa” -program.

I would like to thank my thesis examiners and supervisors, Academy Research Fellow Matti Mäntysalo and Lecturer Jari Kangas, for all of their support and guidance to complete my thesis. I would like to thank Doctoral Researcher Riikka Mikkonen for her support in the screen-printing lab work and the sheet resistance measurements and specially for being nice, supportive, and friendly person.

From May to September 2019, I had the opportunity to work as antenna design engineer intern at Radientum Oy, Tampere Finland. It was incredibly educative to work with such professionals who are applying their knowledge and using it. The CST Microwave Studio simulation results that are reported in this thesis work have been developed during my internship with Radientum Oy.

I am very thankful for my family and my lovely wife Ola for standing by my side through thick and thin in the last two years. They have overwhelmed me with all the support and motivation I could ask for to finalize this thesis, may Allah bless them with endless happiness. I would like to thank my friends Mohamed Khalifa and Mitchel Adel as well for their emotional support.

Tampere, 24 January 2020

Mohamed Rohaim

CONTENTS

LIST OF SYMBOLS AND ABBREVIATIONS

ε_{eff}	Effective dielectric constant
ε_r	Dielectric constant
Γ_L	Reflection coefficient
G_L	Ground plane Length
G_W	Ground plane width
R_s	Sheet resistance
Z_0	Characteristic impedance
ADS	Advanced Design System software
AUT	Antenna under test
BW	Bandwidth
C	Speed of light
CMA	Characteristic mode analysis
CST	Computer Simulation Technology
D	Directivity
dB	Decibel
dBi	Decibel isotropic
EM simulation	Electromagnetic simulation
G	Gain
IoT	Internet of Things
LTE	Long-Term Evolution
MA	Measurement antenna
MS	Modal significance
MSA	Microstrip antennas
R	Real part of impedance
RFID	Radio frequency identification
RL	Return loss
V1 antenna	First final version antenna
V2 antenna	Second final version antenna
V3 antenna	Third final version antenna
VNA	Vector Network Analyzer
X	Imaginary part of impedance
λ	Wavelength
σ	Electrical conductivity (sigma)
Ω	Ohm
ρ	Electrical resistivity (rho)

1. INTRODUCTION

Antennas are needed nowadays in various applications where compact size, light weight, and ease of mass production are of interest. For such applications, alternative construction techniques such as printable electronics are preferred. In addition, many wireless standards are used nowadays, and current wireless communication devices are required to support several standards simultaneously [7]. It is cost inefficient to use separate antenna for each band as it requires a lot of space and complicated feed network [7]. In this context, multiband antennas offer a very efficient solution as it can support multiple frequency bands using one antenna and one feeding network.

The aim of this thesis work was to design a multiband antenna for a wireless sensor sticker application. The antenna and application circuitry are aimed to be integrated on same substrate. Screen printing is the technology to be used to construct the antenna. Conductive ink with high conductivity ($\sigma \approx 5e6$ S/m) is used to draw the antenna pattern on the substrate. The substrate material used is PREPERM® TP20556. It is special flexible film with tailored dielectric constant. The dielectric constant is $\varepsilon_r \approx 11$ and the dielectric loss is very low (~0.001). PREPERM® TP20556 is designed for flexible antennas with thicknesses from 0.2 up to 1 mm.

The application requirements were to design a compact planar three-band antenna to cover LTE common bands (0.8, 1.8, 2.6 GHz) with -10 dB return loss bandwidth of 100 MHz at each band. In addition, the antenna should achieve as much realized gain for higher read range. Also, these characteristics should not be degraded much when the antenna is bent or attached to any material. More discussion about the required specifications is presented in subchapter 3.1.

The wireless sensor sticker (antenna and application circuitry) is aimed to be attached to glass or a wall of any material. Thus, our initial idea was to design an antenna with grounded structure, microstrip patch antennas MSA. Considering the radiation characteristics of patch antenna, it should be top candidate for our antenna design. The existence of the ground plane on the other side of the substrate makes the patch antenna less sensitive to the electrical properties of the materials it is attached to.

Many ideas for multiband patch antennas are available in literature. However, as mentioned in [4], [19], [28], and [33]; the bandwidth and efficiency of a patch are decreased

by decreasing substrate thickness and by increasing the dielectric constant of the substrate. Unfortunately, the substrate material used in this thesis work is very thin (which makes it more flexible with thickness of 0.275 mm) and has very high dielectric constant $\varepsilon_r \approx 11$. Therefore, our initial simulation results (for a conventional rectangular microstrip patch antenna resonating at 800 MHz) showed a bandwidth of 10 MHz bandwidth and around 15 percent efficiency. Thus, patch antenna design did not seem suitable on the PREPERM substrate.

Many other antenna structures have been examined where multiband and flexibility were challenges. Printed monopole antennas share many advantages with microstrip antennas. They are both light weight antennas with small volume and low-profile planar configuration [25] [28] [29] [31]. This allows them to be conformal to the host circuit surface and makes them easier to be integrated with the driving electronics circuit [1] [28] [29] [30]. Both antennas allow for mass production using printed circuit technology which reduces the fabrication cost [1] [25] [28] [29].

Moreover, the planar printed monopole antennas demonstrated multiband operation with reasonably good performance in numerous designs [1] [8] [20] [25] [30] [34] [36]. In addition, the flexibility attribute of the printed monopole antenna presented in [18] was experimentally studied with promising results. Thus, planar monopole antenna was a promising candidate for our design. Similar geometrical configuration is used for these antennas where a microstrip line is printed on top of the substrate to feed the antenna, and a ground plane is printed on the other side of the substrate.

The idea of the printed double-T monopole antenna for dual-band operation is proposed in [18] and [20]. The antenna comprises two T-shaped monopoles of different sizes, which generate two separate resonant paths for the desired dual-band operations. The idea of the dual-band F-shaped monopole antenna is proposed in [34] which should achieve a noticeable size reduction from the double-T monopole antennas of [18] and [20].

Our idea was to use the F-shaped idea of [34] to achieve a size reduction and by varying the widths of the F-shaped meandered strips we can utilize the higher order modes as reported in [8]. This will make the longer strip of the lower band active at the higher band which form an array to enhance the results of the higher band as reported in [9] [30]. Moreover, we aim for three-band operation to cover the LTE common bands (0.8, 1.8, 2.6 GHz). Thus, we add a third strip to allow for a third resonance path. Figure 1-1 shows one of the final designs, the monopole arm on top of the substrate with letter F–like shape and the ground with a slit below the substrate. In [37], they showed that the radiation

pattern of the higher band can improver by cutting four slots from the ground plane which increase the effective current path of the ground plane. We will utilize this idea to improve the radiation pattern of the final version antenna at the 2.6 GHz.

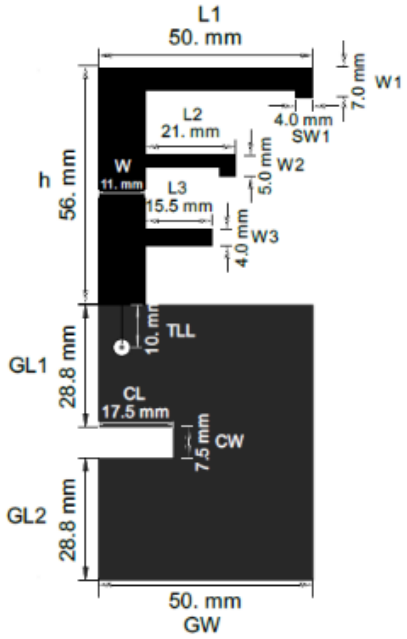

Figure 1-1. *Layout of three-band final version antenna V2*

In chapter 2, we present the theoretical background information that is necessary to understand our research problems described later in the thesis. We start with introducing Maxwell equations and antenna fundamentals. Then we expand on the antenna pattern measurement techniques. Finally, we discuss the characteristic mode analysis CMA topic. Unfortunately, the CMA has been used at late stage of this thesis work. However, it supported the results that we achieved through the hard optimization way. Also, it has explained and introduced many ideas to enhance the results which will be discussed in the simulation and results chapters 4 and 5 respectively.

In chapter 3, we present the technical requirement and the aim of this thesis work. In addition, we expand more on the theoretical background and review the existing literature background on planar printed monopole antennas.

In chapter 4, the working principle of the proposed antenna is studied. First, a simple printed monopole antenna working at 800 MHz is considered and the impact of all its geometry parameters is examined. Next, an L-shaped monopole antenna is considered, especially, the differences between straight and L-shaped radiating elements. Finally, two L-shaped arms are added. These arms should support operation at 1.8 GHz and 2.6 GHz. The study is done with frequency domain solver on ADS software and supported

with characteristic mode analysis CMA (with multilayer solver) and time domain solver on CST microwave studio.

In chapter 5, we discuss three final versions that have been developed based on the ideas of the previous chapter. For the second final version, we show how CMA has been utilized to fix radiation pattern of the 2.6 GHz band. Final versions V1 and V2 antennas have been constructed with screen printing technology and copper tape. The antennas were tested with a VNA and in the Satimo antenna measurements anechoic chambers. Final version V3 antenna has been designed to enhance the measured results of the second final version V2.

2. THEORETICAL BACKGROUND

In this chapter, we present the theoretical background information that is necessary to understand the research problems described later in the thesis. We start with introducing Maxwell equations and antenna fundamentals. Then we expand on the antenna pattern measurement techniques. Finally, we discuss the characteristic mode analysis CMA topic.

2.1 Maxwell Equations

James Clerk Maxwell composed a universal field theory "Maxwell Equations" that connected electricity with magnetism [35]. Table 2-1 shows the four Maxwell equations in their integral, differential, and phasor forms [26].

Table 2-1 *Maxwell Equations in Differential, Integral and Phasor forms [26]*

Differential form	Integral form	Phasor form	Designation
$\nabla \times \boldsymbol{E} = -\frac{\partial \boldsymbol{B}}{\partial t}$	$\int_{\partial S} \boldsymbol{E} \cdot d\boldsymbol{l} = -\frac{\partial}{\partial t}\int_{S} \boldsymbol{B} \cdot d\boldsymbol{s}\, \forall S$	$\nabla \times \boldsymbol{E} = -j\omega \boldsymbol{B}$	Faraday's law
$\nabla \times \boldsymbol{H} = \boldsymbol{J} + \frac{\partial \boldsymbol{D}}{\partial t}$	$\int_{\partial S} \boldsymbol{H} \cdot d\boldsymbol{l} = \int_{S} \boldsymbol{J} \cdot d\boldsymbol{s} + \frac{\partial}{\partial t}\int_{S} \boldsymbol{D} \cdot d\boldsymbol{s} \forall S$	$\nabla \times \boldsymbol{H} = \boldsymbol{J} + j\omega \boldsymbol{D}$	Ampère-Maxwell's law
$\nabla \cdot \boldsymbol{D} = \rho$	$\int_{\partial V} \boldsymbol{D} \cdot d\boldsymbol{s} = \int_{V} \rho\, dv = Q \forall V$	$\nabla \cdot \boldsymbol{D} = \rho$	Gauss' law for electricity
$\nabla \cdot \boldsymbol{B} = 0$	$\int_{\partial V} \boldsymbol{B} \cdot d\boldsymbol{s} = 0 \forall V$	$\nabla \cdot \boldsymbol{B} = 0$	Gauss' law for magnetism

Quantity	Symbol	Unit
Electric field intensity	$\boldsymbol{E}$	V/m
Magnetic field intensity	$\boldsymbol{H}$	A/m
Electric flux density	$\boldsymbol{D}$	Coul/m^2
Magnetic flux density	$\boldsymbol{B}$	Wb/m^2
Electric current density	$\boldsymbol{J}$	A/m^2
Electric charge density	ρ	Coul/m^3

Gauss' law for electricity states that the net electric flux over a closed surface is proportional to the charges enclosed by it [35]. On the other hand, Gauss' law for magnetism states that the closed surface integral of magnetic flux, no matter where, equal zero [35]. Thus, there is a profound difference between electricity and magnetism; that is, separated positive or negative electrically charged objects exist. While, with magnetism, magnetic poles always come in pair, or as physicists always say, "magnetic monopole does not exist" [35].

Faraday suggested that a steady magnetic field would produce a steady electric field. However, he found that it is only the changing magnetic field that would produce electric field. Faraday's law forms the basis of electric motors and electric generators. [35]

Maxwell's contribution was to amend Ampere's law about magnetic fields with the introduction of the displacement current term. Before Maxwell, Ampere's law stats that the integral of a magnetic field over a closed path is only proportional to the current enclosed by the surface of this path. Maxwell suggested that a changing electric field should give rise to a changing magnetic field. Maxwell introduced the displacement current term to Ampere's law which represent how changing electric field give rise to a changing magnetic field. [35]

By the introduction of the displacement current term to Ampere's law, Maxwell has predicted that radio waves should exist. Wave equation can be deuced from the Maxwell laws which predicts the wave velocity of propagation. [35]

2.2 Antenna fundamentals

Radiation is the transformation of electric signal into electro-magnetic waves [11]. It turned out that every object that has an electric charge is able, to some extent, to radiate [11]. Lumped elements inductors and capacitors have radiation losses associated with them; even though they are not designed to radiate [26]. In this context, antenna is simply a device that has been designed carefully to be an efficient radiator [28]. That is, it can transform most of the input electric power into electromagnetic waves. Antenna is reciprocal device; that is, it can also receive the radiated electromagnetic by another device and transform it into electrical signal [4].

Maxwell equations states that a changing magnetic field produces a changing electric field and vice versa. A steady electric current produces steady magnetic field, but not radiation. Current must continuously change to generate radiation. A time-varying alternating current accumulates the charges resulting in a changing electric field. Accumulation of charges and time-varying current are both responsible for radiation. [4]

The region around the antenna can be classified into two regions; near and far field [28]. It is only in the far field region that the radiation wave exhibits local plane wave behaviour and does not change shape rapidly [28]. The near field region can be further divided into two regions; the reactive and radiative near field. The reactive near field region is closest to the antenna and the reactive fields dominate over the radiative fields. Between the reactive near field and the far field region, there is the radiative near field region where

the radiative fields dominate. Table 2-2 show the boundaries between these three regions where λ is the wavelength and D is the maximum extent of any finite antenna. [28]

Table 2-2. *Radiation field region distances for cases where D ≫ λ [28].*

Region	Distance from antenna (r)
Reactive near field	0 to $0.62 * \sqrt{D^3/\lambda}$
Radiative near field	$0.62 * \sqrt{D^3/\lambda}$ to $2D^2/\lambda$
Far field	$2D^2/\lambda$ to ∞

2.2.1 Input impedance and return loss

The impedance measured at the terminal of the antenna is called the input impedance [28]. Antenna input impedance describe the relation between the current and the voltage on the antenna, and generally it has a complex form with imaginary and real part [4]. Real part is associated with either radiated or losses power. Radiation resistance is associated with the desired radiated power away from the antenna. Where, the ohmic or losses resistance is associated with the power that dissipated in the form of heat. Ohmic resistance is due to the finite conductivity of the materials used to construct the antennas. The imaginary part of the complex input impedance represents the stored power in the near field radiation. [4] [28]

$$\boldsymbol{Z_A = R_A + j\,X_A} \tag{2.1}$$

Input impedance changes with different antenna types. Even for the same antenna type, input impedance depends on the material and the geometrical dimensions. In addition, the excitation setup can change the input impedance of the same antenna significantly (as will be shown in the characteristic mode analysis subchapter) [4]. Input impedance of an antenna will also be affected by other objects (or any other antennas) that exist near the antenna [28].

Figure 2-1 shows an equivalent circuit model of an antenna [4]. Antenna input impedance is represented by its imaginary part X_A; losses resistance R_L; and radiation resistance R_r. The source (or generator) that excite the antenna is represented by its impedance $Z_G = R_G + \mathrm{j}\,X_G$. Any impedance discontinuity in the transmission medium of an electromagnetic wave will cause reflection [26]. That is, part of the electromagnetic wave will be reflected to the source [26]. It turned out that, with simple calculation, the maximum power transfer from the generator to the antenna happen when the Z_g is the complex

conjugate of Z_A (Z_g = $Z_A{}^*$). That is, the real parts of both impedances are equal (R_g = R_A), and the imaginary parts are equal wit opposite sign (X_g = $-X_A$); therefore, the reactance of the imaginary parts of both impedances resonate each other. This is known as the conjugate matching condition, and results in maximum power transfer. [26]

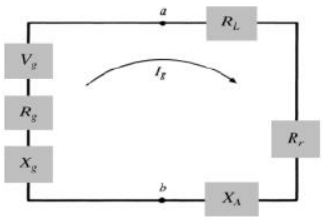

Figure 2-1. *Antenna Thevenin equivalent [4]*

For an antenna fed by a transmission lines with specific characteristic impedance Z_0, the ratio between the reflected wave V^- from the antenna to the wave arriving V^+ at the antenna is defined as the reflection coefficient Γ_L [26].

$$\Gamma_L = \frac{V^-}{V^+} = \frac{Z_A - Z_0}{Z_A + Z_0} \tag{2.2}$$

Further, reflection coefficient Γ_L is used to calculate the power delivered to the antenna P_A and the power reflected from it P_r [26].

$$\boldsymbol{P_A = P_{avg} * (1 - |\Gamma_L|^2)} \tag{2.3}$$
$$\boldsymbol{P_r = P_{avg} * |\Gamma_L|^2} \tag{2.4}$$

The decibel value of the factor $1/|\Gamma_L|^2$ is describing (for general source with any available power) the power of the reflected wave due to antenna mismatch and defined as return loss $RL_{(dB)}$ [26].

$$\boldsymbol{RL_{(dB)} = 10 * log_{10} |\Gamma_L|^2} \tag{2.5}$$

That is, a return loss of -3 dB means that the reflected power is 3 dB smaller than the available power (half of the available power from the generator will be reflected and half will be delivered to the antenna). A complex conjugate matching is always desired as it results in maximum power transfer to the antenna [4]. However, complex conjugate matching is hard to be achieved over a wide band of frequencies. A practical value is usually defined around -10 dB; therefore, only 10 percent of the available power from the generator will be reflected and 90 percent will be delivered to the antenna. Many impedance matching techniques are sometimes used to decrease the reflected power and increase power transfer to the antenna. Passive lumped components inductor and capacitors are widely used for antenna matching [28]. Also, low-loss transmission lines are used for antenna impedance matching specially with high frequencies when the required size is small [28].

2.2.2 Radiation pattern

Radiation pattern describes the angular variation of the antenna radiation properties at a fixed distance (usually in far field region) from the antenna when it is transmitting [28]. It is a 3D graphical representation that help visualising how the antenna radiate in all directions. This can be done by measuring (or simulating) the antenna transmitted power density S in all direction at a fixed distance from the antenna [28]. Radiation pattern can represent different properties of the antenna, as field or power pattern, in linear or decibel scale [28]. The antenna pattern measurements and the coordinate system used in antenna measurements will be discussed in subchapter 2.3.

There are some common forms of antennas' radiation pattern; isotropic, directional, and omnidirectional [28]. Isotropic antenna is an ideal non-existent antenna that radiate equally in all directions [11]. Directional antennas concentrate the radiated power in a beam at certain direction. Directional antennas are of great interest when radiation is only required in certain directions; thus, radiation in undesired directions is considered to be wasted [11]. Figure 2-2 shows the radiation pattern of a patch antenna, a common directive antenna.

(a) 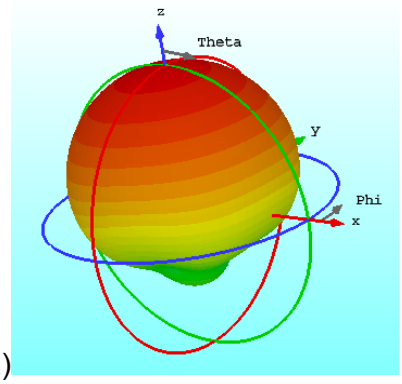

(b) 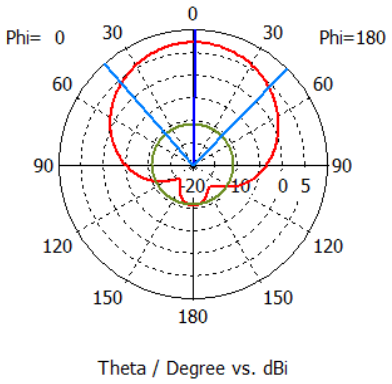

***Figure 2-2**. Radiation from directive patch antenna. (a) 3D plot of radiation pattern. (b) polar plot 2D cut of Phi=0°*

On the other hand, in the mobile phone case (and many other cases) the desired direction of radiation is not well defined, and directional antenna may lose the connection in the directions with less radiation [11]. Omnidirectional antennas can come very close to the ideal (non-existent) isotropic antenna. Omnidirectional antenna radiates equally in the plane perpendicular to it as shown in figure 2-3 [11].

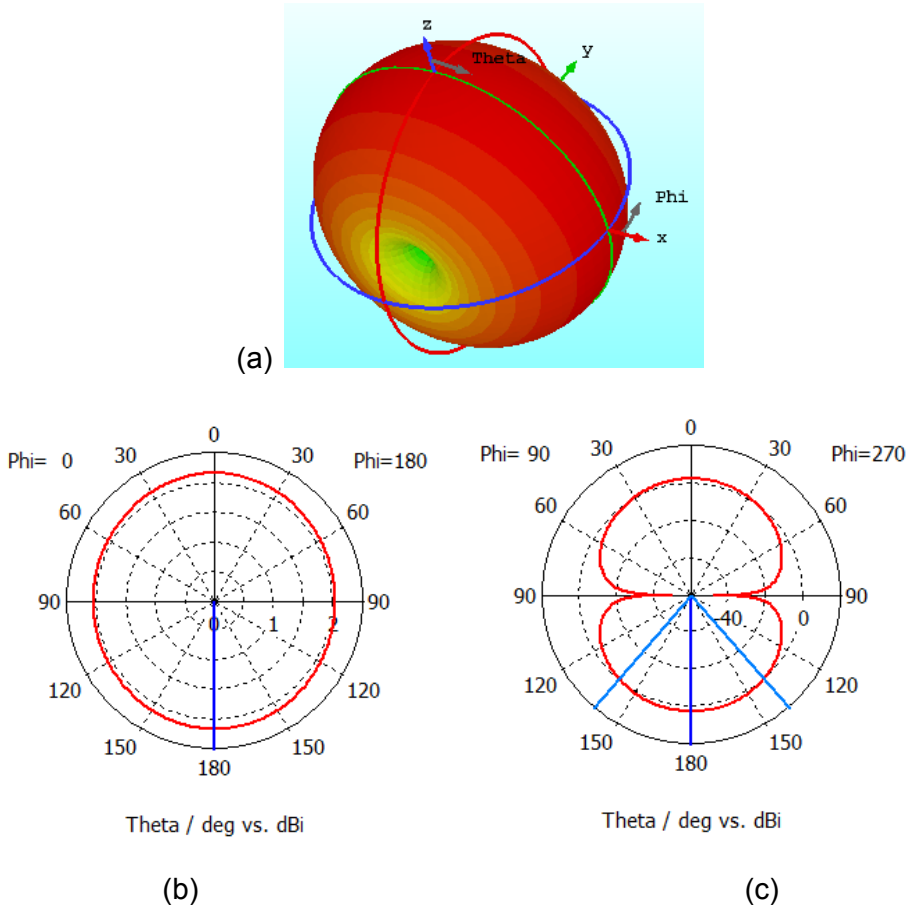

Figure 2-3. *Radiation pattern of dipole antenna. (a) 3D plot of radiation pattern. (b) polar plot 2D cut of Phi=0°. (c) polar plot 2D cut of Phi=90°*

Radiation from differnet parts of the antenna arrive at the far field with different phases and magnitudes [28]. They enterfere with each other constructively or distructively to form the radiation pattern with lobing effect [28]. As shown in figures 2-2 and 2-3, the radiation pattern of any antenna is usually formed as many lobes. The maximum direction of radiation is described as the main lobe [28]. Minor lobes descibe the directions with less radiation than the main lobe [28]. Back lobe, if exists, is in the opposite direction of the main lobe [28]. Beam width, measured in degree, is another important parameter that describes the width of the main lobe with half of the maximum radiation intensity, the -3 dB beam width [28]. In figures 2-2 and 2-3, the blue lines define the -3 dB beam width of the antenna.

2.2.3 Directivity and gain

As discussed, Isotropic antenna is an ideal non-existent antenna that radiate equally in all directions, and directional antennas concentrate the radiated power in a beam at certain direction. The ratio of the radiated power in one direction to the average radiated power from a directive antenna is defined as the directive gain in that direction [11]. The

directive gain along the direction of maximum radiation (e.g. main lobe) is defined as the antenna directivity D [11]. In the direction of maximum radiated power, we get D time more power than the average radiated power that we would get if the same power has been radiated from an isotropic antenna [11].

Notice that the directivity is a pure radiation pattern parameter; that is, it is calculated for the radiation pattern considering the actual radiated power pattern. Radiation efficiency and return loss are parameters that affects the radiated power from an antenna. However, antenna with high return loss and poor efficiency would have high directivity [28]. Power gain G_p is defined as the directivity multiplied by the radiation efficiency [28]. Realized gain $G_{realized}$ is defined as the directivity multiplied by the radiation efficiency and the return loss factor. That is, in the direction of maximum radiated power, we get $G_{realized}$ time more power than what we would get if the same source available power is feeding an ideal isotropic antenna. [28]

It should be noted that antennas are passive dvices which cannot amplify the input power [11]. Antenna can just rearrange the radiated power so that it concentrates the radiated power it certain directions while decrease (or even eliminate) radiation in other direction [11]. Therefore, as the antenna gain increase, the narrower become its radiation [11]. As gain and directivity are measured with respect to isotropic antenna, their decible value are usually written as dBi (not dB) to define the reference state [11]. As discussed before, antenna is a reciprocal device. Considering the antenna as a receiver, the effective aperture of the antenna increased in certain direction by G_{power} times (the power gain in that direction). [11]

2.2.4 Polarization

Another important factor is the polarization of an antenna. Polarization of the antenna is describing how the radiated electromagnetic wave from the antenna is polarized in certain direction [28]. The radiated electromagnetic wave induce force on the electric charges in a direction perpendicular to the direction of propagation, not along the direction of propagation [28]. The direction of the electromagnetic wave field vectors components of the propagated wave defines its polarization. The direction of the electric field is usually used to define the polarization direction of the wave [28]. When the direction of the electric field vector moves back and forth along a fixed line, the wave is said to be linearly polarized. A very common example of a linearly polarized antenna is the dipole antenna. [28]

It is also possible that the electric field is time dependent; that is, the electric field vector changes its direction with time. If the strength of the electric field vector remains constant but rotates with time in circular path, then it is called circularly polarized wave [28]. More general case is when the direction of the electric field rotates with time in circular path but its strength changes, then it is called elliptically polarized wave [28]. More discussion about the polarization and the design of circularly polarized antennas will come in the characteristic mode analysis subchapter.

2.3 Antenna pattern measurements

Antenna pattern measurement refers to “the determination of the radiation pattern of an antenna under test (AUT). That is, the measurement of the relative magnitude and sometimes phase of an electromagnetic signal received from the AUT” [3]. A passive antenna is reciprocal; that is, it can be used either as the transmitter or receiver in order to measure its pattern information [3] [16]. On the other hand, transmit and receive pattern of active antenna could be considerably different [3]. Thus, both patterns (transmit and receive) of active antenna are required [3].

Normally these measurements are performed in an anechoic antenna test chamber. The anechoic chamber is designed to absorb reflections of waves within the chamber and minimize echo. In addition, anechoic chamber provides shielding from outside interference. There are different types of antenna test chambers that are used for wireless testing and antenna measurements. [3]

The most basic technique for antenna pattern measurement is the single axis rotational pattern [3]. The AUT is placed on a 360° rotating table and the measurement antenna (MA) measure the response as function of angle. A dual polarized (e.g. horn) antenna is used as the MA to be able to measure two ortho-normal field components [3]. Figure 2-4 shows a polar pattern test setup [3]. Figures 2-2 and 2-3 show some 2D polar patterns for some typical antenna types.

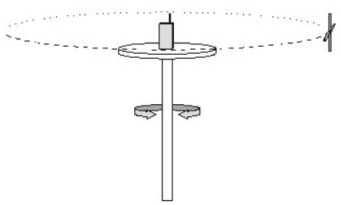

Figure 2-4. *Test setup for single axis polar pattern measurement [3].*

A full spherical pattern can be generated by changing the orientation of the AUT and repeating the previous polar test [16]. The second axis must be perpendicular to and

intersect the first axis. These two axes correspond to the θ and ϕ angles of the spherical coordinate system, and are referred to as elevation and azimuth respectively [3]. The standard spherical coordinate system used in antenna measurements is shown in Figure 2-5 [16]. A full spherical pattern measurement can be acheived If the turntable rotates through 180° while arc MAs rotates through 360°, or vice versa. [3] [16]

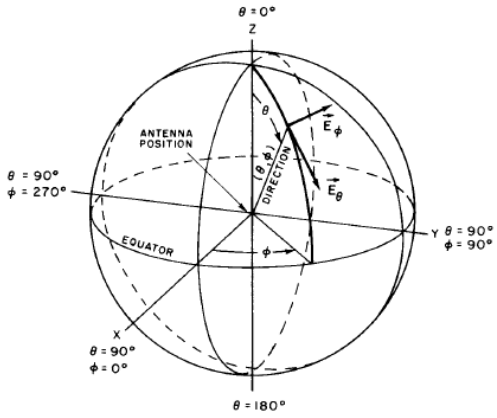

Figure 2-5. *Standard spherical coordinate system for antenna measurements [16]*

2.3.1 Satimo antenna measurement device

The Satimo antenna measurement device is special type of anechoic chambers designed specifically for characterizing the field patterns from antennas [12]. The Satimo antenna measurement device has a number of MAs embedded in a ring structure that surrounds the AUT antenna [12]. The AUT is placed on a turntable and the MAs are moved around the AUT as illustrated in Figure 2-6 [3]. The turntable provides the ϕ rotation, while the MAs is raised or lowered around the AUT to provide the θ rotation. One axis needs to be rotated through 360° while the other is only rotated through 180° [3].

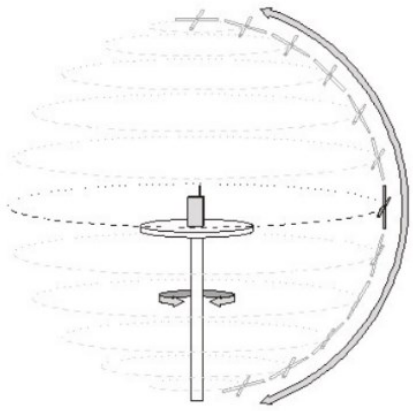

Figure 2-6. *Illustration of the Satimo antenna measurement device for spherical antenna pattern measurement [3].*

2.4 Characteristic mode analysis

Characteristic mode analysis is the numerical calculation of a weighted set of orthogonal current modes supported naturally by a metallic structure [14]. Theses Characteristic modes are the natural resonance modes of a metallic structure independent of any excitation [14]. The theory has been introduced by Garbacz [14] in early 1970's, and later developed by Harrington [15]. Characteristic modes are obtained by solving eigenvalue equation of the MoM impedance matrix [Z] with standard algorithms [6].

$$[\boldsymbol{Z}] = [\boldsymbol{R}] + \boldsymbol{j}\,[\boldsymbol{X}] \tag{2.6}$$

$$[\boldsymbol{X}][\boldsymbol{I}]_{\boldsymbol{n}} = \boldsymbol{\lambda_n}[\boldsymbol{R}][\boldsymbol{I}]_{\boldsymbol{n}} \tag{2.7}$$

where R and X are the real and imaginary parts of the impedance and, λ_n and I_n are the eigen function and eigen current.

Thus, the characteristic mode analysis results in getting the characteristic modes current distribution and the characteristic eigenvalues of the resonance modes as a function of frequency. It is somehow like the calculation of the waveguide modes, where the fields are decomposed into its fundamental modes. While with CMA, the current is decomposed into the individual current modes [32].

This is a valuable information as it provides physical insight about the antenna working principle and allows for a systematic antenna design approach [6]. At early stage of this thesis work, we were able to design a three-band antenna by optimizing the antenna dimensional configuration to get the desired results. We followed this road without really understand why certain dimensions have these impacts, or what modifications can be done in order to improve the antenna performance. CMA brings us back to basics and allow for a systematic antenna design approach to be followed [2].

So, by solving the eigenvalue equation we get the characteristic eigenvalues of the resonance modes as a function of frequency. The magnitude of the characteristic eigenvalue λ_n, associated with certain mode nth, is proportional to the reactive power [6] [15]. Mode is storing magnetic energy when $\lambda_n > 0$ at any certain frequency and called inductive mode [15]. While, mode is storing electric energy when $\lambda_n < 0$, and called capacitive mode [15]. Therefore, at resonance frequency $\lambda_n = 0$, when no reactive power is stored. As mentioned, these characteristic modes are the natural resonance modes of the antenna structure (without feed). They depend only on the shape and size of the structure [15]. Thus, these resonance modes with $\lambda_n = 0$ are called externally resonant mode of the structure itself [15]. Few modes are needed to characterize and model electrically small antennas as the case of this thesis [6] [15].

The response of an excitation driven antenna at certain frequency is a combination of all these weighted set of orthogonal modes at a frequency [2]. Figure 2-7 shows a well-known idea for creating a circularly polarized patch antenna [2]. It is a square patch antenna (simulated on Rogers RT5880 with a ground plane) with two triangular cuts as shown. The idea of this structure is to excite two modes which are 90° out of phase; therefore, the response of the antenna will be the combination of these two modes which results in a rotating current and consequently circularly polarized antenna [2].

Figure 2-7 shows the characteristic eigenvalues CMA simulation results of this patch simulated on CST MW studio (with multilayer solver). As mentioned, the magnitude of the characteristic eigenvalue λ_n is proportional to the reactive power stored in the system. Results show two characteristics modes at resonance around 2.4 GHz with λ_n = 0.

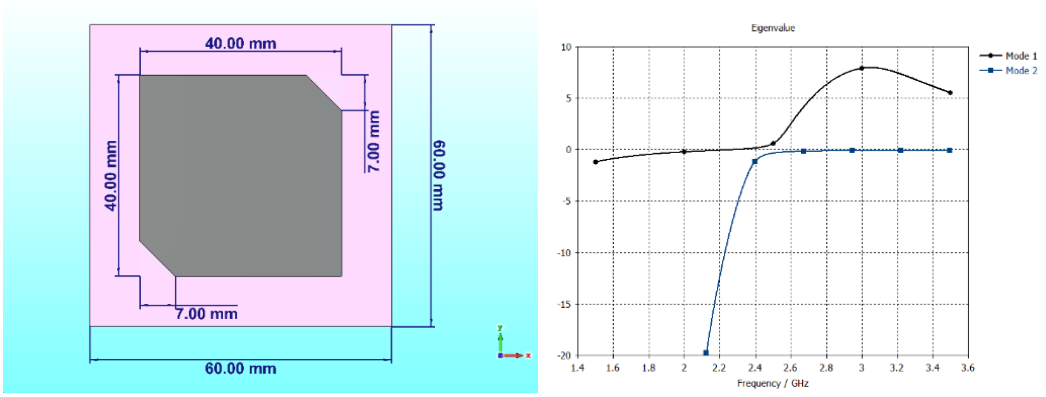

Figure 2-7. *Circularly polarized patch antenna [2], and its characteristic eigenvalues of the two dominant modes at 2.4 GHz*

Figure 2-8 shows the simulated characteristic modes current distribution results of these two modes. The current path of one mode (the one that resonate at 2.3 GHz) is the longer diagonal without cuts. The current path of second mode (the one that resonate at 2.6 GHz) is the shorter diagonal with cuts. These two modes are around 90 out of phase at 2.4 GHz due to the introduction of the two cuts. This will create rotational current and consequently left-hand circularly polarized driven antenna.

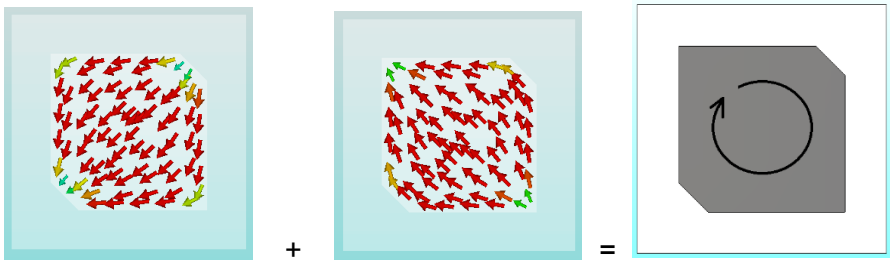

Figure 2-8. *Characteristic current distribution of the two dominant modes at 2.4 GHz (for the circularly polarized patch antenna depicted in figure 2-7)*

In practice, other parameters are defined to allow for a better visualization of the resonating characteristics of the modes. These two quantities are called modal significance and characteristic angel. [6]

$$\boldsymbol{Modal\ Significance\ MS} = \left|\frac{\mathbf{1}}{\mathbf{1}+j\boldsymbol{\lambda_n}}\right| \tag{2.8}$$

$$\boldsymbol{Characteristic\ angel\ \alpha_n} = \mathbf{180°} - \boldsymbol{tan^{-1}\,\lambda_n} \tag{2.9}$$

When mode is at resonance with $\lambda_n = 0$, the modal significance (MS) attains it maximum value MS = 1. On the other hand, when mode is at resonance with $\lambda_n = 0$, the characteristic angle α = 180°. Figure 2-9 shows the simulated results of these two quantities for the circularly polarized patch antenna of figure 2-7. Both quantities are deduced from the characteristic eigenvalue λ_n, but they allow for better visualization of the results [6]. The potential bandwidth can be visualized better on the modal significance (MS) graph, while the exact resonance frequencies of modes is clearer on the characteristic angle results.

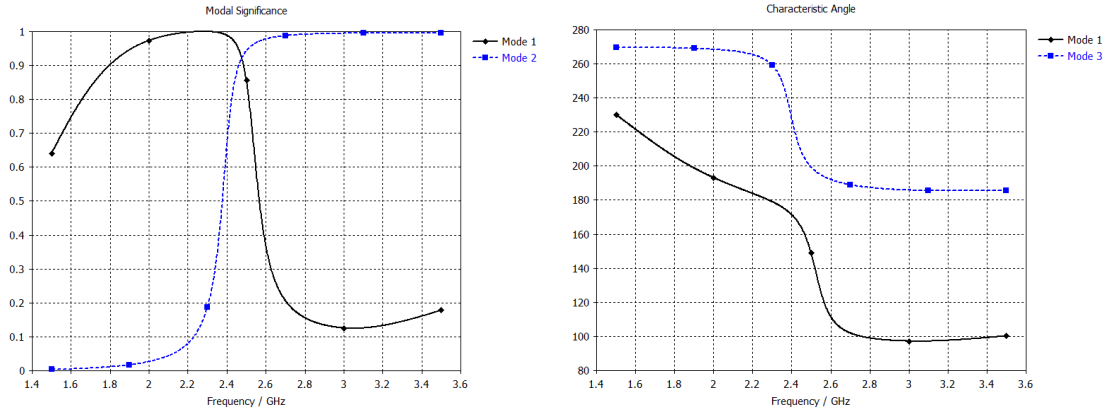

Figure 2-9. *Modal significance (MS) and Characteristic angle of the two dominant modes at 2.4 GHz (for the circularly polarized patch antenna depicted in figure 2-9)*

Figure 2-10 shows the S-parameters simulation results of the patch antenna of figure 2-9, but excited with discrete port (driven model simulated on CST microwave studio with time domain solver). It is clear that we have two resonance frequencies around 2.4 GHz as the CMA results suggest. Notice that the feed position has been optimized, according to the CMA results, to achieve good results at both bands. This would have been harder to achieve with only the driven model as the result is a combination of these two weighted modes at a 2.4 GHz and we cannot visualize the results of each mode alone.

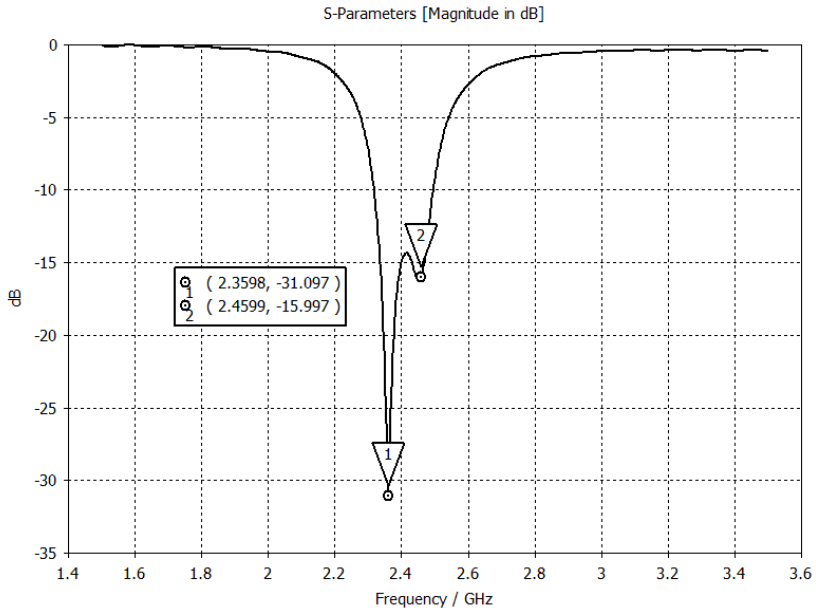

Figure 2-10. *Simulated return loss for the excited circularly polarized patch antenna depicted in figure 2-9*

Finally, figure 2-11 shows the simulated radiation pattern axial ratio and realized gain at X-Z plane (Phi = 0) cut. It shows that the axial ratio is less than 3 dB over the patch direction of radiation.

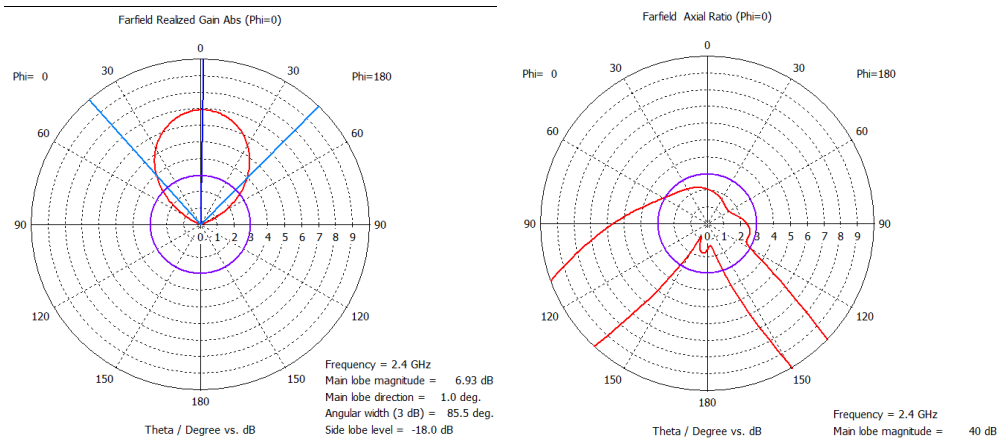

Figure 2-11. *Simulated radiation pattern polar plot and axial ratio* |*AR*| *at 2.4 GHz*

Thus, the CMA enable us to understand the antenna fundament properties and allows for a systematic antenna design approach. The CMA results can be utilized in many applications as mentioned in [2], [6], and [32]. It can be used to suppress certain undesired modes with proper excitation. It can also be used to study how to decrease the coupling of multi antenna devices. Many other examples are presented in [2], [6], and [32].

3. SCREEN PRINTED MULTIBAND MONOPOLE ANTENNA

In this chapter, we present the technical requirement and the aim of this thesis work. In addition, we expand more on the theoretical background and review the existing literature background.

3.1 Application requirement

The aim of this thesis work was to design a multiband antenna for a wireless sensor sticker application. The antenna and application circuitry are aimed to be integrated on same substrate. The required antenna characteristics are:

- Three-band antenna to cover LTE common bands (0.8, 1.8, 2.6 GHz).
- Bandwidth BW of 100 MHz at each band.
- Planar antenna.
- High gain for longer read range.
- Flexible antenna.
- Compact in size (near to ID card size).
- Stable results with different materials, as the sticker will be attached to wall or glass.

Bandwidth of an antenna can be defined as the range of frequencies over which certain characteristics are achieved [28]. Usually antenna bandwidth is defined in term of its return loss as the range of frequencies over which the antenna has a return loss of certain value. The -10dB bandwidth is commonly used term to define the antenna bandwidth in term of its return loss.

However, as discussed in the theoretical chapter, an antenna with bad radiation efficiency would have -10dB return loss over the required band. Thus, it also required that the antenna achieved certain radiation characteristics over that -10dB return loss band. It could be required that the antenna keep certain radiation pattern (directional or omnidirectional) over the whole band. A certain radiation efficiency would also be required. In case of directional antenna, a minimum gain would be required in direction of maximum radiation. In many cases, it is required that the antenna keeps certain polarization (linearly or circularly) over the whole band.

The substrate used to construct the antenna and application circuitry is PREPERM® TP20556. It is special flexible film designed for flexible antennas with thicknesses from

200 micron up to 1 mm. However, the antenna should be designed to keep certain return loss and radiation characteristics when it is bent. That is, it is not enough that the substrate itself is flexible, but also the antenna should be designed to work properly when it is bent. In addition, the wireless sensor (antenna and application circuitry) is aimed to be as a sticker mounted on different material (wall, glass, wood, conductor, etc). Thus, antenna should maintain stable results with different materials. However, this condition was very hard to achieve with the PREPERM® TP20556 due to its properties (dielectric constant $\varepsilon_r \approx 11$ and thicknesses of 275 micron), more discussion about this point will come in the literature review subchapter. Thus, this condition was not considered in this thesis work.

3.2 Screen printing technology

Antennas are needed nowadays in various applications where ease of mass production are of interest. For such applications, alternative construction techniques such as printable electronics are preferred. Screen printing is the technology used to construct the antenna of this thesis. Screen printing or silkscreen printing is a printing technique where a stretched mesh is used to transfer ink onto a substrate to draw a specific required pattern [5]. A screen is a stretched mesh over a frame to keep the mech under the required tension. The screen stretched mesh have an area of open apertures that form the required pattern, and other areas are blocked. Thus, when the screen touches the substrate, ink will transfer to the substrate only from the open apertures and draw the required pattern [5]. Figure 3-1 shows one of the final versions' antenna constructed by screen printing technology. The antenna is intended to be integrated on same substrate with an application circuit. Antenna is printed on one side of the substrate and a common ground plane (for the antenna and the application circuit) is below it on the other side of the substrate.

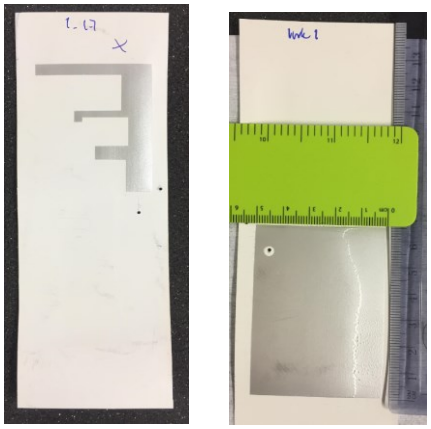

Figure 3-1. *Screen printed antenna (one of the final versions V1)*

3.2.1 Ink and sheet resistance

Screen printing draw the antenna and ground plane as a thin layer of conductive ink with thickness of 10 μm. The electric properties of such very thin layers are usually characterized by measuring the sheet resistance. Considering a 3D chunk of conductor, the resistance can be expressed as in equation 3.1 [24].

$$R = \boldsymbol{\rho} \frac{\boldsymbol{L}}{\boldsymbol{A}} = \boldsymbol{\rho} \frac{\boldsymbol{L}}{\boldsymbol{t} * \boldsymbol{W}} \tag{3.1}$$

where ρ is the resistivity of the conductor, L is the length, and A is the cross-sectional area. The cross-sectional area can be further expressed as the width and the thickness of the conductor layer. Combining the resistivity and the layer thickness, the resistance can be expressed as equation 3.2 [24].

$$R = \boldsymbol{R_s} * \frac{\boldsymbol{L}}{\boldsymbol{W}} \tag{3.2}$$

Where R_S is the sheet resistance of the material in unite Ω/square [24]. Sheet resistance can be easily measured for the conductive ink using four-probe method [24]. Thus, by measuring the sheet resistance and knowing the conductive ink thickness, we can easily get an estimation about the resistivity and conductivity of the ink.

3.2.2 Substrate material and effective dielectric constant calculations

In practical applications, antennas are usually mounted or printed on dielectric substrate [38]. Whether substrate is needed as an active part of the antenna or just for mechanical support, substrate choice is very important due to its impact on almost all the antenna characteristics [38]. The substrate material used in this thesis work is PREPERM® TP20556. It is special flexible film with tailored dielectric constant ε_r = 11, and the dielectric loss is very low (~0.001). PREPERM® TP20556 is designed for flexible antennas with thicknesses from 200 micron up to 1 mm.

Substrates are used in either grounded or ungrounded structures [38]. Microstrip antennas MSA are one commonly used example of grounded substrate. Printed dipole and monopole antennas are commonly used examples of ungrounded substrate. [38]

Microstrip antenna consist of a radiating patch on top of a grounded substrate with a ground plane on the other side [19]. The fringing fields around the patch are not fully confined in the substrate layer but also spread in the air to create radiation [19]. During the analysis of MSA a semi-empirical approximation is used to replace the dielectric constant ε_r by an infinite homogeneous effective dielectric constant ε_{eff} [38]. This facilitate

the study of MSA antennas and the calculation of its resonance frequency and feed location. Approximate formula for the calculation of the infinite homogeneous effective dielectric constant ε_{eff} of an MSA can found in any antenna and RF book [4] [19] [26] [28].

$$\varepsilon_{eff} = \frac{\varepsilon_r+1}{2} + \frac{\varepsilon_r-1}{2} * [1 + 12 * \frac{h}{W}]^{-1/2}, \quad (3.3)$$

Where ε_r and h are dielectric constant and height of the substrate and W is the patch width. According to Maxwell equations, electromagnetic wave travel in vacuum with the speed of light. In general medium, the phase velocity is scaled down by the square root of the dielectric constant [26]. Thus, during the analysis of MSA, the phase velocity and wavelength are scaled down by the square root of the effective dielectric constant ε_{eff} as in equation 3.4 [28].

$$\lambda_g = \frac{\lambda_o}{\sqrt[2]{\varepsilon_{eff}}} = \frac{v_o}{f * \sqrt[2]{\varepsilon_{eff}}} \quad (3.4)$$

where λ_0 and v_0 are the wavelength and speed of light in free space. Microstrip antennas are resonant; that is, the antenna resonate at the design frequency with $\frac{\lambda_g}{2} \approx \mathrm{L}$ for the dominant mode TM_{010} [28].

Substrate choice significantly affect the MSA characteristics. According to equation 3.4, size reduction can be achieved by using substrate with higher dielectric constant [19]. Also, decreasing the substrate thickness will increase the effective dielectric constant ε_{eff} (according to equation 3.3) and consequently more size reduction [19]. On the other hand, it turned out that increasing the dielectric constant of the substrate or decreasing the substrate height decrease the patch fringing fields. Therefore, bandwidth decreases and all radiation characteristics (directivity, efficiency, and gain) are degraded [19].

Ungrounded substrate is the case when a planar conductor is printed on a substrate and surrounded by free space with no conductor on the other side [38]. Printed dipole and monopole antennas are commonly used examples of ungrounded substrate. They are widely used with RFID and IoT applications. It would be convenient (as the case of MSA) to find a formula or a technique for calculating the effective dielectric constant ε_{eff} of such structure. This facilitate the analysis of the antenna as if it was in a homogeneous medium having dielectric constant ε_{eff}. [38]

The resonant dimensions of such ungrounded substrate structure are often found by trial and error method or by optimizing the antenna dimensional configuration to get the desired results [38]. Sometimes, the formula $\varepsilon_{eff} = \frac{(\varepsilon_r+1)}{2}$ is used to approximate the effective dielectric constant ε_{eff} [36]; however, this is an inappropriate approximation as it

is only valid for semi-infinite substrates [38]. Zivkovic, and his team, examined a systematic approach in [38] to estimate the effective dielectric constant of a dipole antennas. Their idea is that the effective dielectric constant can be approximated by finding the ratio between the resonant frequency of ungrounded antenna in free space and the same antenna printed on examined substrate. Thus, effective dielectric constant of the antenna structure substrate ε_{eff} can be approximated by equation 3.5, as presented in [38].

$$\varepsilon_{eff} = (f_{res.fr}/f_{res.diel})^2, \tag{3.5}$$

where $f_{res.fr}$ denotes the resonance frequency of the antenna with substrate dielectric constant equal 1 (free space), and $f_{res.diel}$ denotes the resonance frequency of the printed antenna on substrates (dielectric constant equal 11). The effective dielectric constant of substrate depends generally on relative dielectric constant ε_r and the geometrical dimensions of specific antenna [38]. They, in [38], simulated and printed dipole antennas on substrate with three different dimensional shapes (length, width, and orientation). In first probe A, the substrate width was same as the antenna. In second probe B, the substrate is wider than the dipole by 1.6 mm on each side. In probe C, the dielectric is wider than the antenna by 14.2 mm and slanted with respect to the dipole. For each case (probe A, B, and C), four commonly used dielectric substrate thicknesses were used (d = 0.5 mm, 0.8 mm, 1.2 mm and 1.6 mm) and three standard dielectric constants were used (Teflon: ε_r = 2.54, FR4: ε_r= 4.6 and Duroid: ε_r= 10.2). Thus, they have examined 36 samples.

Their simulated and experimental results showed that the effective dielectric constant of substrate increased as the dielectric size and dielectric constants ε_r increase. In addition, their results showed that the effective dielectric constant of substrate increased linearly by increasing the thickness of the substrate (with specific dielectric constant). Generally, their results showed that the effective dielectric constant of such ungrounded antennas is far below the substrate dielectric constants ε_r. Table 3-2 shows the calculated effective dielectric constants for probe B (the nearest to our antenna) with different substrates and different thickness. In addition, their results showed that the antenna input capacitance is directly proportional to the effective dielectric constant.

Table 3-1. *Calculated effective dielectric constants for probe B (the nearest to our antenna) with different substrates and different thickness [38].*

Substrate thickness (mm)	**Teflon (ε_r= 2.54)**	**FR4 (ε_r= 4.6)**	**Duroid (ε_r= 10.2)**
0.5	1.24	1.38	1.58
0.8	1.29	1.48	1.71
1.2	1.34	1.56	1.85
1.6	1.37	1.62	1.96

In [36], they started with the formula $\varepsilon_{eff} = \frac{(\varepsilon_r+1)}{2}$ to approximate the effective dielectric constant ε_{eff}. Then, they optimized the dimensions by numerical simulation to get their antenna resonate at $\lambda_g/4$. As will be shown in the simulation and results chapters 4 and 5, these results agree very well with our results. We used ADS frequency domain solver and CST time domain solver to simulate the antennas presented in this thesis work. We performed characteristic mode analysis to study the impact of various geometrical features. Our results agree with results presented by Zivkovic, and his team, in [38]. In addition, we found that the antenna radiation efficiency increases as the substrate thickness decreases (these results and more discussion can be found in subchapter 5.3). This could be a result of decreasing the antenna input capacitance (which agree with our simulation results and the results reported in [38]) and consequently the storing reactive power decreases. This could be considered as a good result as decreasing the substrate thickness also increases the antenna flexibility.

3.3 Multiband printed antennas

Many wireless standards are used nowadays, and current wireless communication devices are required to support several standards simultaneously [7]. It is cost inefficient to use separate antenna for each band as it requires a lot of space and complicated feed network. In this context, multiband antennas offer a very efficient solution as it can support multiple frequency bands using one antenna and one feeding network [7]. In addition, multiband antenna may be even preferred over wideband antenna (that cover all the required bands) as the multiband antenna is considered to be cost-effective by removing filters which may be needed to remove undesired frequencies bands [36].

3.3.1 Multiband microstrip patch antennas

Considering our requirements mentioned in subchapter 3.1, microstrip patch antennas should be top candidate for our antenna design. Microstrip antenna consist of a radiating patch on top of a grounded substrate with a ground plane on the other side [19]. The existence of the ground plane on the other side of the substrate concentrates the radiated power in the main beam in the side of the patch and decreases the radiated power in the back lobe as shown in Figure 2-2. Consequently; (1) if attached from the GND plane side to any material, there is less coupling with the antenna and less impact on its results; (2) concentrating the radiated power in the main beam in the side of the patch makes it directive antenna with higher gain. Although the directivity of patch antenna is influenced by substrate height and the width of the patch, but on average it varies between 5-8.5

dBi [4]. On the other hand, for example dipole antenna is omnidirectional directional antenna with directivity around 2 dBi [4].

Many ideas for multiband patch antennas are provided in [19], [21-23], and [33]. However, as mentioned in [4], [19], [28], and [33]; the bandwidth and efficiency of a patch are decreased by decreasing substrate thickness and by increasing the dielectric constant of the substrate. Unfortunately, the PREPERM® TP20556 substrate material used in this thesis work is very thin (with thickness of 0.275 mm to increases the antenna flexibility) and has very high dielectric constant $\varepsilon_r \approx 11$. Therefore, our initial simulation results (for a conventional rectangular microstrip patch antenna resonating at 800 MHz) showed a bandwidth of 10 MHz bandwidth and around 15 percent efficiency. Thus, patch antenna design did not seem suitable on the PREPERM substrate.

3.3.2 Multiband printed monopole antenna

Planar monopole antennas share many advantages with microstrip antennas. They are both light weight antennas with small volume and low-profile planar configuration [25] [28] [29] [31]. This allows them to be conformal to the host circuit surface and makes them easier to be integrated with the driving electronics circuit [1] [28] [29] [30]. Both antennas allow for mass production using printed circuit technology which reduces the fabrication cost [1] [25] [28] [29].

Moreover, the planar monopole antennas printed or etched on thin substrate demonstrated multiband operation with reasonably good performance in numerous designs [1] [8] [20] [25] [30] [34] [36]. In addition, the flexibility attribute of the printed monopole antenna presented in [18] was experimentally studied with promising results. Thus, planar monopole antenna was a promising candidate for our design.

In [25], they presented the dual-band printed G-shaped monopole antenna as shown in Figure 3-2. Very similar ideas are presented in [17] and [27]. In [36], they presented a printed antenna for triple-band applications. The antenna consists of three circular-arc-shaped strips that looks like “ear” type as shown in Figure 3-3 [36]. In [1], they presented a U-shaped inkjet-printed monopole antenna for triple-band applications, as shown in Figure 3-3. Similar geometrical configuration is used for these antennas where a microstrip line is printed on top of the substrate to feed the antenna, and a ground plane is printed on the other side of the substrate. The width of the microstrip line varies according to the substrate material used with each antenna. Size reduction is achieved in these antennas ([1], [17], [25], [27], and [36]) by using meandered strips [1] [17] [25] [27], or

strips with arc shape [36]. It is mentioned in [36] that an arc with smaller radius on the upside can be used to achieve more sized reduction.

These antenna in [1], [17], [25], [27], and [36] achieve the multiband operation by optimizing the strips length to resonate at the desired frequencies. For example, in the dual-band printed G-shaped monopole antenna proposed in [25], it resonates at two frequencies, where the longer strip and shorter strip resonate at lower band and higher band, respectively. They mentioned in [1], [17], [25], [27], and [36] that the length of each strip is optimized to be a quarter of the guided wavelength at the desired resonant frequency. It is mentioned in [36] that the couplings between strips provide a contribution for the final exact working bands. That is, there is no single design parameter that tune only one frequency band [17].

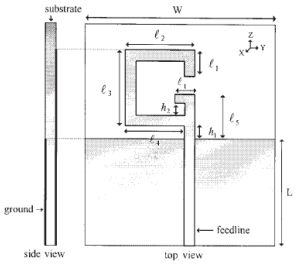

Figure 3-2. *Geometrical configuration of the printed dual-band G-shaped monopole antenna [25]*

(a)  (b) 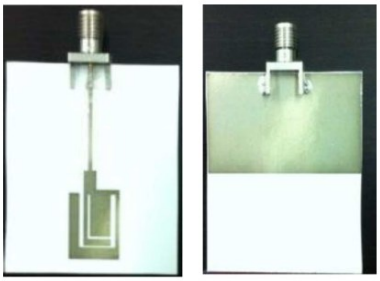

Figure 3-3. *Printed antenna for triple-band applications. (a) looks like "ear" [36], and (b) Inkjet-printed U-shaped [1]*

The achieved gain of the proposed antennas in [1], [17], [25], [27], and [36] varied according to (1) antenna size; (2) ground plane size. In [36] they achieved gain of around 2 and 2.5 dBi at the lower and mid-band (2.5 and 3.5 GHz) respectively while achieving 4 dBi at the high band (5.5 GHz). Gain increase as frequency increase because the ground plane is becoming electrically larger at higher frequencies [1]. Similar results are presented in [17] [25] [27]. In [1], they achieved much size reduction for both antenna and ground plane, as shown in Figure 3-3, on the expense of the realized gain. Thus, their measured realized gain, in [1], dropped to -6 dBi for the 1.57 GHz band and around 1.5 dBi for the 3.2 and 5 GHz bands.

In [9], they presented the idea of using two identical strips for the same band which form an array to enhance the antenna performance. The antenna forms a U-shape with four strips (two identical strips for each band), as shown in Figure 3-4, to achieve the dual-band operation at 2.4 and 5.8 GHz. In [30], they utilize the same idea to enhance the performance of the higher band (5.2 GHz) only, while using one strip for the lower band (2.4 GHz). This results in a trident shape monopole antenna as shown in Figure 3-4. In addition, the proposed antenna in [30] has a relatively large ground plane. Therefore, they have achieved gain of around 4 dBi at the lower band (2.4 GHz) and around 5 dBi at the higher band (5.2 GHz).

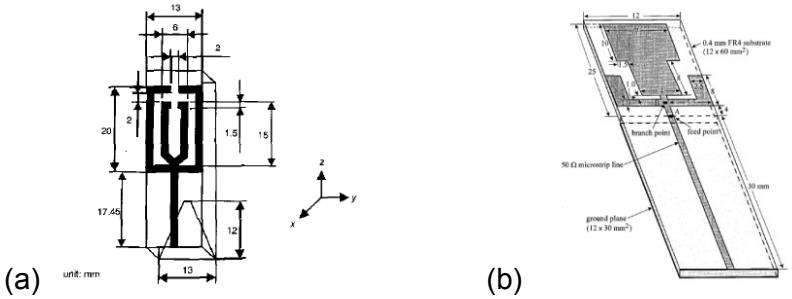

Figure 3-4. *Geometrical configuration of the printed dual-band antennas. (a)U-shaped monopole antenna [9], and (b) trident monopole antenna [30]*

In [8] and [31], the multiband operation is achieved by one meandered strip of different widths. Figure 3-5 shows the antenna proposed in [8]. It is an inverted-L monopole modified by introducing a meandered wire and a conducting triangular section. In [8] and [31], they utilize the higher order modes of the antenna and they were able to achieve good impedance matching for the two bands by varying the width of each section of the meandered strip.

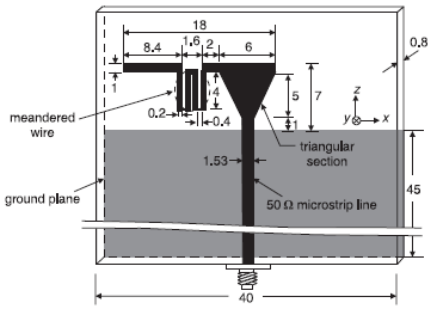

Figure 3-5. *Geometrical configuration of the modified inverted-L monopole antenna for 2.4 GHz and 5 GHz dual-band operations [8]*

The idea of the printed double-T monopole antenna is proposed in [18] and [20]. Figure 3-6 shows the antenna proposed in [20]. The antenna comprises two T-shaped monopoles of different sizes, which generate two resonant paths for dual-band operation. It is mentioned in [20] that the larger T-shaped monopole controls the lower operating band

while the smaller T-shaped monopole controls the higher operating band. The idea of the dual-band F-shaped monopole antenna is proposed in [34] which should achieve a noticeable size reduction from the double-T monopole antennas of [18] and [20].

The idea of these three antennas in [18] [20] [34] is to generate two separate resonant modes where the length of each resonance path is optimized to be a quarter of the guided wavelength at the desired resonant frequency. The idea of utilizing the higher order modes, reported in [8] and [31], has not been mentioned in [18] [20] [34]. Our idea was to use the F-shaped idea of [34] to achieve a size reduction and by varying the widths of the F-shaped meandered strips we can utilize the higher order modes. This will make the longer strip of the lower band active at the higher bands which form an array to enhance the results of the higher band as reported in [30].

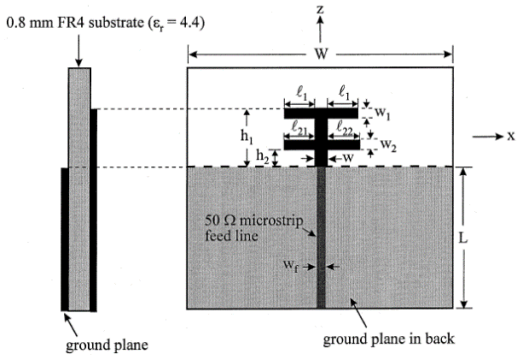

Figure 3-6. *Geometry of the printed dual-band double-T monopole antenna [20]*

In addition, the impact of the ground plane size on dual-band antenna performance is studied in [37]. They studied the impact of the ground plane size on the radiation pattern of the higher band. They showed that the radiation pattern of the higher band can improver by cutting four slots from the ground plane which increase the effective current path of the ground plane. We will utilize this idea to improve the radiation pattern of the final version antenna at the 2.6 GHz. Also, in [29] they introduce the idea of adding two parasitic elements on the ground plane which gives a good performance at the two bands and achieves a size reduction.

Finally, the flexibility attribute of the printed monopole antenna presented in [18] was experimentally studied with promising results. The thin and flexible printed antenna, in [18], was rolled on foam cylinders with different radii to test the performance of the antennas under different bending extents. Their results showed that resonance frequencies have shifted up by around 10–25 MHz and 10–30 MHz for the lower and higher bands, respectively. However, it is mentioned in [18] that as the impedance bandwidths at each band is relatively large, it could overcome this minor shift in resonance frequency caused by bending.

4. MULTIBAND PRINTED MONOPOLE ANTENNA, WORKING PRINCIPLE WITH SIMULATION RESULTS

In this chapter, the working principle of the proposed antenna is studied. First, a simple printed monopole antenna working at 800 MHz is considered and the impact of all its geometry parameters is examined. Next, an L-shaped monopole antenna is considered, especially, the differences between straight and L-shaped radiating elements. Finally, two L-shaped arms are added. These arms should support operation at 1.8 GHZ and 2.6 GHz. The study is done with frequency domain solver on ADS software and supported with characteristic mode analysis CMA (with multilayer solver) and time domain solver on CST microwave studio. Table 4-1 lists the 3D electromagnetic EM simulators software that have been used along with the type of solvers. Throughout this chapter and the next chapter, it will be mention clearly which EM simulators and which solver is used to get the presented results.

Table 4-1. *3D EM simulators software that have been used and the type of solvers.*

3D EM simulation software	Version	EM Solver	Simulation task
Advanced Design System (ADS)	2016.01	Frequency domain	Excited driven model
CST MICROWAVE STUDIO	2018.00	Time domain	Excited driven model
CST MICROWAVE STUDIO	2018.00	Multilayer	Characteristic mode analysis

4.1 Conventional 800MHz printed monopole antenna

For a simple monopole antenna simulated with the conductive ink (σ = 5e6 S/m) and printed on PREPERM® TP20556 substrate ($\varepsilon_r = 11$ and dielectric loss = 0.001), a simulation model has been developed on ADS software as shown in figure 4-1. The dimensions have been optimized so that the antenna resonates at 800 MHz.

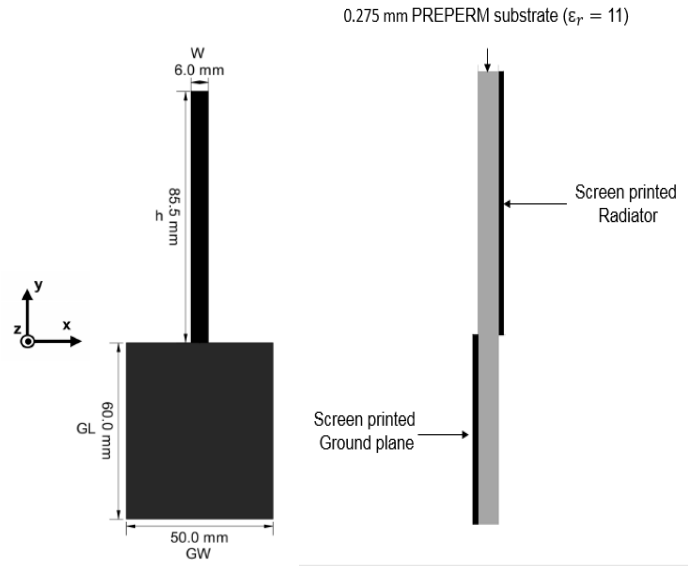

Figure 4-1. *Simple monopole planar antenna layout simulated on ADS*

The antenna is being excited without transmission line at this early stage of simulation. One port P1 is assigned to the antenna and two reference ports P2 and P3 are assigned to the ground plane. Exciting the antenna through a 50 Ω microstrip feedline should not affect the return loss results noticeably if the antenna is matched to 50 Ω. However, it changes the phase of the input impedance which rotates it on smith chart according to the electrical length of the line at each frequency [26]. Thus, to focus the study on the antenna input impedance and other results, it was better not to include this segment of 50 Ω microstrip feedline. One port P1 is assigned to the antenna and two reference ports P2 and P3 are assigned to the ground plane as shown in figure 4-2.

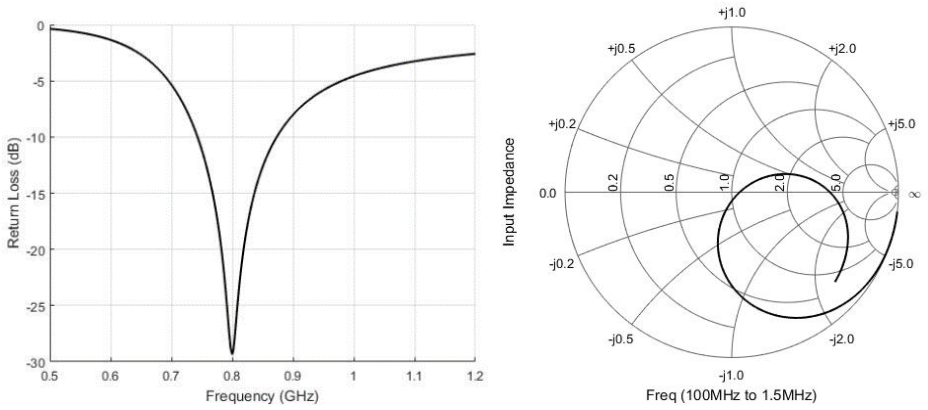

Figure 4-2. *Simulated return loss and input impedance*

Simulation results of figure 4-2 show -10 dB return loss bandwidth of around 130 MHz at the 800 MHz band, which is more than required. Figure 4-3 and 4-4 show the simulated radiation pattern at 800 MHz. Results showed a monopole-like radiation pattern in the E-plane (y-z plane) and the H-plane (x-z plane), where the antenna is oriented in the x-y plane. Simulation results showed a maximum gain of 1.94 dBi with directivity of 2.2 dBi and efficiency of 94%.

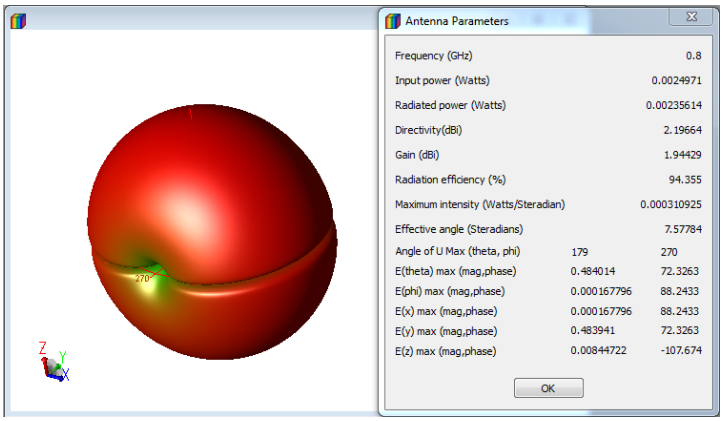

Figure 4-3. *Simulated 3D-radiation pattern at 800 MHz*

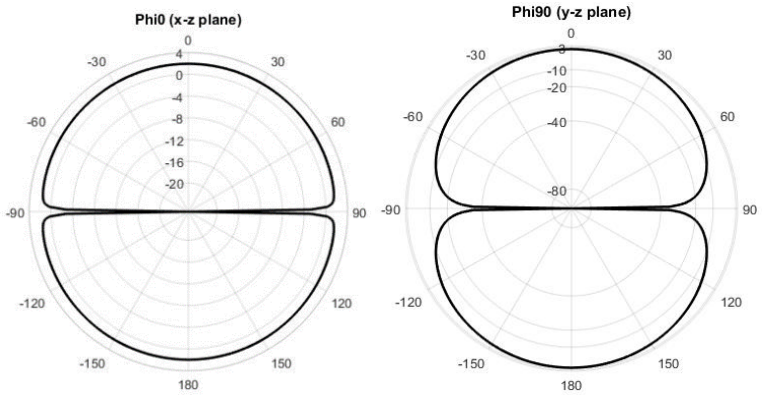

Figure 4-4. *Simulated radiation pattern polar plot (power gain) at 800 MHz*

Results of figure 4-5 show that the antenna radiates a linearly polarized wave (in E-plane direction) with axial ratio |AR| minimum value of 34 dB. These results of the radiation pattern and other antenna parameters were stable over the whole bandwidth of the 800 MHz band.

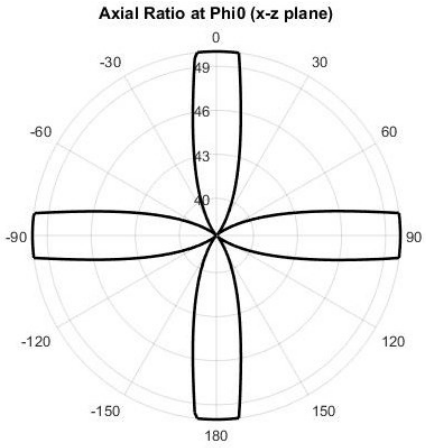

Figure 4-5. *Simulated axial ratio |AR| at 800 MHz*

These results agree with the characteristic mode analysis (CMA) on CST microwave studio using multilayer solver. Figure 4-6 shows the simulated model on CST with the

same dimensions as in figure 4-1. As mentioned in the characteristic mode analysis (CMA) subchapter 2.4 in the theoretical background chapter, lossy materials are not supported for the characteristic mode analysis on CST MW studio. Thus, lossless PREPERM® TP20556 substrate (dielectric constant ε_r = 11) and perfect electric conductor are used to build the model.

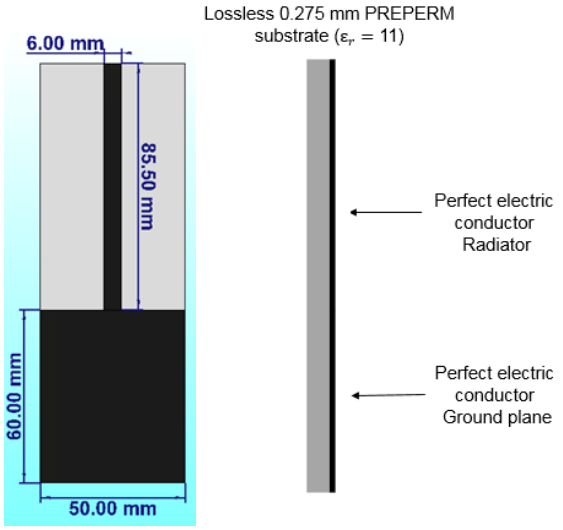

Figure 4-6. *Simple monopole planar antenna layout simulated with CMA on CST*

Figure 4.7 shows the modal significance simulation results of the most three significant modes at 800 MHz. A clear dominant mode exists at 800 MHz which agrees with the ADS frequency domain solver simulation results. Higher order modes have very small modal significance value which should not affect the results of the dominant mode at 800 MHz.

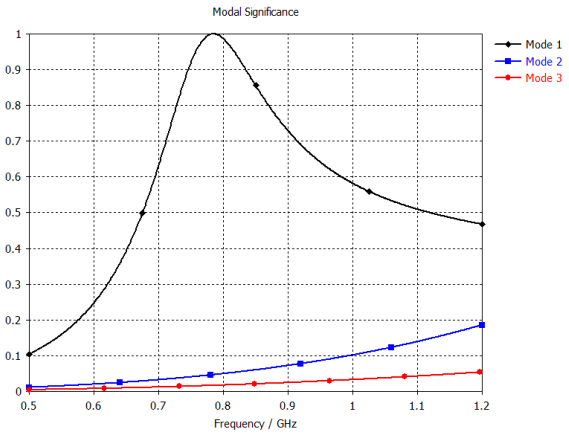

Figure 4-7. *Modal significance (MS) of three modes at 800 MHz (for modal depicted in figure 4-6 simulated with CMA on CST)*

Figure 4-8 shows the characteristic angle and eigenvalue simulation results of the dominant mode (mode 1). Results show that the dominant mode is resonating around 800 MHz with characteristic angle equal 180° and eigenvalue equal 0. The magnitude of the

characteristic eigenvalue λ_n shows also that the mode is storing electric energy (with $\lambda_n < 0$) before the resonance frequency. Thus, the input impedance before resonance should be more capacitive, which agrees with the ADS results on smith chart of figure 4-2. On the other hand, the characteristic eigenvalue λ_n shows that the mode is storing magnetic energy (with$\lambda_n > 0$) after the resonance frequency. Which again agrees with the ADS results on smith chart of figure 4-2.

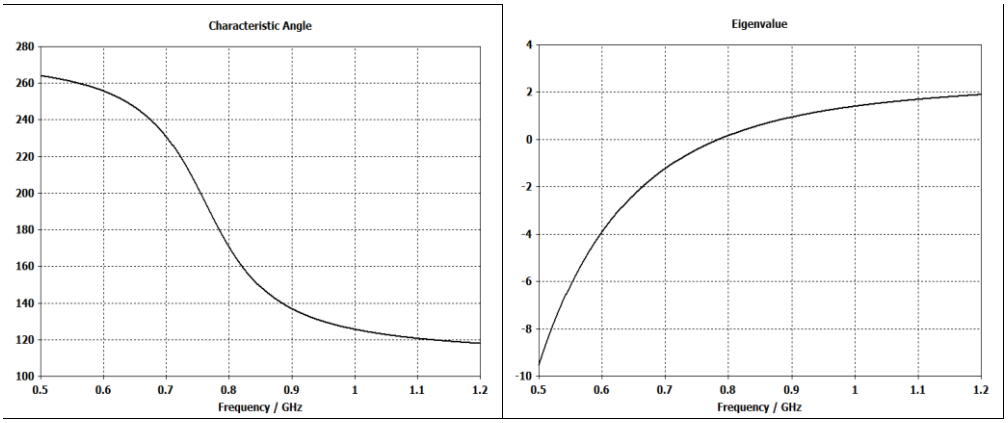

Figure 4-8. *Characteristic angle and eigenvalue of the dominant mode at 800 MHz (for modal depicted in figure 4-6 simulated with CMA on CST)*

Figure 4-9 shows the CMA simulated surface current of the dominant mode at 800 MHz, which agrees with the ADS driven model simulation results. results show a quarter-wave monopole-like surface current distribution over the antenna arm. Current is more confine to the edges ground plane, which agrees with the results reported in [37]. This will be discussed more and utilized later in the ground plane size subchapter.

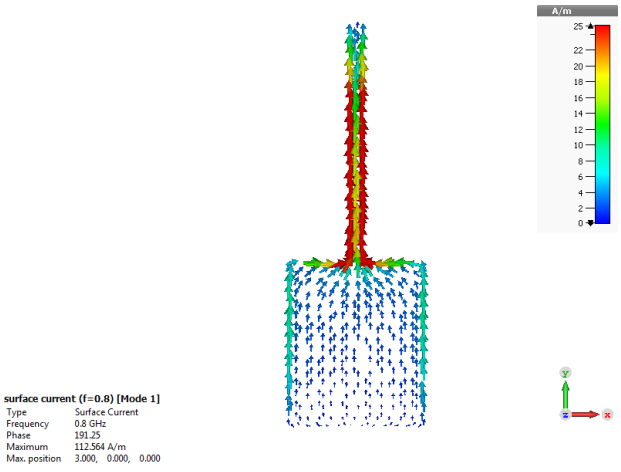

Figure 4-9. *CMA simulation results for the surface current of the dominant mode at 800 MHz (for modal depicted in figure 4-6 simulated on CST)*

Figure 4-10 shows the simulated 3D-radiation pattern of the dominant mode at 800 MHz, with a nice monopole-like donut. The results are in a very good agreement with the ADS driven model results as higher order modes are not significant at 800 MHz.

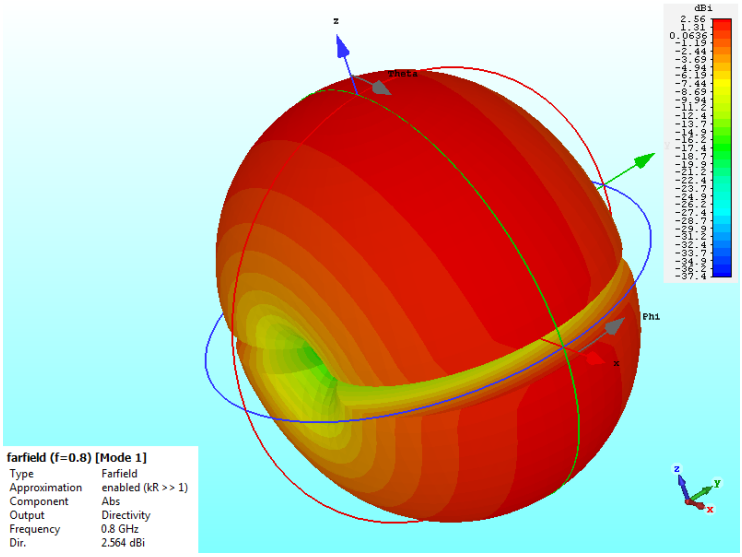

Figure 4-10. *CMA simulation results for the 3D-radiation pattern of the dominant mode at 800 MHz (for modal depicted in figure 4-6 simulated on CST)*

As discussed in the theoretical chapter, the effective dielectric constant of the antenna structure substrate ε_{eff} can be approximated by equation 4.1, as presented in [38].

$$\varepsilon_{eff} = (f_{res.fr}/f_{res.diel})^2, \tag{4.1}$$

where $f_{res.fr}$ denotes the resonance frequency of the antenna with substrate dielectric constant equal 1, and $f_{res.diel}$ denotes the resonance frequency of the printed antenna on substrates (dielectric constant equal 11). Simulation results for the antenna with the same parameters as in figure 4-1, but with air ($\varepsilon_r = 1$) replaced PREPERM ($\varepsilon_r = 11$) showed that resonance frequency ($f_{res.fr}$) increased to 860 MHz. Using equation 4-1, ε_{eff} can be calculated to be 1.15, which agrees with the experimental results reported in [38] for such thin substrate.

4.2 Antenna width

For conventional wire dipole or monopole antenna, increasing the wire radius decrease the resonance frequency [28]. This is happening due to the fringing fields which increase with increasing the wire radius; consequently, the effective length of the antenna increases, and the input reactance is becoming more inductive for frequencies near the first resonance frequency. Thus, resonance frequency decreases. For a wire dipole antenna, to be at resonance, with a real input impedance, the antenna length decreased as the wire diameter increases as shown it Table 4-2 [28].

Table 4-2. *Wire lengths required to produce a resonant half-wave dipole for a wire diameter of D and length L [28].*

Length to diameter ratio L/D	Percent shortening required	Resonate length L	Dipole thickness class
5000	2	0.49 λ	Very thin
50	5	0.475 λ	Thin
10	9	0.455 λ	Thick

However, the simulation results for our planar monopole antenna (figure 4-1) showed different behaviour. Increasing the antenna width, increased the resonance frequency, and vice versa. These results agree with the results reported in [20]. Figure 4-11 shows simulation results for the antenna in figure 4-1 with different widths W = 4 mm, 6 mm and 12 mm (all other parameters remain same). Results showed that as the width increases, input resistance decreases. In addition, the input reactance impedance component is becoming more capacitive as the width increases. This could happen as a result of decreasing the input inductance or capacitance of the antenna (notice that $Z_L = j\omega L$ and $Z_C = \mathrm{j}/J\omega C$). As a result, the resonance frequency increases as the width increases and input impedance curve on smith chart shift toward low impedance and more capacitive region as shown in figure 4-11.

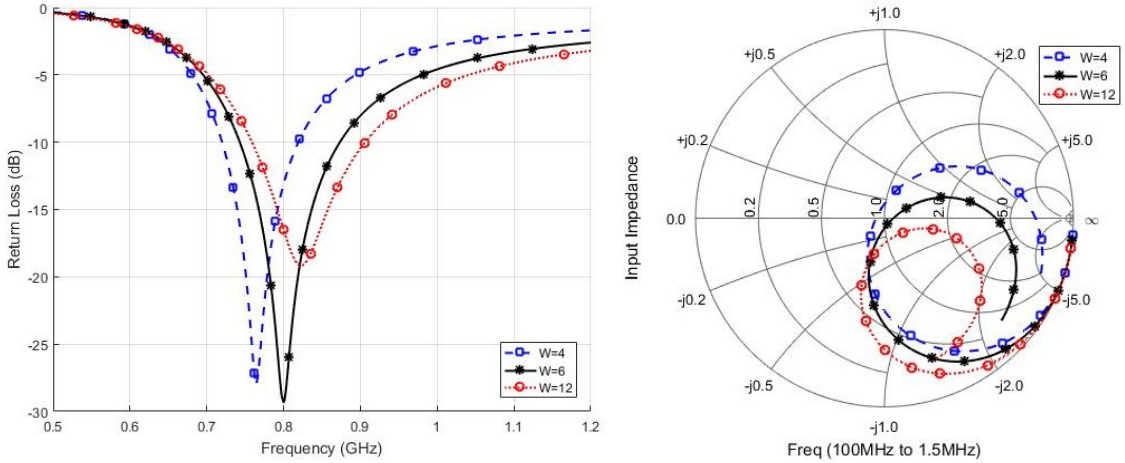

Figure 4-11. *Simple monopole planar antenna simulated with different width*

Characteristic mode analysis (CMA) results on CST MW studio supported these results. figure 4-12 shows the modal significance (MS) and the characteristic angle for the antenna in figure 4-1 with different widths W = 4 mm, 6 mm and 12 mm. It is clear that the resonance frequency of the dominant mode is increasing as the width increases which agrees with the ADS results.

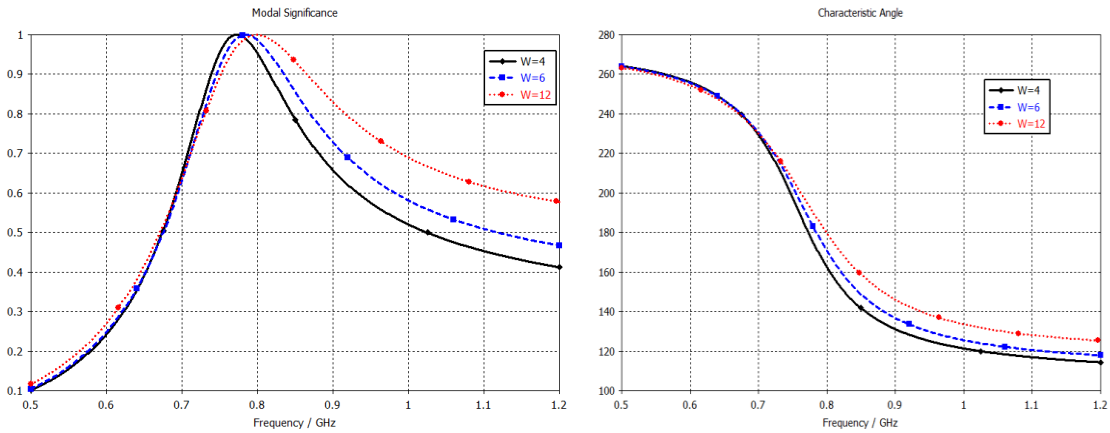

Figure 4-12. *Modal significance and characteristic angle of the dominant mode at 800 MHz simulated with different width (for modal depicted in figure 4-6)*

The characteristic eigenvalues CMA simulated results, shown in figure 4-13, showed that the dominant mode is becoming more capacitive near 800 MHz as the width increase (mode is storing electric energy when $\lambda_n < 0$, and called capacitive mode). This explains why the input impedance of the ADS driven antenna shifts toward more capacitive region as the width increase. In addition, the CMA simulated surface current of the dominant mode at 800 MHz suggested higher current as the antenna width increase, which could explain why input impedance curve on smith chart shift toward low impedance. Also, results of the modal significance suggested that the potential bandwidth of the CMA external resonance frequency increases as the antenna width increases. Same results are reported in [20] that by increasing width the bandwidth can be effectively enhanced. The driven model results on ADS suggested the same results, but matching started to degrade as width increases which in return affected the bandwidth. Notice that the characteristic mode analysis (CMA) does not consider excitation nor matching as discussed.

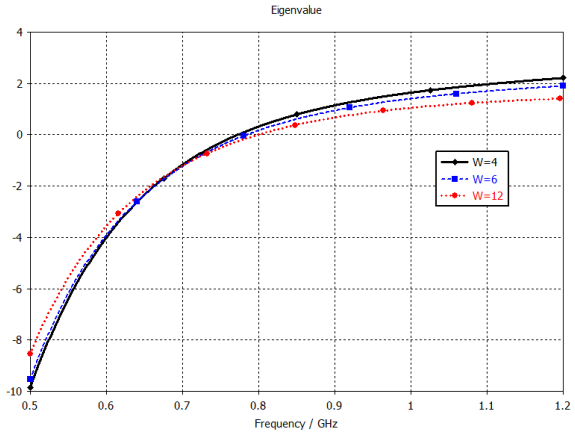

Figure 4-13 *Eigenvalue of the dominant mode at 800 MHz simulated with different widths (for modal depicted in figure 4-6)*

To keep the resonance frequency at the desired frequency, 800 MHz in this case, the antenna length has to be increased (if the width increased) or decreased (if the width decreased). Table 4-3 shows the required antenna's length for different widths to keep the resonance frequency at 800 MHz with the antennas simulated results.

Table 4-3. *Required antenna length for different widths and related results*

Width (mm)	Length (mm)	Directivity (dBi)	Radiation Efficiency (%)	Max Gain (dBi)
4	83	2,18	94,12	1,92
6	86	2,19	94,32	1,94
8	87	2,2	94,37	1,95
10	88	2,2	94,42	1,96
14	89	2.22	94.45	1.97

The simulated results for these five antennas are shown in figure 4-14. Results show that BW increases slightly with increasing the antenna width. More noticeably, circles on smith chart are getting smaller and shifts toward low impedance and more capacitive region with increasing the antenna width. For W = 14, circle got much smaller, which affects matching and BW starts to decrease again. Thus, increasing the width will increase the BW slightly until impedance become far from matching which starts to decrease the BW again. On the other hand, Directivity, efficiency, and gain showed slight enhancement as the antenna width (and consequently length) increases, as shown in Table 4-3. This small enhancement could be regarded to increasing the antenna length.

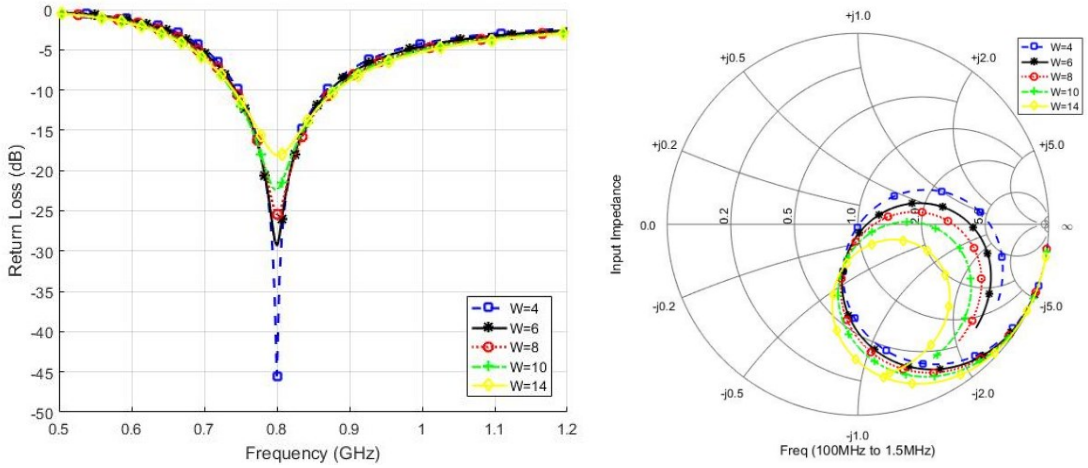

Figure 4-14. *Simulation results for the antennas in Table 4-2*

4.3 Trumpet structure

Another interesting result happens when the antenna width at the feed point or at the end of the line increases as shown in Figure 4-15. Increasing the width at the feed point

from 6 mm to 12 mm, increases the resonance frequency. On the other hand, increasing the width at the end of the line from 6 mm to 12 mm, decrease the resonance frequency. Figure 4-15 shows the CMA simulation results of the modal significance of these two ideas with different width at the feed point or end of the line. Other dimensions of the antenna are same as in figure 4-1.

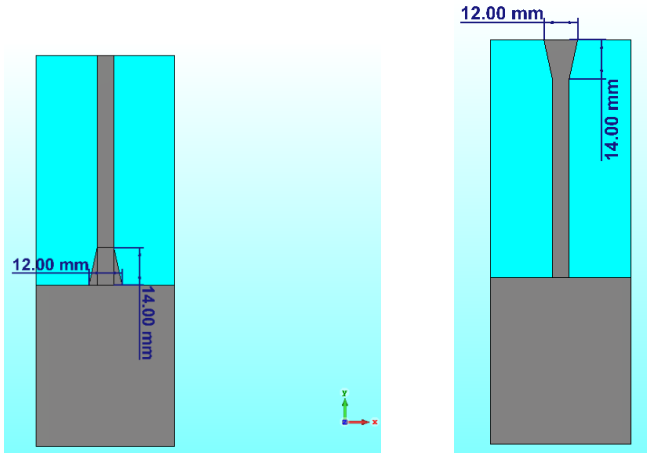

Figure 4-15. *Trumpet structure model simulated with CMA on CST*

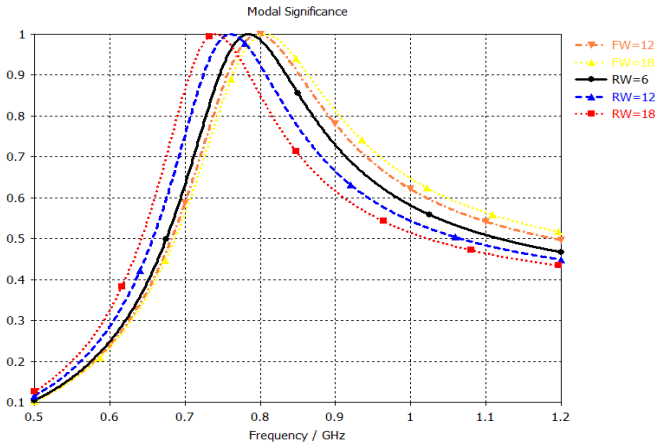

Figure 4-16. *CMA modal significance simulation results for the antennas in figure 4-15 with different feed-width or radiating edge width*

For the driven excited model on ADS, Increasing the width at the feed point from 6 mm to 12 mm, increases the resonance frequency as input resistance decreases and the input reactive impedance component is becoming more capacitive. This agrees with eigenvalue results of the CMA simulations. Consequently, the antenna length has to be increased from 85.5 mm to 88 mm to keep the frequency at 800 MHz as shown in figure 4-17. On the other hand, increasing the width at the radiating edge from 6 mm to 12.7 mm, decrease the resonance frequency as input resistance increases and the input reactive impedance component is becoming less capacitive. Antenna length has to be decreased from 85.5 mm to 81 mm to keep the frequency at 800 MHz as in figure 4-17.

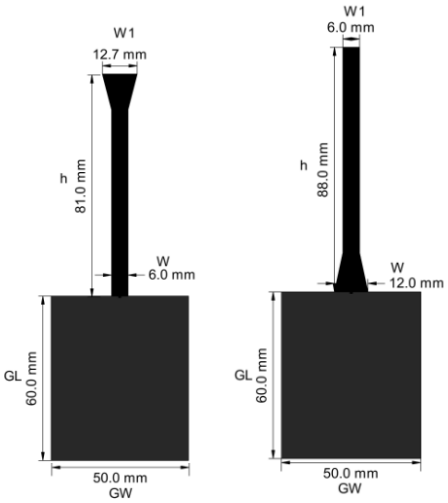

Figure 4-17. *Trumpet structure*

The simulation results for these two antennas against the conventional one are shown in figure 4-18. Increasing the width at the radiating edge and decrease the antenna length has less impact on the input impedance while achieving size reduction. Other simulation results showed that more size reduction can be achieved by increasing the width of radiating edge. Although the CMA simulation results suggested better potential BW as the width at the feed point increases, Increasing the width at the feed point and increasing the antenna length move the input impedance curve toward low impedance and more capacitive region which affects input impedance and matching. Thus, there was no significant change in the BW in the driven ADS cases. Other simulation results showed that input impedance and matching can be controlled by adjusting the width at the feed point or at the radiating edge accordingly.

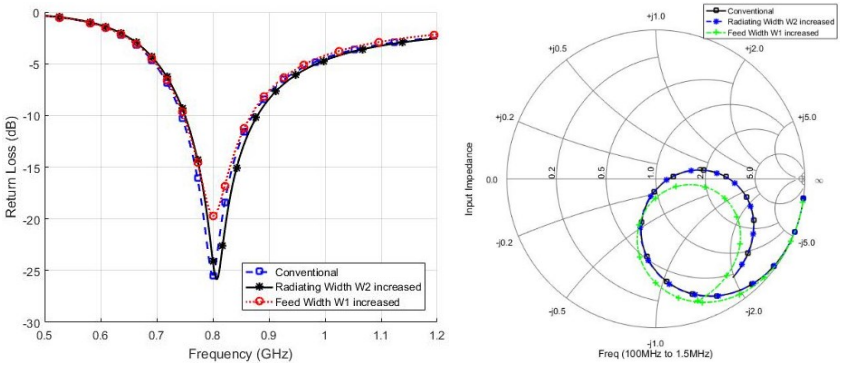

Figure 4-18. *Simulation results for the antennas in figure 4-17 compared with the original one in figure 4-1*

These results can be understood by viewing the surface current distribution over the antenna at 800 MHz as shown in figure 4-19. As mentioned in [28]; “for a dipole less than a half wavelength long, maximum current on the antenna always occurs at the centre”. Thus, Maximum current of a centre-feed dipole is happening near the feed point and increasing the width at this point pulls down the point of maximum current, so the antenna

resonates at higher frequency. Increasing the width near the radiating edge, increase the fringing fields which, consequently, increases the effective length of the antenna and the resonance frequency decreases.

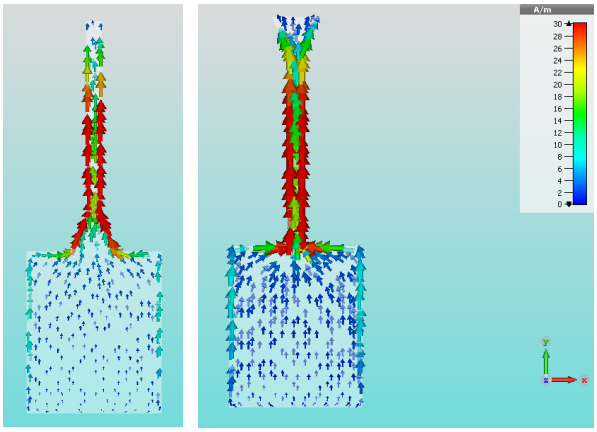

Figure 4-19. *Trumpet structure surface current distributions simulation at 800 MHz*

The results of section 4.2 showed that increasing the total width of the antenna increases the resonance frequency. This highlight that the impact of the width near the feed point is more dominant, unlike the conventional wire monopole antennas. This could be regarded to the planar structure where the conductive ink layer is very thin (10 micron). Thus, increasing the width, affect the current more. Same results are reported indirectly in [20], which will be discussed in section 4.6.These results will be utilized to control the size of the antenna and its input impedance; (1) antenna length can be decreased by decreasing the width; (2) matching and input impedance can be controlled by changing antenna's dimensions.

4.4 Ground plane size

The ground plane is indeed part of the radiation structure and its dimensions affect the results and the overall characteristics of the antenna [20] [37]. In this subchapter, the impact of the ground plane dimensions is studied.

4.4.1 Ground plane width G_W

It would be expected that the ground plane width G_W should have the same impact on the resonance frequency as the antenna width; however, this was not the case. The conventional antenna simulated in figure 4-1 has ground plane dimensions G_L= 60 mm and G_W=50 mm. Figure 4-20 shows the parametric simulation results for the conventional antenna with different ground plane width G_W= 30 mm, 50 mm, and 75 mm, while other parameters are not changed. Unlike the antenna width, increasing G_W decreased the

resonance frequency, and vice versa, similar results are reported in [20]. Input impedance on smith chart decreased as G_W increases. The shape of the circle did not change noticeably as the frequency decrease. Bandwidth increased slightly as the G_W increases.

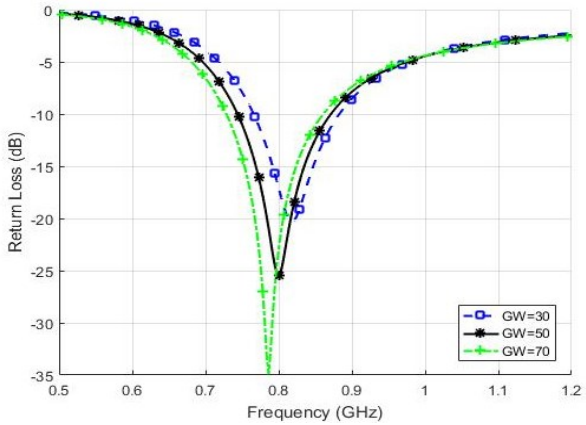

Figure 4-20. *Simulation results for the antennas in figure 4-1 with different* $\boldsymbol{G_W}$

Figure 4-9 shows the simulated current distribution over the antenna and the ground plane. It is clear that the current distribution over the ground plane is more confine to the edges with much higher value of current density. It is mentioned in [20] and [37] that these results could be probably because the G_W is comparable to the wavelength at 800 MHz. Thus, decreasing G_W decreases the current path and frequency increases, and vice versa. Decreasing G_W shift Input impedance curve toward high capacitive region which consequently decreased the BW.

4.4.2 Ground plane Length G_L

Increasing the ground plane length G_L, decreases the resonance frequency. Figure 4-21 shows parametric simulation results for the conventional antenna in figure 4-1 with G_L=60 mm, 65 mm and 70 mm, while other parameters are not changed. it is clear that as G_L increases the resonance frequency decreases.

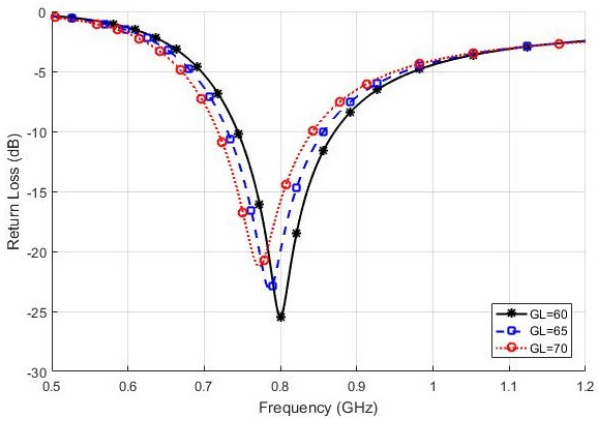

Figure 4-21. *Simulation results for the antennas in figure 4-1 with different* $\boldsymbol{G_L}$

The resonance frequency can be readjusted to 800 MHz again by decreasing the antenna length. Figure 4-22 compare the simulated results for the conventional antenna ($A_L = 86\ and\ G_L = 60$), and the case ($A_L = 83\ and\ G_L = 65$).

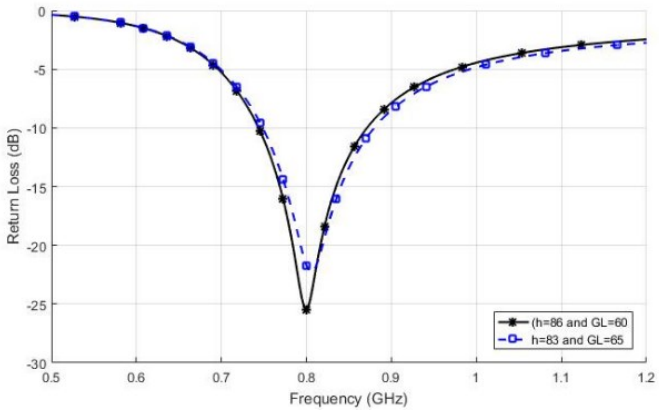

Figure 4-22. *Simulation results for case 1 ($\boldsymbol{A_L = 86\ and\ G_L = 60}$) in black, and case 2 ($\boldsymbol{A_L = 83\ and\ G_L = 65}$) in blue*

The two cases have the same resonance frequency; however, input impedance is quite different (which will be utilized in designing the final version). Matching and input impedance enhanced by increasing G_L. Notice that the ground plane dimensions will affect the results of the higher bands, 1.8 GHz and 2.6 GHz. Thus, G_W and G_L will be decided after examining their impact on the higher bands.

4.5 Shifting the antenna to the ground plane edge

So far, all simulations were done with antenna located at the centre of the ground plane. For the final versions, the antenna should be shifted to the edge of the ground plane as shown in figure 4-23.

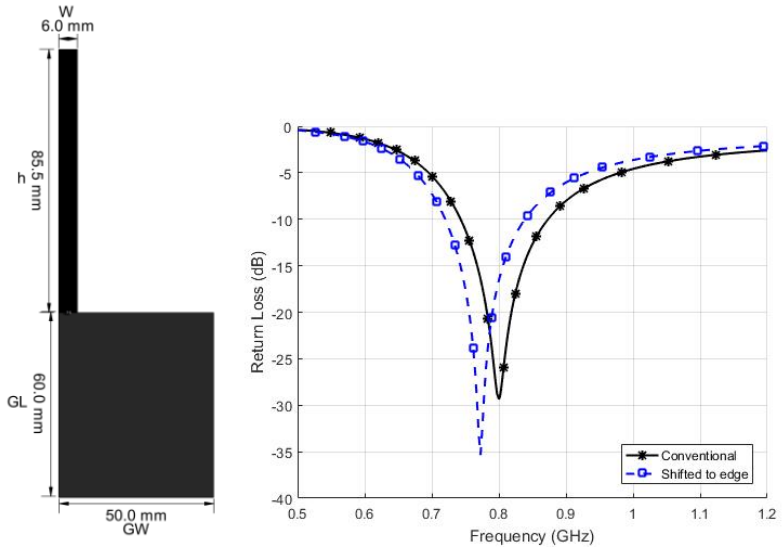

Figure 4-23. *Simple monopole planar antenna shifted to the ground plane edge with its simulated results in blue vs the original simulation results in black*

Simulation results, as shown in figure 4-23, showed that shifting the antenna to the edge of the ground plane has the same impact as increasing the ground plane length G_L; Resonance frequency decreases and input impedance decreases. This can be understood by viewing the surface current distribution over the antenna at 800 MHz, as shown in figure 4-24. Current distribution over the antenna is same as before; however, on the ground plane it is different. The effective length of the ground plane that the current follow can be considered as the diagonal of the ground plane, which is longer than the ground plane length. Thus, shifting the antenna to the edge of the ground plane, increases the effective length of the ground plane.

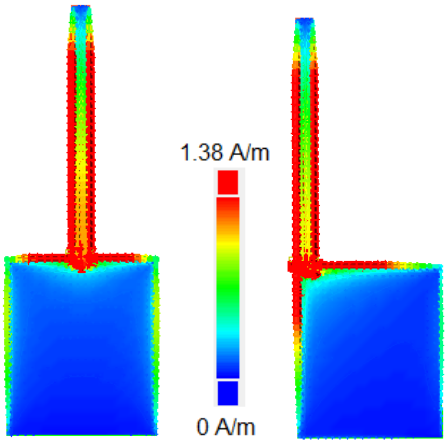

Figure 4-24. *Surface current distributions at 800 MHz with antenna located at the center and the edge of the ground plane*

As the resonance frequency has decreased, the antenna length has to be decreased from 85.5 mm to 81 mm to adjust the resonance frequency again to 800 MHz, as shown in Figure 4-25. There was no noticeable change for the input impedance and BW. Directivity, gain, and efficiency have enhanced slightly. Radiation pattern keeps almost the same characteristics with no noticeable change.

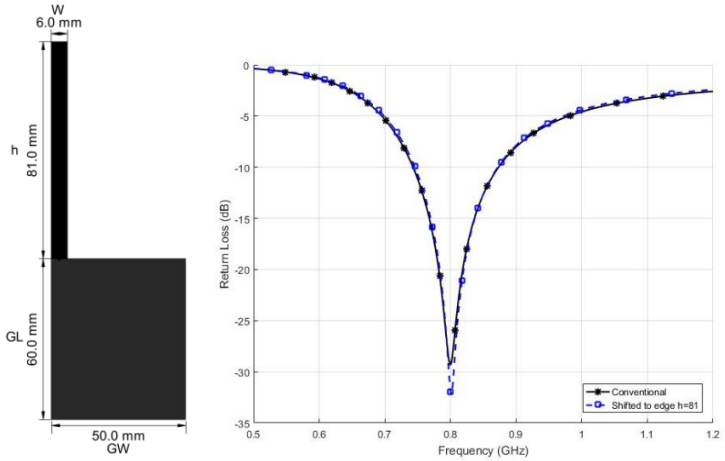

Figure 4-25. *Antenna shifted to the ground plane edge h = 81 mm with its simulated results*

4.6 L-shape monopole arm (compact antenna)

In this subchapter the idea of L-shape antenna (resonate at 800 MHz) will be developed. Four different structures will be introduced to show the impact of different parameters. Figure Figure 4-26 shows the first two structures, S1 and S2. For S1, the antenna height h = 54 mm and the arm length L1 = 39 mm. While for S2 more size reduction has been achieved by decreasing the antenna height to h = 47 mm and increasing the arm length to L1 = 48 mm.

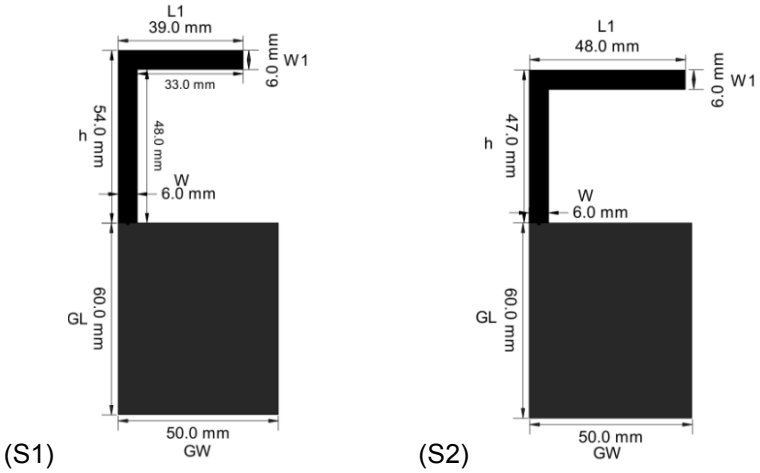

Figure 4-26. *L-shape structures S1 and S2*

Simulated results for these two antennas (S1 and S2) are shown in figure Figure 4-27 against the results of the straight antenna at the edge of figure Figure 4-25. Results show that input impedance decreases as the antenna height h decreases (and consequently increase the arm length L1 to keep the resonance frequency at 800 MHz). As a result, matching degraded and the BW decreased.

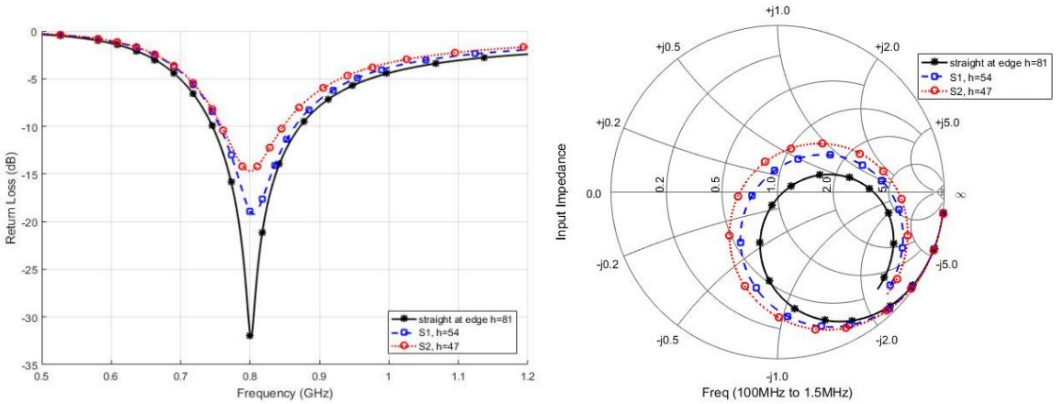

Figure 4-27. *Simulation results for L-shape antennas S1 and S2*

CMA simulation results on CST MW studio suggested losing potential BW as a cost for achieving size reduction for S2 antenna. Figure 4-28 shows the simulated modal significance of these two antennas S1 and S2.

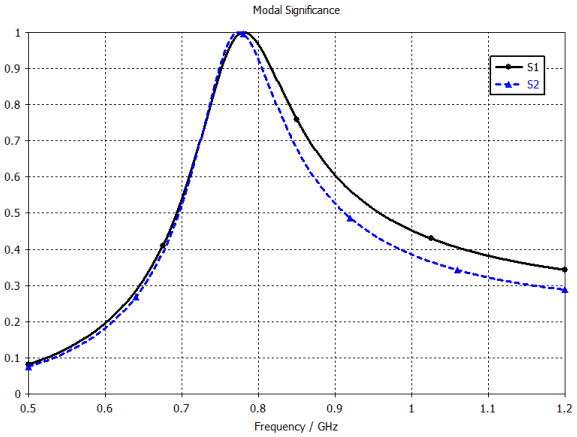

Figure 4-28. *CMA modal significance simulation results for S1 and S2 antennas*

Figure 4-29 shows the current distribution of antenna S1 at 800MHz. It turned out that current path is controlled with the inner length of the antenna, which agrees with the results reported in [31]. The inner length of antenna S1 is (48 mm +33 mm) 81 mm, which is the same length for the straight antenna at the ground edge. The inner length of antenna S2 is 83 mm.

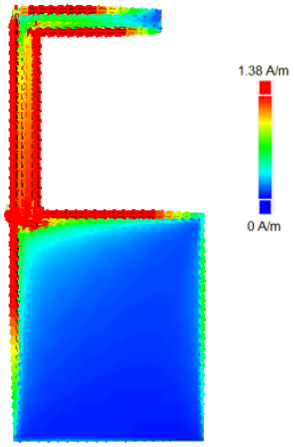

Figure 4-29. *Simulated current distribution of antenna S1*

Notice that W and W1 in this L-shape are playing the same rules as the feed point's width and the radiating edge width discussed explained in the trumpet structure section 4.3. Thus, they have the same impact as explained before. Figure 4-30 shows the third L-shape structure S3 with its simulation results against antenna S1. Antenna S3 has same parameters as S1 except for the width of the radiating edge W1 (increased from 6 mm to 10 mm). Increasing W1 decreases the current path which should increase the resonance frequency. On the other hand, according to the results of the trumpet structure section, frequency should decrease by increasing the radiation edge width. Simulation results showed that the resonance frequency decreased as shown in Figure 4-30, which agrees with the results of the trumpet structure section 4.3; the CMA simulation results; and the results reported in [20].

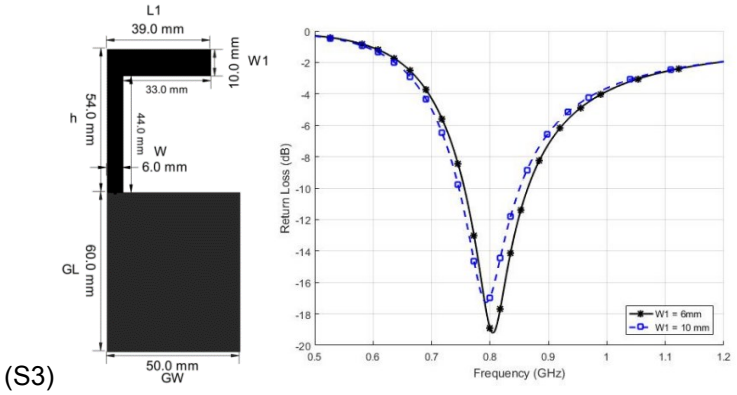

(S3)

Figure 4-30. *L-shape structures S3 and its simulation results against S1*

Finally, Figure 4-31 shows the fourth structure S4 with its simulation results against S1 and the results of the straight antenna at the edge. By increasing antenna width at the feed W (from 6 mm to 11 mm), resonance frequency increases. The frequency can be adjusted back by increasing the arm length L1 (from 39 mm to 50 mm), which is same as the ground plane width. Simulation results showed that matching and BW of S4 has enhanced noticeably, compared with S1.

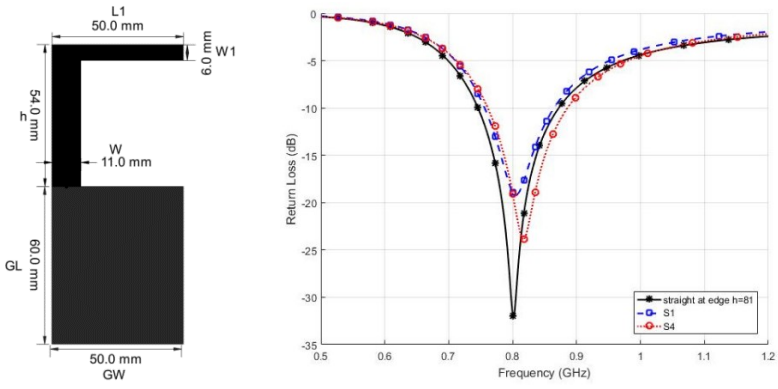

(S4)

Figure 4-31. *L-shape structures S4 and its simulation results against S1*

Many other structures have been simulated to improve the results. decreasing the antenna height as in antenna S2 results in size reduction but matching and BW degraded. The idea of antenna S3 results in better BW than S2 but it will affect the BW of the 1.8 GHz band as will be explained in next section. Increasing the feed width W, as in antenna S4, enhance the matching and the BW, but increase the antenna length L1. However, L1 is still 50 mm same as the ground plane width which means that the overall width of the structure has not increased. Considering the size and the BW requirements, antenna S4 offers the good compensated results.

Figure 4-32 show the simulated radiation pattern of antenna S4 (at 800 MHz) in E-plane (y-z plane) and H-plane (z-x plane), where the antenna is oriented in the x-y plane. Results showed no significant change in the radiation pattern from the conventional straight antenna of Figure 4-4. Radiation efficiency remains at 94%, as the straight antenna.

However, as a result of decreasing the antenna length, directivity has decreased to 2dBi, as shown clearly in Phi = 90° (y-z plane) cut. Consequently, maximum gain dropped to 1.7 dBi. Results showed that the antenna radiates a linearly polarized wave with axial ratio |ARI minimum value of 13 dB (within the beam width). These results of the radiation pattern and other antenna parameters were stable over the whole bandwidth of the 800 MHz band.

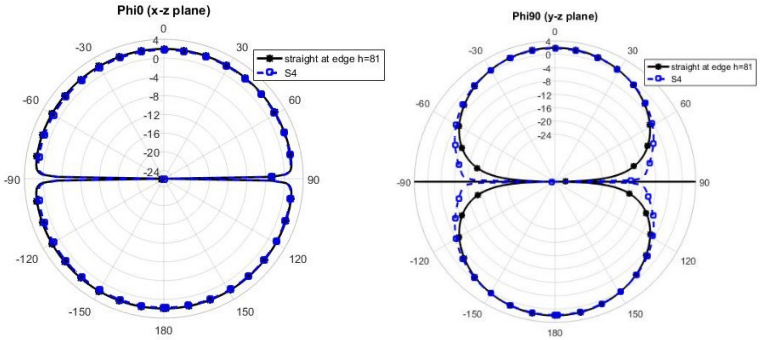

Figure 4-32. *Simulated radiation pattern polar plot (power gain) of S4 antenna at 800 MHz against the straight antenna at the edge of Figure 4-23*

4.7 Two-band antenna, Adding the 1.8 GHz arm

By adding a second horizontal strip with the dimensions shown in Figure 4-33, to the L-shape antenna S4 of Figure 4-31, another resonant frequency at 1.8 GHz is obtained. Figure 4-34 show the simulated return loss and input impedance. Results show that dual-band operation at 800 MHz and 1.8 GHz has been created. For simplicity and to avoid confusion, we will call the first arm (with length L1=50 mm) the 800 MHz-arm, while this new second horizontal strip the 1.8 GHz arm. The dimensions of these two arms are not the only factor to control the results at each band as has been shown for the 800 MHz band and will be shown for the 1.8 GHz band. However, we call them as so (800 MHz-arm and 1.8 GHz arm) just to avoid confusion.

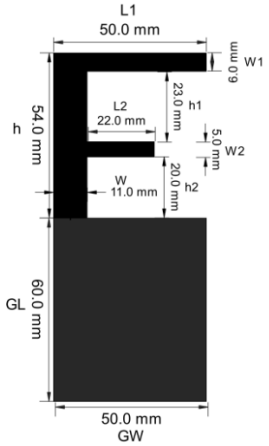

Figure 4-33. *Two-band antenna*

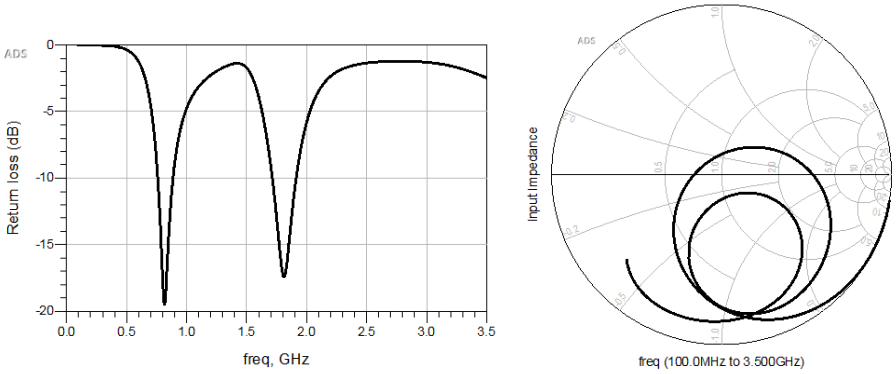

Figure 4-34. *Simulation results of the two-band antenna depicted in Figure 4-33*

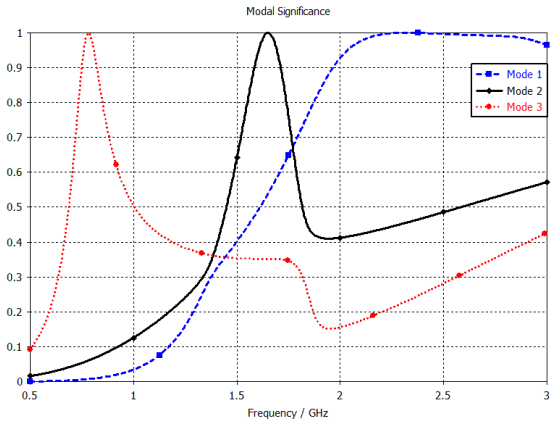

Figure 4-35. *CMA modal significance simulation results of the two-band antenna for the most three significant modes around 1.8 GHz*

The CMA simulation results show similar results. Figure 4-35 shows the modal significance simulation results (of the two-band antenna in Figure 4-33) for the most three significant modes around 1.8 GHz. A clear dominant mode around 1.8 GHz has been created by the introduction of the 1.8 GHz arm. It seems that the resonance mode of the 800 MHz affects at 1.8 GHz but with lower significance. One higher order mode (2.4 GHz) seems to be significant and could affect the results at 1.8 GHz. However, the CMA simulated surface current of this mode at 1.8 GHz shows that this mode will be suppressed with our excitation setup. The excitation setup is introduced at the beginning of this chapter and it will be discussed in detail in the results and discussion chapter.

It is mentioned in [1], [20] and [34] that adding the second horizontal strip (1.8 GHz arm) creates a second resonant path starting from the feed point to the second horizontal strip open end, which will mainly control the new resonance frequency (1.8 GHz in our case). In both [20] and [34], they mentioned that this new resonant path will form one-quarter wavelength current distribution at the new resonance frequency (1.8 GHz in this case).

However, our simulation results showed that the new resonant path is indeed forming three-quarter wavelength current distribution: (1) one-quarter wavelength current distribution starting from the feed point to the second horizontal strip (1.8 GHz arm) open end (h2 + L2); and (2) two-quarter wavelength starting from the second horizontal strip (1.8 GHz arm) open end to the upper horizontal strip (800 MHz arm) open end (L2 + h1 + L1). Figure 4-36 shows the CMA simulated surface current of the dominant mode at 1.8 GHz (mode 2 in Figure 4-35), which agrees with the ADS driven model simulation results very nicely. It also confirms that the 800 MHz mode is not significant at 1.8 GHz, and the higher order mode has been suppressed by our excitation setup.

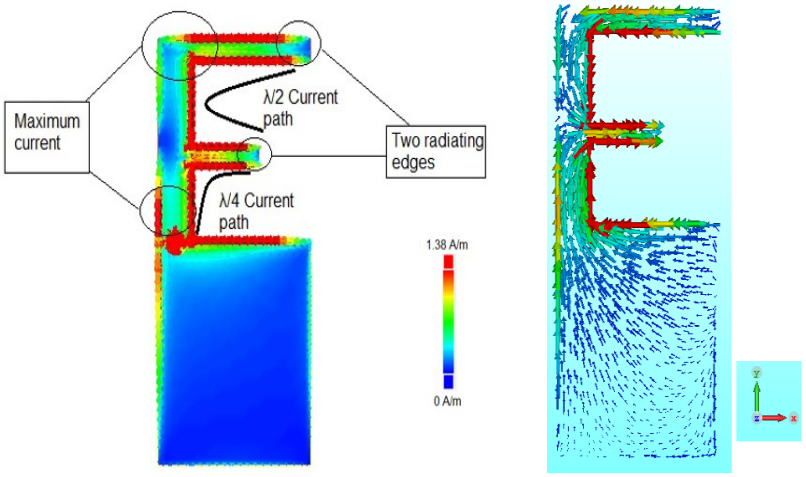

Figure 4-36. *Surface current distributions simulation results at 1.8 GHz for the two-band antenna. ADS driven model on right and CST CMA on left*

Different simulations have been done to prove that the new resonant path is indeed forming three-quarter wavelength current distribution not only one-quarter wavelength. First, Shifting the second horizontal strip (1.8 GHz arm) down by 3 mm (h1 = 26 mm and h2 = 17 mm) decreases the length from feed point to the second horizontal strip (1.8 GHz arm) open end, while increasing the length from the second horizontal strip open end (1.8 GHz arm) to the upper horizontal strip (800 MHz-arm) open end. Simulation results showed that the resonance of the 1.8 GHz band has increased by 20 MHz. Second, decreasing the length of the upper horizontal strip by 3 mm (L1 = 47 mm) will decrease the length of the two-quarter wavelength current path (the length from the second horizontal strip open end (1.8 GHz arm) to the upper horizontal strip (800 MHz-arm) open end). Simulation results showed that the resonance of the 1.8 GHz band has increased by 20 MHz. Third, decreasing the length of the second horizontal strip (1.8 GHz arm) by 3 mm (L2 = 19 mm) affects both current paths. Simulation results showed that the resonance of the 1.8 GHz band has increased by 140 MHz. Figure 4-37 shows the CMA MS simulation results of these three cases against the original one in Figure 4-33. It seems

that the potential BW increase as the length (h2 + L2) approaches one-quarter wavelength current distribution and the length (L2 + h1 + L1) approaches two-quarter wavelength. This result will be utilized to optimize the final versions.

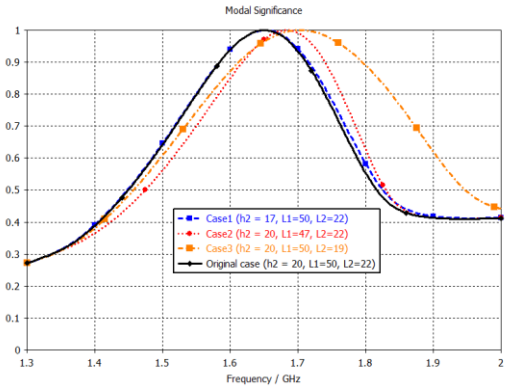

Figure 4-37. *CMA MS simulation results for the dominant mode at 1.8 GHz for the three cases described in previous paragraph against the original two-band antenna*

This current distribution shown in Figure 4-36 form two radiating edges and two points of maximum current. Other simulation results showed that they are acting as explained in the trumpet structure section. Increasing the width at the radiating edges increases the effective length and decreases the resonance frequency. On the other hand, Increasing the width at the feed point increasing the resonance frequency and affect input impedance. These results will be used to optimize the final versions.

Results of the 800 MHz band have not been affected by adding the 1.8 GHz arm strip. With this dimension, we were able to achieve -10 dB return loss bandwidth of around 200 MHz at the 1.8 GHz band, which is more than required. Decreasing the height of the 1.8 GHz arm h2 to 20 mm affects the results of the 2.6 GHz band, as it will be explained in next section. Therefore, we will have to shift the second horizontal strip up by decreasing h1 and increasing h2. This will affect the matching and consequently the BW of the 1.8 GHz band. Figure 4-38 shows another structure where h2 has increased to 30 mm (and L2 increased to 23 mm to adjust the resonance frequency). Simulation results of these two structures show that by shifting the second horizontal strip up, matching and BW have degraded. This is happening as now the two-quarter wavelength starting from the second horizontal strip (1.8 GHz arm) open end to the upper horizontal strip (800 MHz-arm) open end (L2 + h1 + L1) has decreased. On the other hand, the one-quarter wavelength current distribution starting from the feed point to the second horizontal strip (1.8 GHz arm) open end (h2 + L2) increased. Thus, input impedance increased significantly which affected the BW.

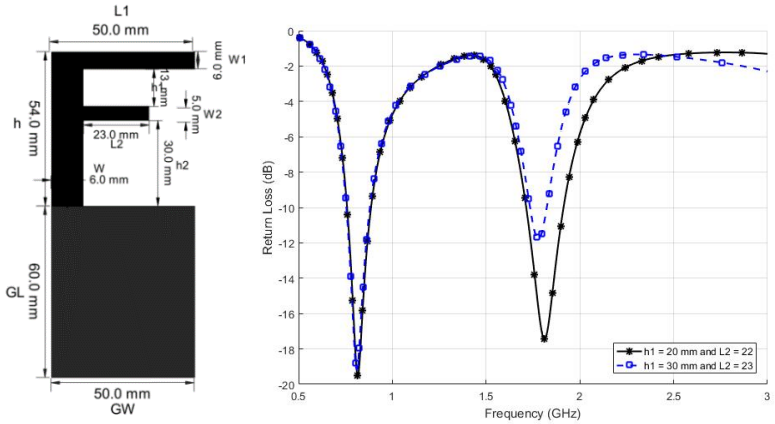

Figure 4-38. *Two-band antenna with h2 = 30 mm and its simulation results against the results with h2 = 20 mm*

Other simulation results showed that increasing the ground plane length GL enhance the matching and BW of the 1.8 GHz band. This will be utilized for the final version.

The simulated radiation pattern at 1.8 GHz showed a monopole-like radiation pattern in the E-plane (y-z plane) and the H-plane (x-z plane) as showed in Figure 4-39 (where the antenna is oriented in the x-y plane). Simulation results showed a maximum gain of 3.4 dBi with directivity of 3.77 dBi and efficiency of 91.3%.

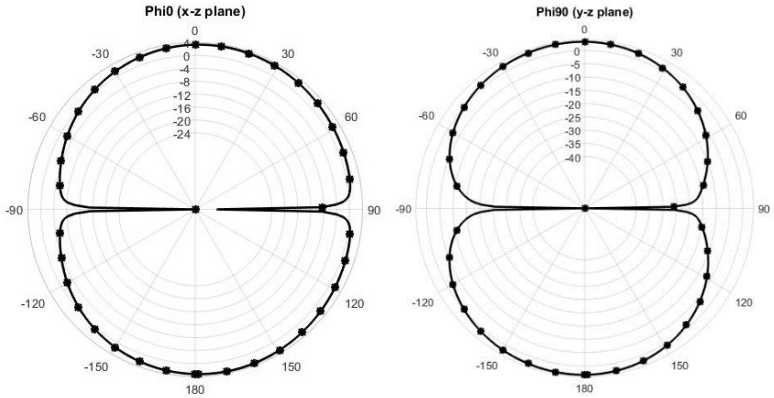

Figure 4-39. *Simulated radiation pattern polar plot (power gain) of the antenna in Figure 4-38 at 1.8 GHz*

4.8 Adding the 2.6 GHz arm

By adding a third horizontal ink strip with the dimensions shown in Figure 4-40, to the antenna of Figure 4-38, another resonant frequency at 2.6 GHz is obtained. Figure 4-40 shows the simulated return loss. Results show that triple-band operation at 800 MHz, 1.8 GHz and 2.6 GHz has been created. Results of the 800 MHz and 1.8 GHz bands have been enhanced by adding the third horizontal ink strip as it effectively increased the width at the feed point (point of maximum current at both bands). Enhancement is

clearer for the 1.8 GHz band. For simplicity and to avoid confusion, we will call this new third horizontal strip the 2.6 GHz arm. Similar to what we have discussed in the previous sub-chapter, the dimensions of the 2.6 GHz arm are not the only factor to control the results at 2.6 GHz band, as has been shown for the 800 MHz and 1.8 GHz bands and will be shown for the 2.6 GHz band. However, we call them as so (800 MHz-arm, 1.8 GHz arm, and 2.6 GHz arm) just to avoid confusion.

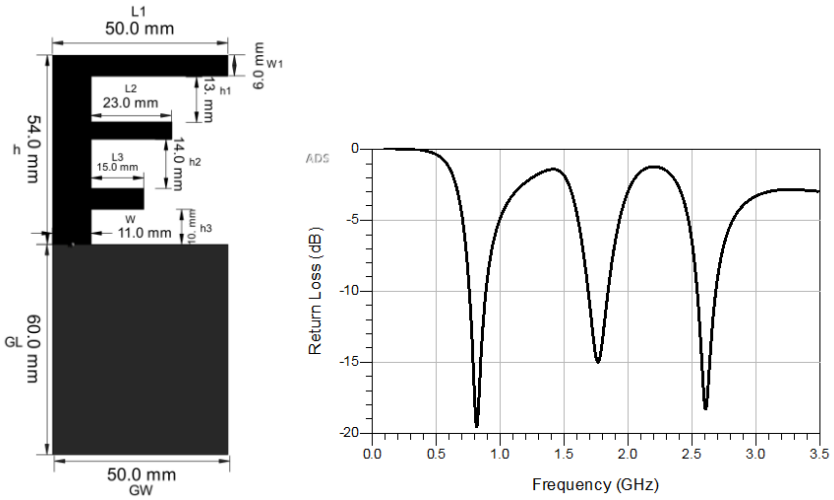

Figure 4-40. *Three-band antenna and its simulated return loss*

The CMA simulation shows quite interesting results. Figure 4-41 shows the modal significance simulation results (of the antenna in Figure 4-40) for the most four significant modes at 2.6 GHz. All the four modes have high modal significance value which means that they may all affect the 2.6 GHz band results. This will depend on their surface current distribution and how the excitation can (or cannot) support (or suppress) each mode. Figure 4-42 shows the surface current distributions simulation results at 2.6 GHz for the four dominant modes of Figure 4-41

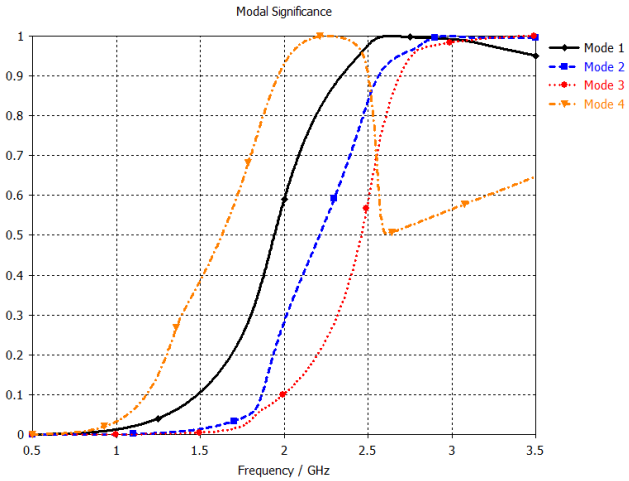

Figure 4-41. *CMA modal significance simulation results of the three-band antenna for the most four significant modes around 2.6 GHz*

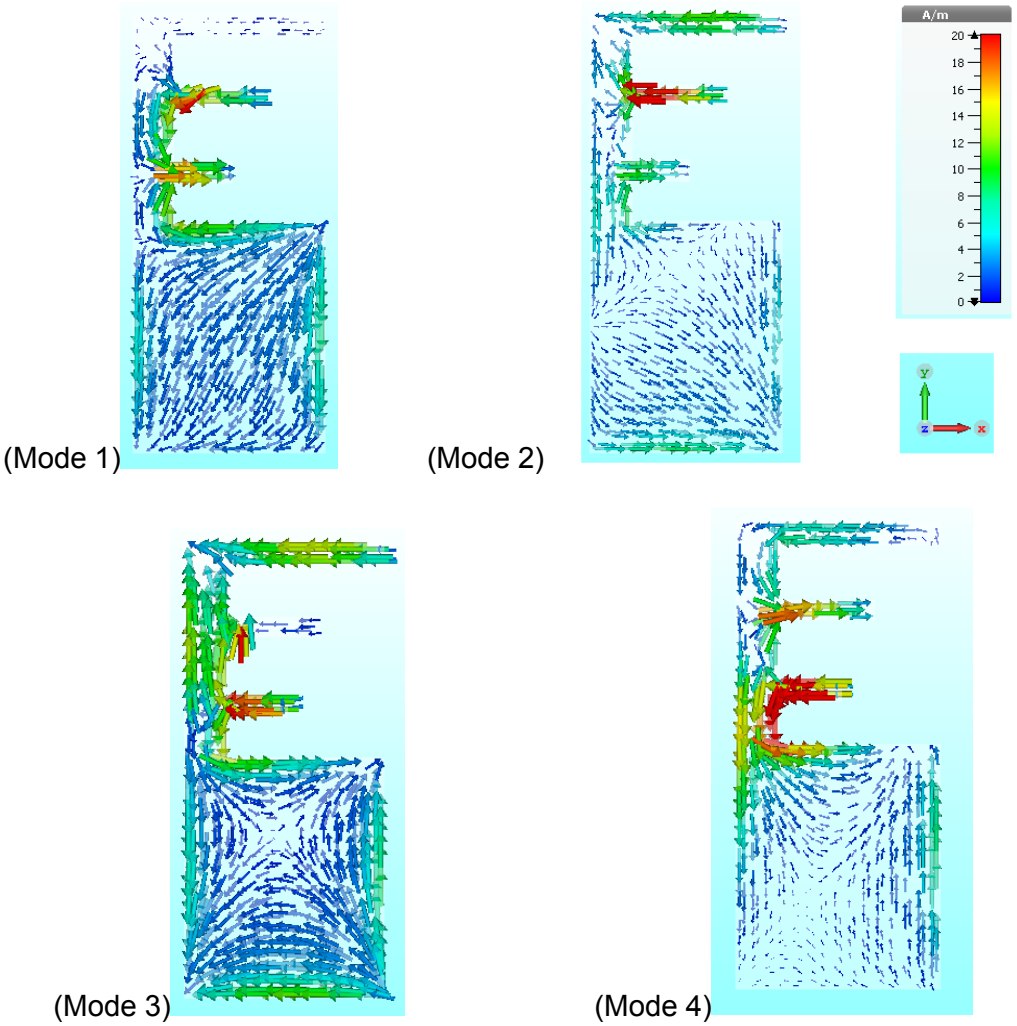

Figure 4-42. *Surface current distributions simulation results at 2.6 GHz for the four dominant modes of Figure 4-41*

Figure 4-43 shows the surface current of the driven model (with excitation) simulated on both ADS (frequency domain solver) and CST (time domain solver), they show a very good agreement. The response of the excitation driven antenna is a combination of all these weighted set of orthogonal modes at 2.6 GHz. It seems that the results are a combination between mode 1 and 4.

Adding the 2.6 GHz arm creates a third resonant path. Simulation results showed that the new resonant path is indeed forming three-quarter wavelength current distribution: (1) one-quarter wavelength current distribution starting from the feed point to the third horizontal strip (2.6 GHz arm) open end (h3 + L3); and (2) two-quarter wavelength starting from the third horizontal strip (2.6 GHz arm) open end to the second horizontal strip (1.8 GHz arm) open end (L3 + h2 + L2).

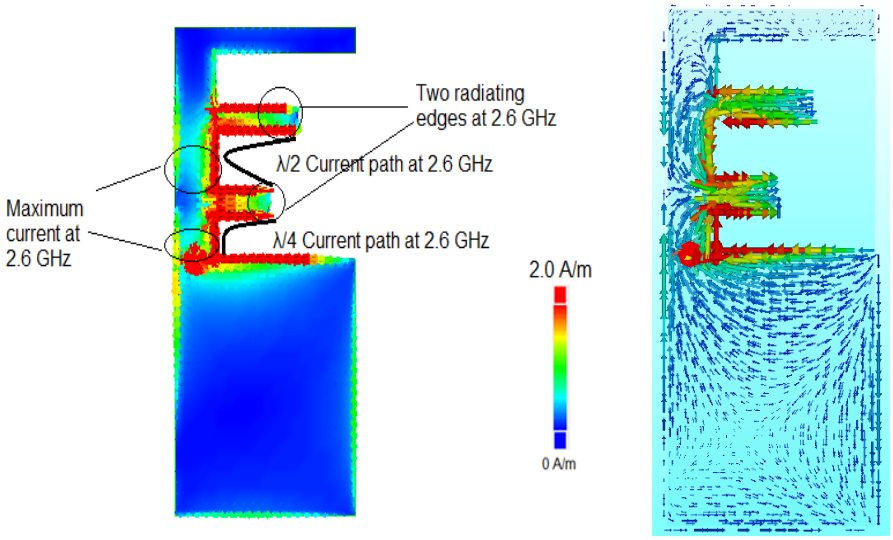

Figure 4-43. *Surface current distributions simulation results at 2.6 GHz. ADS (frequency domain solver) on left and CST (time domain solver) on right*

Different simulations have been done to prove that the new resonant path is indeed forming three-quarter wavelength current distribution not only one-quarter wavelength. First, shifting the 2.6 GHz arm down by 3 mm (h3 = 7 mm) decreases the length from feed point to the 2.6 GHz arm open end while increasing the two-quarter wavelength length from the 2.6 GHz arm open end to the 1.8 GHz arm open end. Simulation results showed that the resonance of the 2.6 GHz band has increased by 60 MHz. in addition, input impedance decreased noticeably. Second, decreasing the length of the 1.8 GHz arm by 3 mm (L2 = 20 mm) will decrease the length of the two-quarter wavelength current path. Simulation results showed that the resonance of the 2.6 GHz band has increased by 55 MHz. Third, decreasing the length of the third horizontal strip by 3 mm (L3 = 12 mm) affects both current paths. Simulation results showed that the resonance of the 2.6 GHz band has increased by 250 MHz.

CMA MS simulation results of these three cases and other cases show that the potential BW increase as the length (h3 + L3) approaches one-quarter wavelength current distribution (starting from the feed point to the third horizontal strip open end); and the length (L3 + h2 + L2) approaches two-quarter wavelength (starting from the 2.6 GHz arm open end to the 1.8 GHz arm open end). This result will be utilized to optimize the final versions.

This current distribution form two radiating edges and two points of maximum current as shown in Figure 4-43. Other simulation results showed that they are acting as explained in the trumpet structure and in the 1.8 GHz sections. These results will be used to optimize the final versions.

The simulated radiation pattern at 2.6 GHz showed a monopole-like radiation pattern in the E-plane (y-z plane) and the H-plane (x-z plane) as showed in Figure 4-45 and Figure 4-45 (where the antenna is oriented in the x-y plane). Simulation results showed a maximum gain of 4.15 dBi with directivity of 4.65 dBi and efficiency of 89%.

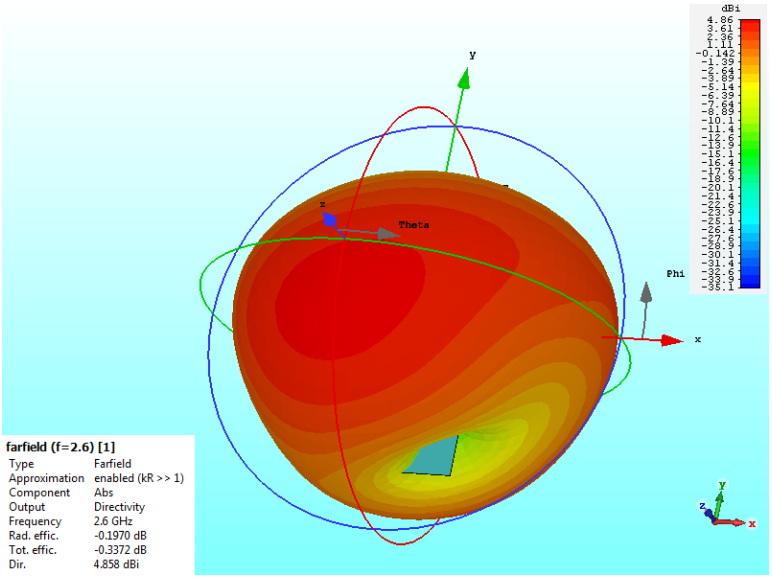

Figure 4-44. *Simulated 3D radiation pattern of the antenna in Figure 4-40 at 2.6 GHz*

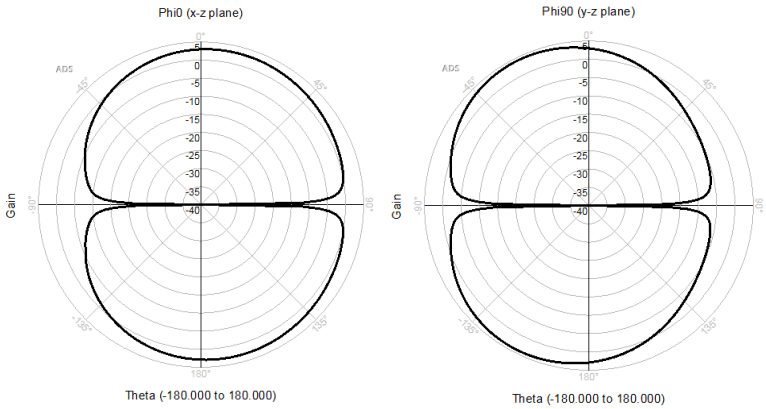

Figure 4-45. *Simulated radiation pattern polar plot of the antenna in Figure 4-40 at 2.6 GHz*

Notice that the angle of maximum radiation is tilted by 27° from z-axis. This is happening as the response of the excitation driven antenna is a combination of all these weighted set of orthogonal modes at 2.6 GHz, mainly modes 1 and 4 are excited. The radiation pattern of mode 1 (at 2.6 GHz) has one lobe nicely centred around z-axis. On the other hand, the radiation pattern of mode 4 (at 2.6 GHz) has 2 lobes with end-fire radiation. Thus, the results are a combination of the radiation pattern of each mode.

5. RESULTS AND DISCUSSION

In this chapter, we discuss three final versions that have been developed based on the ideas of the previous chapter. For the second final version, we show how CMA has been utilized to fix radiation pattern of the 2.6 GHz band. Final versions V1 and V2 antennas have been constructed with screen printing technology and copper tape. Final version V3 antenna has been designed to enhance the measured results of the second final version V2.

5.1 Version V1

Figure 5-1 shows the first final version V1. It has been developed based on the ideas of the simulation chapter. A small segment of 50Ω (W=250 with dielectric constant 11) Microstrip line has been added to the model as it is needed for the final circuit. Exciting the antenna through a 50 Ω microstrip feedline should not affect the return loss results noticeably as the antenna is matched to 50 Ω. In addition, ink and substrate have very small losses; so, they have not added noticeable losses to the return loss simulation results. However, it changes the phase of the input impedance which rotates it on smith chart according to the electrical length of the line at each frequency [26]. A small circle has been cut from the GND plane for the SMA connector for testing the results. Many changes have been introduced on the dimensions of the three-band antenna of Figure 4-40. The aim of these changes is to achieve a better compensated result that all the bands meet the specifications.

First, the ground plane length G_L has been increased from 60 to 65 mm. As discussed in the simulation chapter, matching and input impedance enhanced by increasing G_L (mainly for the 800 MHz band). In addition, directivity and gain increased for all bands as a result of increasing the ground plane length G_L. The direction of peak gain at 2.6 GHz for this V1 antenna was not perpendicular to the antenna-GND plane, as will be discussed later. Increasing the GND length helps to fix the radiation pattern at 2.6 GHz.

Second, the antenna height h has been increased from 54 to 56 mm. As explained in the "L-shape monopole arm" sub-chapter, decreasing the antenna height results in size reduction but matching and BW degraded at the 800 MHz band. By increasing the antenna height h from 54 to 56 mm the matching, BW, and radiation pattern parameters of the 800 MHz band have enhanced. In addition, increasing the antenna height h from 54 to

56 mm increases two-quarter wavelength current distribution at the 1.8 GHz band. Therefore, the BW of the 1.8 GHz has enhanced.

As discussed in the simulation chapter, the current distribution at the 1.8 and 2.6 GHz is forming two radiating edges and two points of maximum current (as shown in Figure 4-36 and Figure 4-43) at each band. they are acting as explained in the trumpet structure section. Increasing the width at the radiating edges increases the effective length and decreases the resonance frequency. On the other hand, Increasing the width at the feed point increasing the resonance frequency and affect input impedance. Thus, thirdly, the antenna widths AW1 = 11 mm, AW2 = 10 mm, and AW3 = 13 mm have been changed to alter the points of maximum current. The width AW3 has been increased from 11 mm to 13 mm to decrease the two-quarter wavelength current distribution at the 1.8 GHz band. This increases the resonance frequency at 1.8 GHz, and the 1.8 GHz arm length has to be increased to bring the resonance frequency back to 1.8 GHz. Although this decreases the BW at the 1.8 GHz, it enhances the BW results at the 2.6 GHz band (which was not good) as it increases the two-quarter wavelength current distribution at the 2.6 GHz band. Same idea for the width AW2, which has been decreases from 11 to 10 mm which increases the two-quarter wavelength current distribution at the 2.6 GHz band. Consequently, the BW and matching of the 2.6 GHz band enhanced.

Fourth, a small square has been added to the open end of the 1.8 GHz arm. This increases the width at the radiating edges of both the 1.8 and 2.6 GHz. This increases the effective length of the 1.8 GHz arm. which increases the two-quarter wavelength current distribution at the 2.6 GHz band. Consequently, the BW and matching of the 2.6 GHz band enhanced. It did not affect the 1.8 GHz band as the dimensions of the square is still small compare with wavelength at 1.8 GHz.

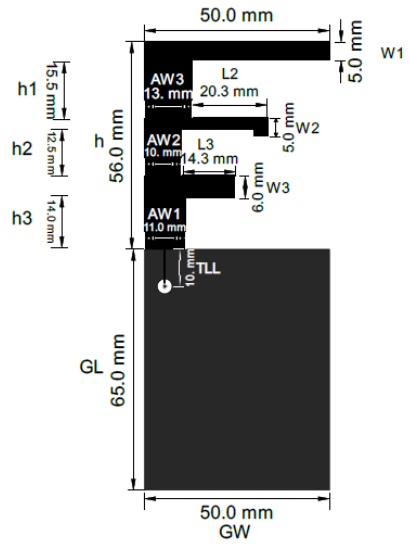

Figure 5-1. *Layout of three-band final version antenna V1*

Figure 5-2 shows the simulated return loss of the first final version V1 (these results have been obtained with ADS frequency domain solver). Results show -10 dB return loss bandwidth of more than 115 MHz at all bands, which is more than required.

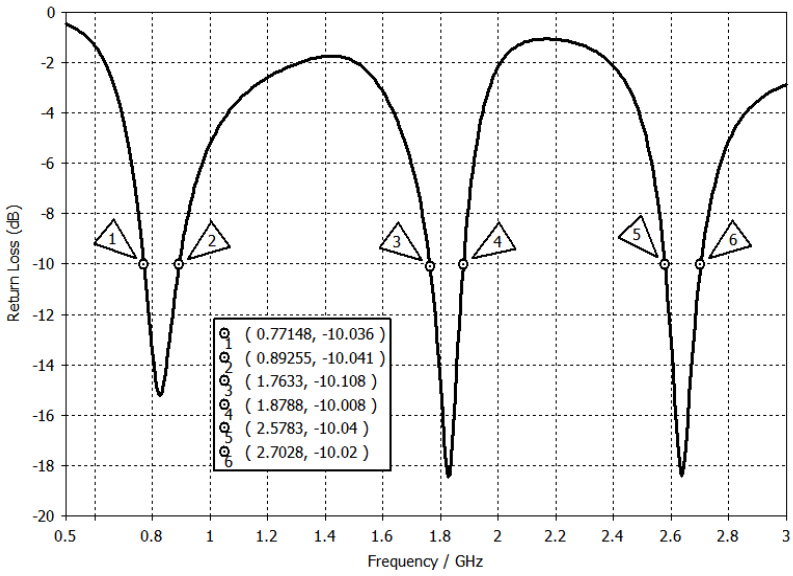

Figure 5-2. *Simulated return loss of final version V1*

Table 5-1 summarizes the simulation results of the V1 antenna which fulfils the specifications with overall size (with the ground plane) of 121 * 50 mm. Simulation results in Figure 5-3 shows a total efficiency of more than 95 % at the three bands. The maximum gain results were 2, 4.2 and 5.1 dBi at the 0.8, 1.8 and 2.6 GHz bands respectively.

Table 5-1. *Final version V1 antenna simulation results summery.*

Band (GHz)	-10 dB Bandwidth (MHz)	Radiation Pattern	Gain (dBi)	Gain Bandwidth
0,8	130	Omnidirectional pattern over whole bandwidth of the 3 bands	2,0	Gain is stable over the 3 bands
1,8	115		4,2	
2,6	125		5,0	

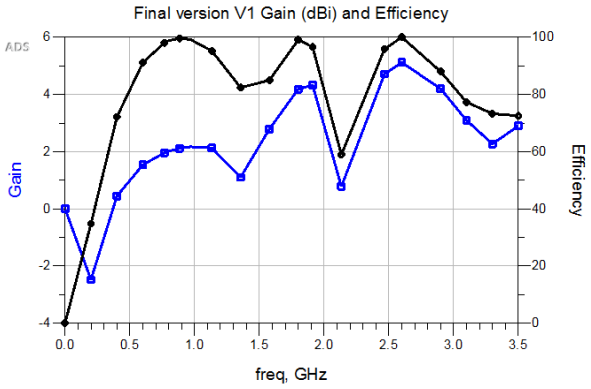

Figure 5-3. *Gain and efficiency ADS simulation results of V1 antenna*

As shown in Table 5-1, results showed a monopole-like radiation pattern for all the band. However, the main disadvantage of this design is that the direction of peak gain at 2.6 GHz was not perpendicular to the antenna-GND plane--it was tilted by 17° as shown in Figure 5-4. The 2.6 GHz has high directivity; so, being 17° tilted is quite significant.

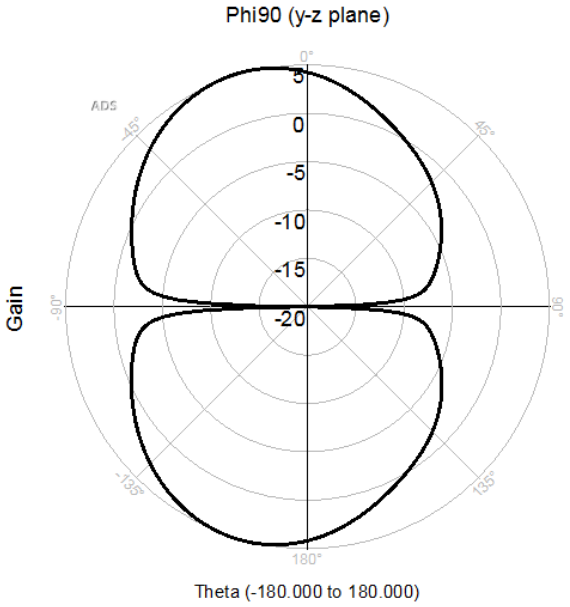

Figure 5-4. *Simulated radiation pattern polar plot Phi=90° (y-z plane) of V1 antenna at 2.6 GHz*

The CMA simulation results of this antenna V1 is like the antenna introduced in the 4.8 subchapter. Although there are some changes in the antenna dimensions and the ground plane length, but the structure and the working principle are same. Figure 5-5 shows the CMA modal significance simulation results (of the antenna V1) for the most four significant modes at 2.6 GHz. All the four modes have high modal significance value which means that they may all affect the 2.6 GHz band results. The CMA simulated surface current of each of the four modes at 2.6 GHz were like the results in Figure 4-42.

The simulated surface current of this final version antenna V1 driven model (with excitation) simulated on ADS show that the response is a combination of all these weighted set of orthogonal modes at 2.6 GHz. Due to our excitation setup, it seems that the result is mainly a combination between mode 1 and 4 (which have surface current similar to Figure 4-42). The radiation pattern of mode 1 (at 2.6 GHz) has one lobe nicely centred around z-axis. On the other hand, the radiation pattern of mode 4 (at 2.6 GHz) has 2 lobes with end-fire radiation. Thus, the results are a combination of the radiation pattern of both modes.

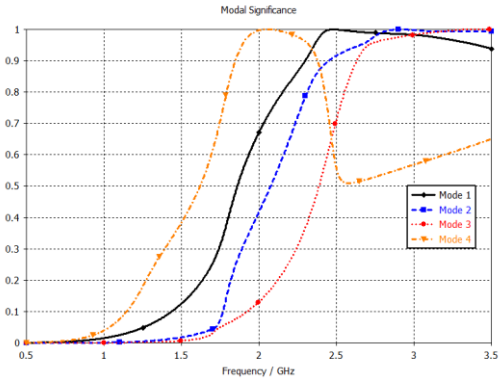

Figure 5-5. *CMA MS simulation results of V1 antenna for the most four significant modes around 2.6 GHz*

Antennas have been constructed with copper tape and screen printing as shown in Figure 5-6. SMA connector is used for testing the results. The SMA connector outer conductor is connected to the ground plane, while the inner conductor is exciting the antenna through the 50 Ω microstrip feedline. Conductive glue is used to connect the SMA connector to the antenna and the ground plane.

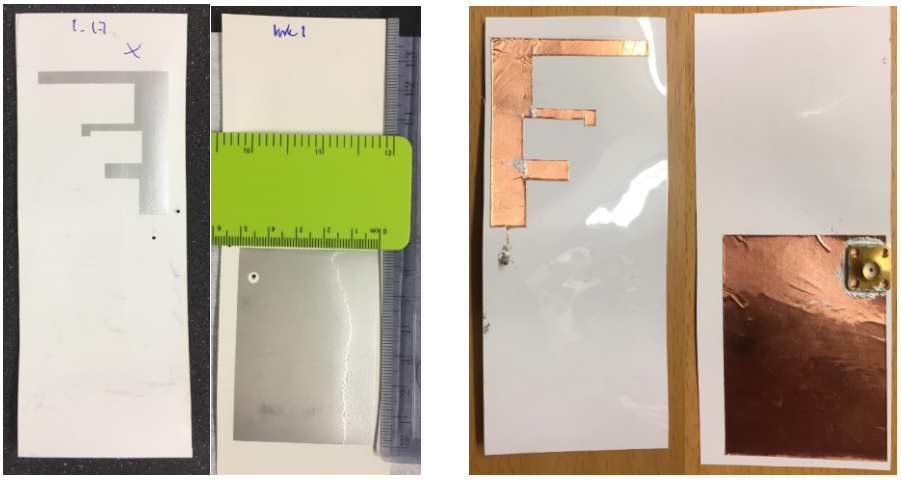

Figure 5-6. *V1 antenna constructed with screen printing technology and copper tape*

Figure 5-7 shows the measured return loss of the constructed antennas (measured with VNA) against ADS simulation results. Both constructed antennas with ink and copper tape seems to match each other. Both constructed antennas keep the overall characteristics of the simulated ones with triple-band operation at 800 MHz, 1.8 GHz and 2.5 GHz.

The measured results at the 800 MHz band are similar to the simulated one with slight decrease in the BW. The 1.8 GHz measured results show a significant decrease in the return loss from -18 dB of the simulated results to around -7 dB in the measured results. the resonance frequency of the higher band has shifted down from 2.6 GHz to 2.5 GHz with some reduction in the return loss and BW.

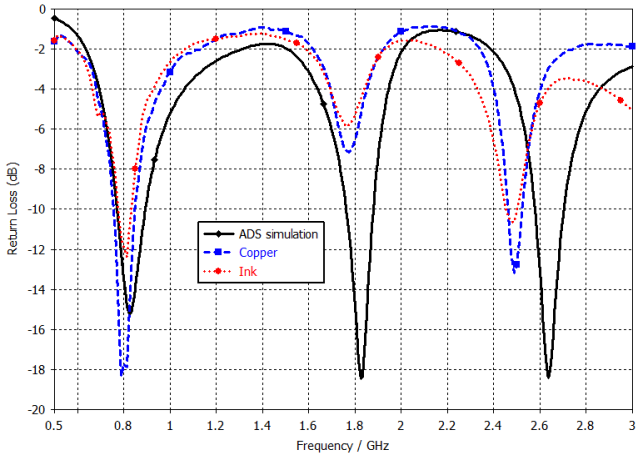

Figure 5-7. *Measured return loss of the constructed V1 antenna against ADS frequency domain simulation results*

As mention before, unfortunately CST simulator has been used at late stage of this thesis work after order the screens for antenna printing. Figure 5-8 shows the measured return loss of the constructed antennas (measured with VNA) against the CST time domain solver simulation results. The CST (time domain solver) results seems more realistic than the ADS (frequency domain solver) and approach the measured results. Similar to ADS, the measured results at the 800 MHz band are similar to the CST simulated one with slight decrease in the BW. The 1.8 GHz CST simulated return loss is degraded from the ADS results. However, the 1.8 GHz measured results are still far from the CST results. the CST simulation results show that the resonance frequency of the higher band should shift down from 2.6 GHz to 2.5 GHz which match the measured results. However, there is a noticeable decrease in the BW of the higher band.

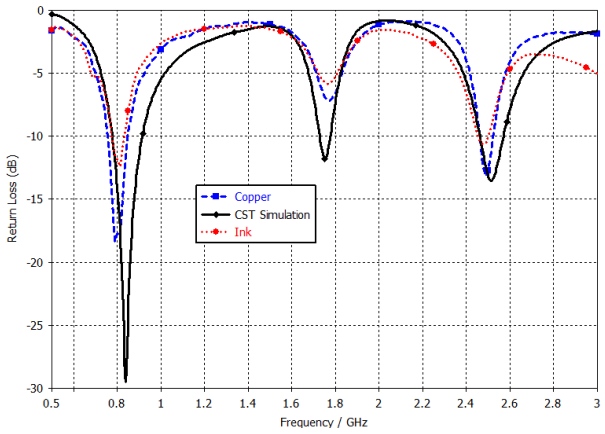

Figure 5-8. *Measured return loss of the constructed V1 antenna against CST time domain simulation results*

This deviation of the measured results could be regarded to many reasons. More discussion and analysis of the results will be discussed in results analysis subchapter after showing the results of the final version V2 antenna.

5.2 Version V2

The main disadvantage of antenna V1 design of the previous sub-chapter is that the direction of maximum radiation at 2.6 GHz was not perpendicular to the antenna-GND plane, it was tilted by 17°. The 2.6 GHz has high directivity (5 dB); so, being 17° tilted is quite significant.

Many ways have been examined in order to try to suppress the undesired mode (mode 4 in Figure 5-5) at the 2.6 GHz to fix its radiation pattern. This has been done by optimizing the antenna dimensional configuration to get the desired results.

The simulated surface current of this final version antenna V1 driven model (with excitation) simulated on ADS shows that the response is a combination of all these weighted set of orthogonal modes at 2.6 GHz. Due to our excitation setup, it seems that the result is mainly a combination between mode 1 and 4 (which have surface current similar to Figure 4-42). The radiation pattern of mode 1 (at 2.6 GHz) has one lobe nicely centred around z-axis. On the other hand, the radiation pattern of mode 4 (at 2.6 GHz) has 2 lobes with end-fire radiation. Thus, the results are a combination of the radiation pattern of each mode.

The undesired mode 4 is resonating at around 2.2 GHz with high modal significance at 2.6 GHz. The idea was to shift its resonance frequency down, so it is not significant at 2.6 GHz. This can be done by increasing its current path length. As shown in Figure 4-42 of the CMA simulated surface current of each of the four modes at 2.6 GHz, current distribution over the ground plane is more confine to the edges with much higher value of current density. In [37], they showed that the radiation pattern of the higher band can improver by cutting four slots from the ground plane which increase the effective current path of the ground plane. Thus, one of the ideas was to introduce a narrow slit in the ground plane which increase the current path length and shift the resonance frequency of mode 4 down. This idea may affect the resonance frequency of the other modes and it would have been better to think about tuning this mode independently of the other modes. However, this was not possible without CMA study.

Figure 5-9 shows the second final version V2 with narrow slit in the ground plan. Some minor changes have been introduced on the dimensions of the final version antenna V1 of Figure 5-1. The aim of these changes is to achieve a better compensated result that all the bands meet the specifications (more discussion about the antenna dimensions will come later after discussing the impact of the ground plane slit).

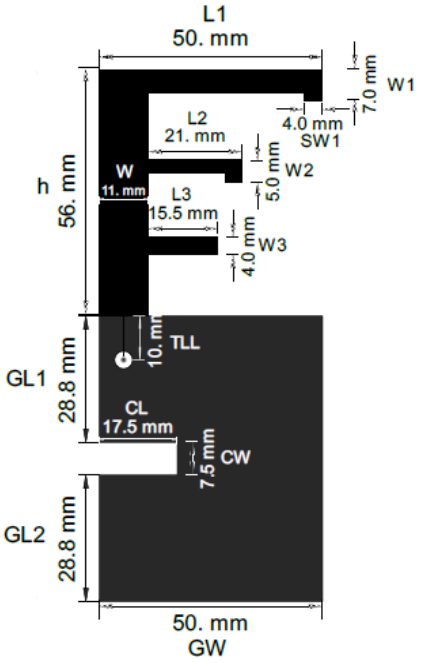

Figure 5-9. *Layout of three-band final version antenna V2*

Figure 5-10 and Figure 5-11 show the CMA modal significance simulation results of this second final version antenna V2 for the most four significant modes at 2.6 GHz without and with the ground plane slit respectively. Results show that we have successfully shifted the resonance frequency of the undesired mode 4 down to around 2 GHz. Resonance frequency of the dominant mode 1 has not been affected noticeably by introducing the ground plane slit. In addition, the resonance frequency of the higher modes 2 and 3 seems to be not affected by the introducing the ground plane slit.

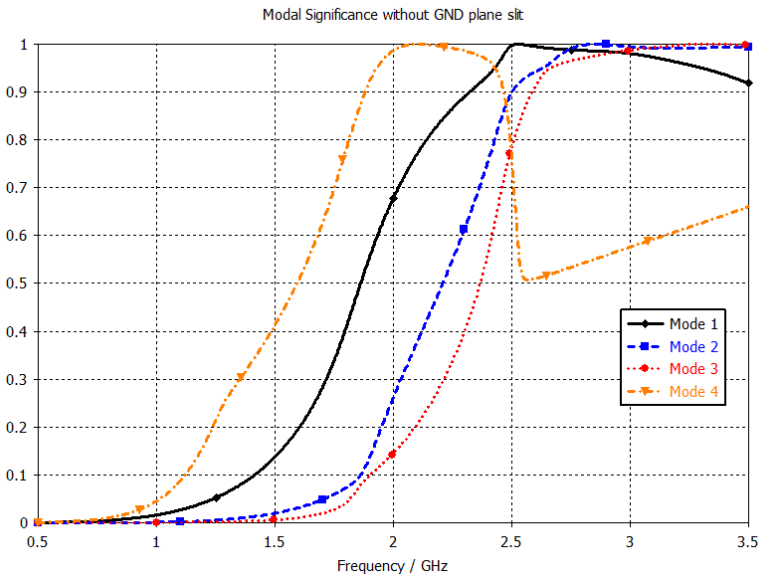

Figure 5-10. *CMA MS simulation results of V2 antenna without ground plane slit for the most four significant modes around 2.6 GHz*

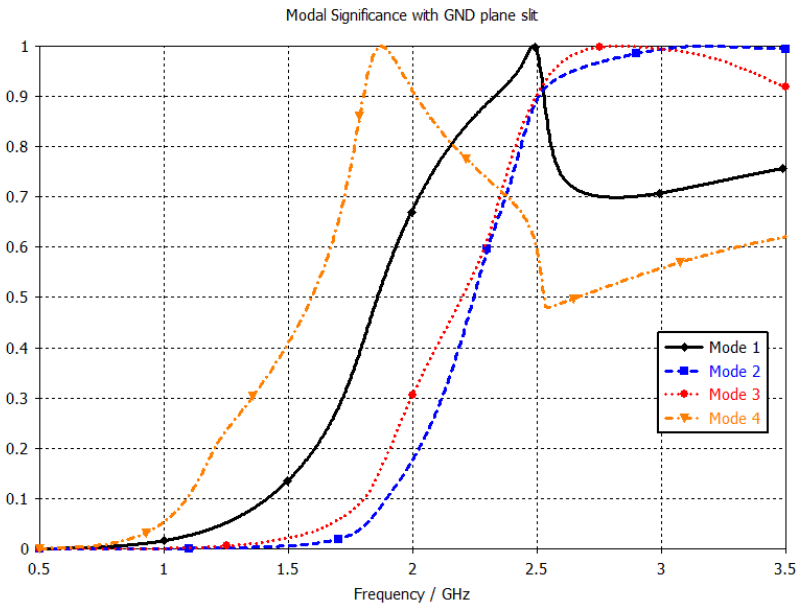

Figure 5-11. *CMA MS simulation results of V2 antenna with ground plane slit for the most four significant modes around 2.6 GHz*

The CMA simulated surface current of each of the four modes at 2.6 GHz suggested that mode 2 should be partially suppressed as it have less current at the feed which results in high input impedance for this mode. This is a good result as the radiation pattern of mode 2 (at 2.6 GHz) has 2 lobes with end-fire radiation which is not desired. On the other hand, the CMA simulated surface current suggested that after introducing the ground plane slit, our excitation setup should support mode 3 as it has maximum current at the feed point (notice that mode 3 before the ground plane slit had less current at the feed point). This is again a very good results as the radiation pattern of mode 3 (at 2.6 GHz) has one lobe nicely centred around z-axis which should support mode 1.

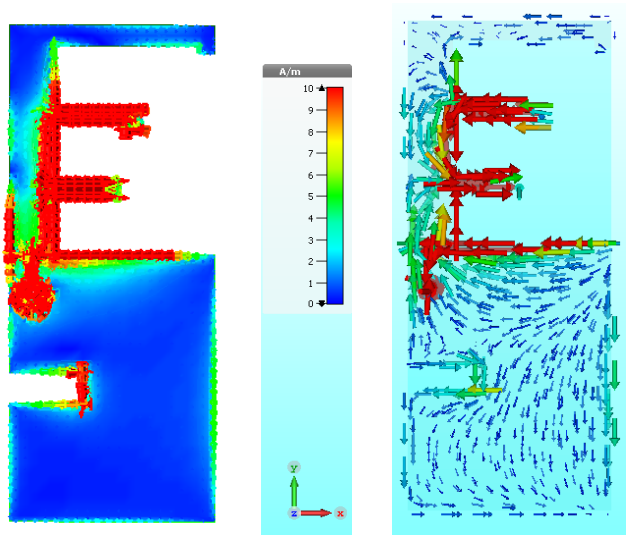

Figure 5-12. *Surface current distributions simulation results of V2 antenna at 2.6 GHz. ADS (frequency domain solver) on left and CST (time domain solver) on right*

Figure 5-12 shows the surface current of the driven model (with excitation) simulated on ADS (frequency domain solver) and CST (time domain solver) at 2.6 GHz, they show a very good agreement. The response of the excitation driven antenna V2 is a combination of all these weighted set of orthogonal modes at 2.6 GHz, mainly modes 1 and 3.

Thus, introducing the ground plane slit has successfully decreased the resonance frequency of the undesired mode 4, and strengthened the significance of the desired mode 3 while unaffecting the dominant mode 1. Consequently, Figure 5-13 shows that the direction of peak gain at 2.6 GHz of V2 antenna is fixed and more perpendicular to the antenna-GND plane compared with the results of V1 antenna in Figure 5-4.

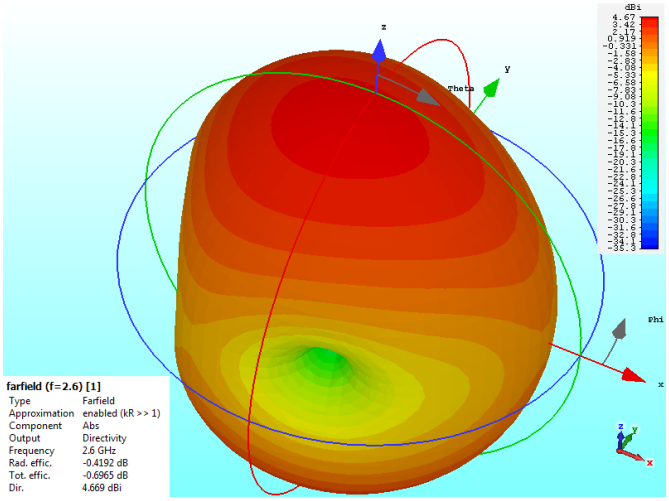

Figure 5-13. *Simulated 3D radiation pattern of V2 antenna at 2.6 GHz*

The main disadvantage of introducing the ground plane slit is that the low frequency mode 4 of the CMA results at 2.6 GHz is shifted down to around 2 GHz which may affect the 1.8 GHz band. Figure 5-14 shows the CMA modal significance simulation results of antenna V2 for the most three significant modes at 1.8 GHz. Results show that there are two significant modes around the 1.8 GHz band. The original dominant mode (which was there before the ground plane slit) resonance frequency has decreased to around 1.55 GHz after introducing the ground plane slit. In addition, the low frequency mode 4 of the CMA results at 2.6 GHz is shifted down to around 2 GHz. When CMA simulation is run at 1.8 GHz, this mode is sorted as the second significant mode and called mode 2 as shown in Figure 5-14. It seems that the resonance mode of the 800 MHz affects at 1.8 GHz but with lower significance.

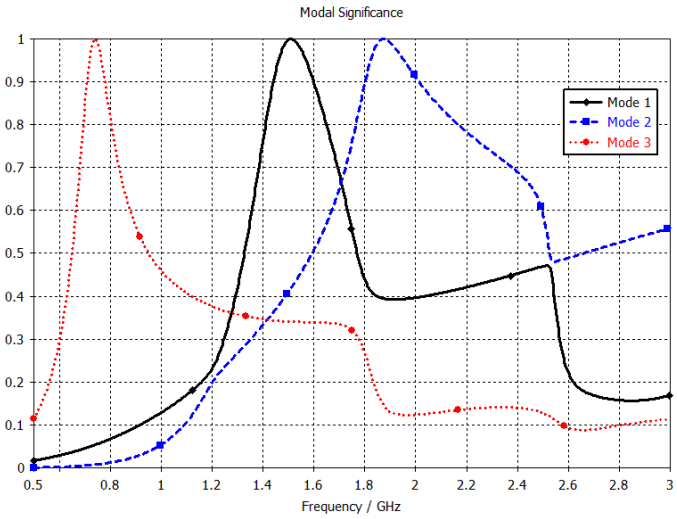

Figure 5-14. *CMA MS simulation results of V2 antenna for the most three significant modes around 1.8 GHz*

The CMA simulated surface current of each of the two modes at 1.8 GHz suggested that our excitation setup should support both modes as they have maximum current at the feed point. Both modes have similar surface current distribution on the antenna; however, their surface current distribution over the ground plane are different. Simulation results showed that the BW of the 1.8 GHz band has been decreased by introducing the ground plane slit. Simulation results showed that the resonance frequency of mode 2 decrease as the slit length (dimension CL in Figure 5-9) increase and the 1.8 GHz band BW decrease also. Thus, the slit length CL has been optimized to be 17.5 mm to achieve a compensation between fixing the radiation pattern of the 2.6 GHz and not to affect the BW of 1.8 GHz much.

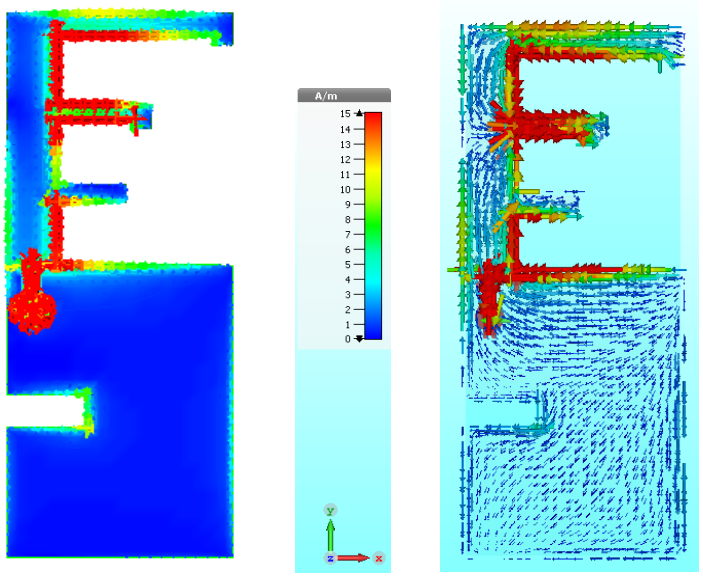

Figure 5-15. *Surface current distributions simulation results of V2 antenna at 1.8 GHz. ADS (frequency domain solver) on left and CST (time domain solver) on right*

Figure 5-15 shows the surface current of the driven model (with excitation) simulated on ADS (frequency domain solver) and CST (time domain solver) at 1.8 GHz, they show a very good agreement. The response of the excitation driven antenna V2 is a combination of all these weighted set of orthogonal modes at 1.8 GHz, mainly modes 1 and 2.

The simulated radiation pattern at 1.8 GHz showed a monopole-like radiation pattern in the E-plane (y-z plane) and the H-plane (x-z plane) as showed in Figure 5-16 (where the antenna is oriented in the x-y plane). Simulation results showed a maximum gain of 3.8 dBi with directivity of 4 dBi and radiation efficiency of 94%.

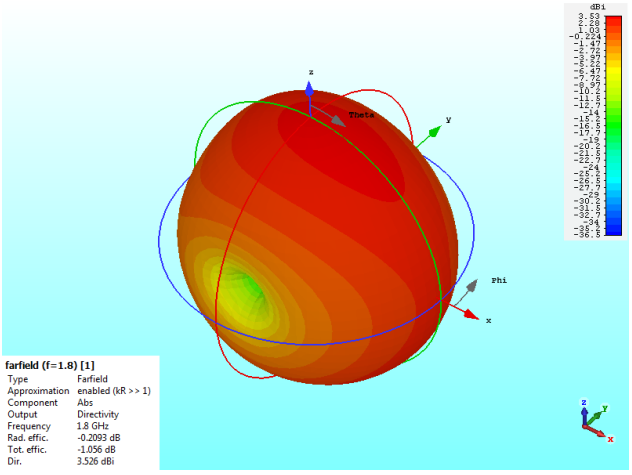

Figure 5-16. *Simulated 3D radiation pattern of V2 antenna at 1.8 GHz*

Results of the 800 MHz band have not been affected noticeably by introducing the ground plane slit. Figure 5-17 shows the surface current of the driven model (with excitation) simulated on ADS (frequency domain solver) and CST (time domain solver) at 800 MHz, they show a very good agreement. The response of the excitation driven antenna V2 at 800 MHz is mainly controlled by the single dominant mode.

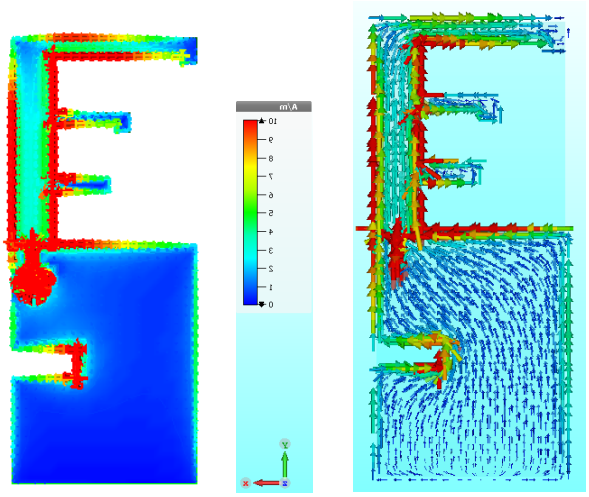

Figure 5-17. *Surface current distributions simulation results of V2 antenna at 800 MHz. ADS (frequency domain solver) on left and CST (time domain solver) on right*

The simulated radiation pattern at 800 MHz showed a monopole-like radiation pattern in the E-plane (y-z plane) and the H-plane (x-z plane) as showed in Figure 5-18 (where the antenna is oriented in the x-y plane). Simulation results showed a maximum gain of 2 dBi with directivity of 2.1 dBi and radiation efficiency of 98.7 %.

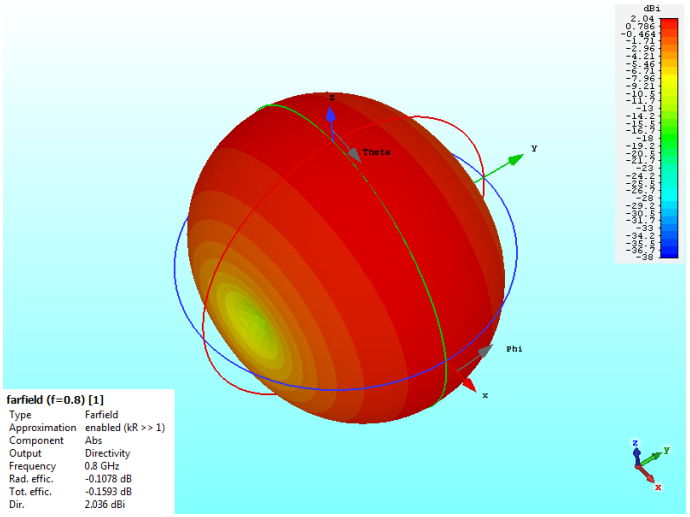

Figure 5-18. *Simulated 3D radiation pattern of V2 antenna at 800 MHz*

Thus, Introducing the ground plane slit has successfully fixed the radiation pattern of the 2.6 GHz band but, on the other hand, decreased the BW of the 1.8 GHz band. Therefore, some changes have been introduced on the dimensions of the antenna V1 of Figure 5-1 to achieve a better compensated result; that is, all the bands meet the specifications.

In antenna V1 the antenna widths (AW1 = 11 mm, AW2 = 10 mm, and AW3 = 13 mm in Figure 5-1) have been changed to alter the points maximum current. The aim of this changes was to increase the BW at the 2.6 GHz on the expense of the 1.8 GHz band. So, there was no need for these modification in this V2 antenna as the BW of the 1.8 GHz band has been decreased by introducing the ground plane slit. The antenna width W has same value 11 mm in this V2 antenna.

Second, a small square has been added to the open end of the 800 MHz arm. This increases the width at the radiating edges of both the 0.8 and 1.8 GHz. This increases the effective length of the 800 GHz arm. which increases the two-quarter wavelength current distribution at the 1.8 GHz band. Consequently, the BW and matching of the 1.8 GHz band enhanced. It did not affect the 0.8 GHz band as the dimensions of the square is still small compare with wavelength at 0.8 GHz.

Figure 5-19 shows the simulated return loss of the second final version V2 (these results have been obtained with ADS frequency domain solver). Results show -10 dB return loss bandwidth of more than 100 MHz at all the band, which meets the specifications.

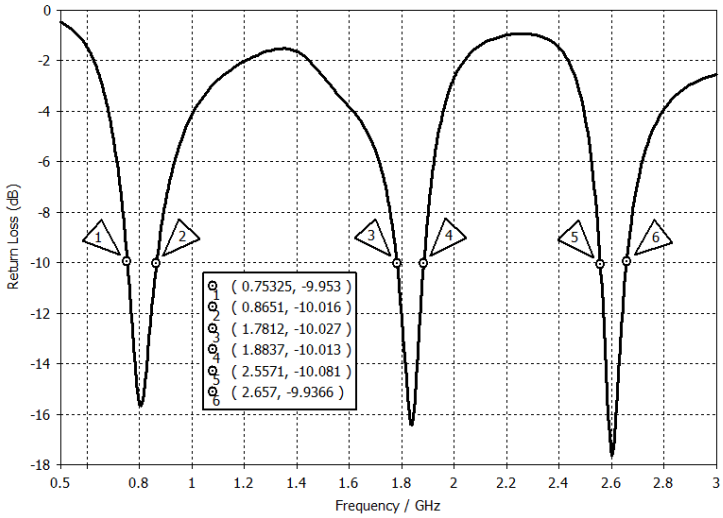

Figure 5-19. *ADS simulated return loss of final version V2*

Table 5-2 summarize the simulation results of the V2 antenna which fulfil the specifications with overall size (with the ground plane) of 121 * 50 mm. Simulation results in Figure 5-20 showed total efficiency of more than 90 % at all bands. Maximum gain results were 2, 3.8 and 5 dBi at the 0.8, 1.8 and 2.6 GHz bands respectively.

Table 5-2. *ADS simulation results of the V2 antenna*

Band (GHz)	-10 dB Bandwidth (MHz)	Radiation Pattern	Gain (dBi)	Gain Bandwidth
0,8	112	Omnidirectional pattern over whole bandwidth of the 3 bands	2,0	Gain is stable over the 3 bands
1,8	107		3.8	
2,6	100		5,0	

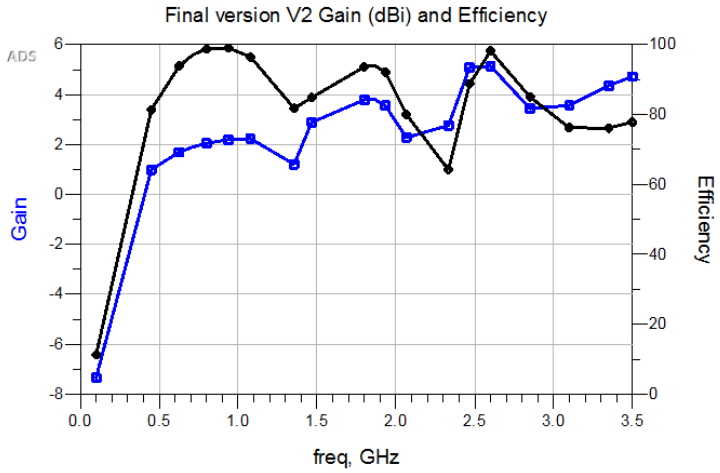

Figure 5-20. *Gain and efficiency ADS simulation results of V2 antenna*

Antennas have been constructed with copper tape and screen printing as shown in Figure 5-21. Three different types of ink have been used to construct the antenna screen printing. SMA connector is used for testing the results. The SMA connector outer conductor is connected to the ground plane, while the inner conductor is exciting the antenna through the 50 Ω microstrip feedline. For the ink versions, conductive glue is used to connect the SMA connector to antennas and the ground plane. Conventional soldering is used to connect SMA connector to copper tape version of this V2 antenna.

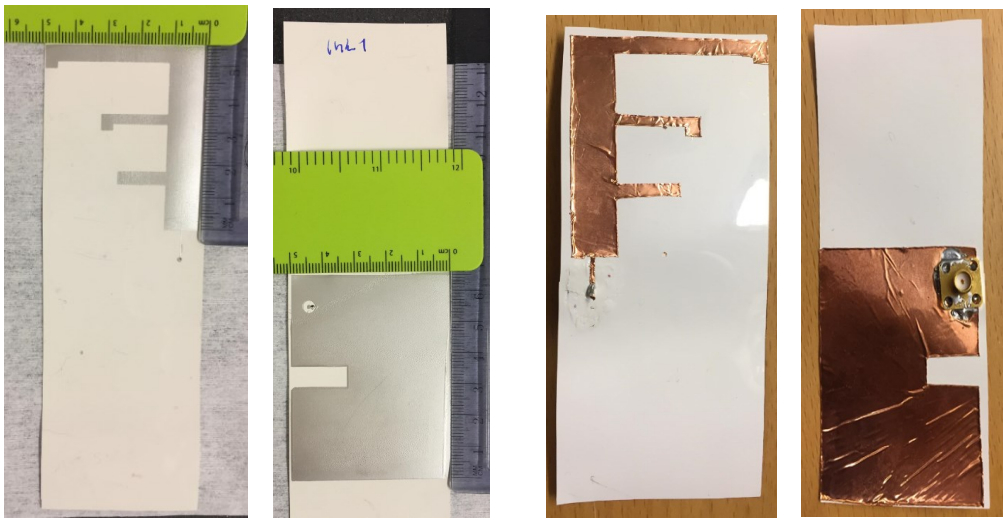

Figure 5-21. *V2 antenna constructed with screen printing and copper tape*

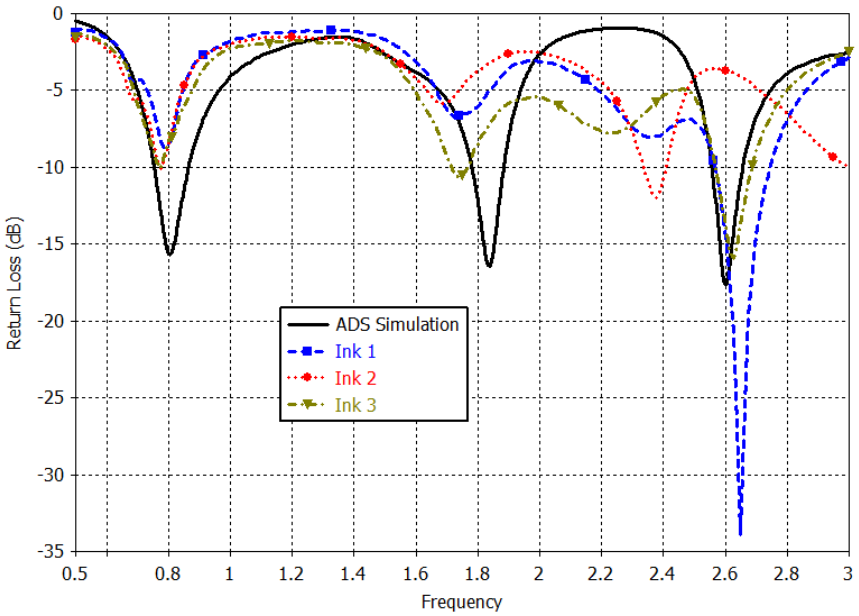

Figure 5-22. *Measured return loss of the screen printed V2 antenna against ADS frequency domain simulation results*

Figure 5-22 shows the measured return loss of the constructed antennas with ink 1, 2, and 3 (measured with VNA) against ADS simulation results. All the ink constructed antennas keep the overall characteristics of the simulated ones with triple-band operation.

The measured results of the three antennas show a noticeable decrease in return loss and BW at the lower band (800 MHz). There is a slight shift in the resonance frequency of the mid-band (1.8 GHz). Ink 3 antenna measured results show better return loss results at the mid-band. The resonance frequency of the higher band (2.6 Ghz) is shifted down to 2.4 GHz with ink 2 antenna. On the other hand, ink 1 and 3 antennas showed very good results at the higher band.

Ink 3 antenna showed the best measured results of the printed antenna. Figure 5-23 shows the measured return loss of the constructed antennas with ink 3 and copper tape (measured with VNA) against ADS (frequency domain solver). The copper tape antenna measured results show very good agreement with the ADS (frequency domain solver) at the lower and higher bands, 0.8 and 2.6 GHz. However, the copper tape antenna measured results at the 1.8 GHz show that the return loss results are degraded from the ADS results -17 dB to around -10 dB with copper tape antenna. These results agree with the ink 3 antenna measured results at the 1.8 GHz mid-band.

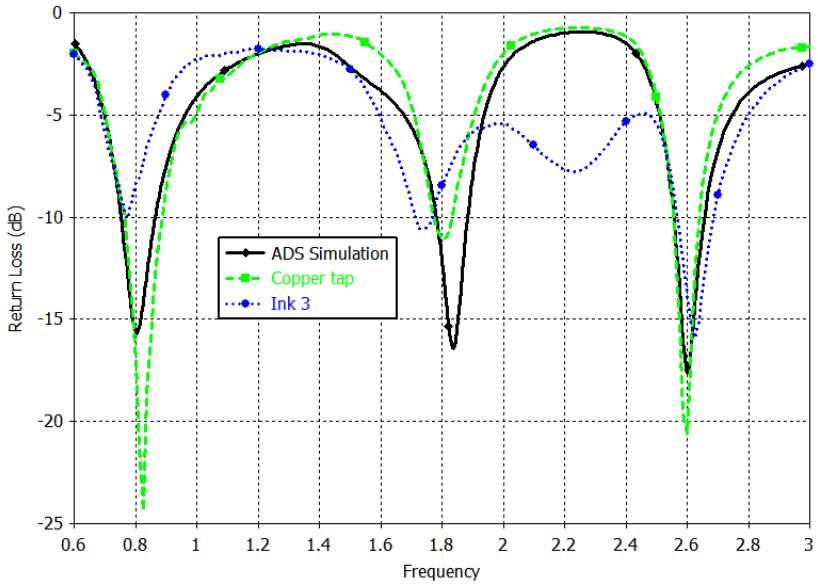

Figure 5-23. *Measured return loss of the constructed V2 antenna with ink 3 and copper tape against ADS frequency domain simulation results*

Figure 5-24 shows the simulated input impedance results of CST (time domain solver) against ADS (frequency domain solver). The simulation results of the CST (time domain solver) showed a very good agreements with the ADS (frequency domain solver) at the lower and higher bands 0.8 and 2.6 GHz respectively. However, CST results showed that the input impedance of the mid-band (1.8 GHz) has decreased much and its circle on smith chart is much smaller. Therefore, the return loss results are degraded from the ADS results -17 dB to around -10 dB.

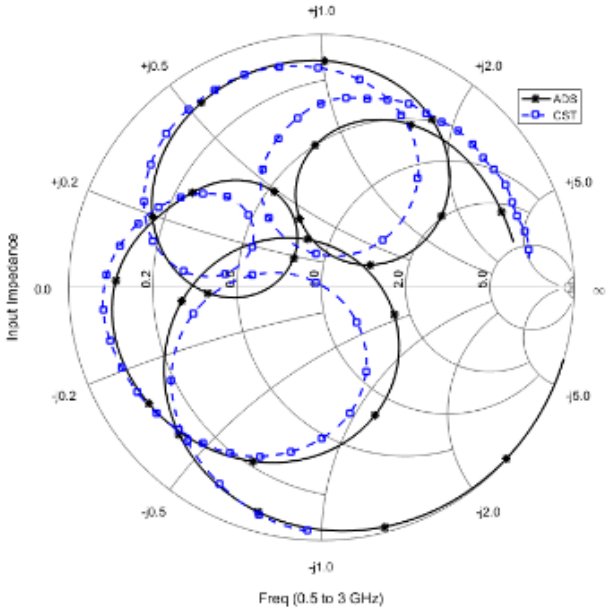

Figure 5-24. *Simulated input impedance results of CST (time domain solver) against ADS (frequency domain solver)*

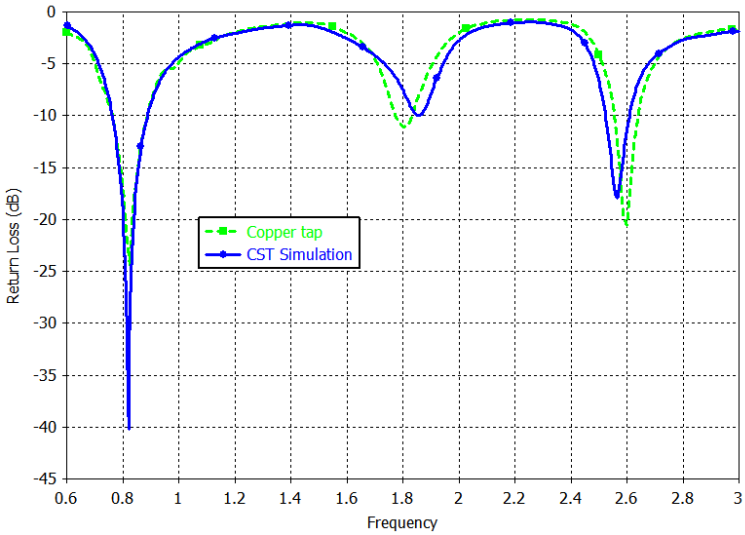

Figure 5-25. *Measured return loss of the copper tape V2 antenna with against CST time domain solver simulation results*

Thus, the CST (time domain solver) simulation results explains the degradation of the 1.8 GHz return loss of the copper tape antenna. Figure 5-25 shows a very good agreement between copper tape antenna measured results with the CST (time domain solver) simulation results at all the bands. The copper tape antenna measured results show also good agreement with the ADS (frequency domain solver) except for the mid-band (which is clear after having the CST results).

Figure 5-26 shows the smith chart input impedance of the copper tape antenna measured results against the CST (time domain solver) simulation results. The actual electrical

length of the copper tape transmission line is decreased from the simulation. Therefore, the measured input impedance did not rotate on smith chart as the stimulated one. This happens due to the existence of a thin layer of adhesive (30 micron) under the copper tape. This layer increases the overall thickness of the substrate and decrease its electrical length. It also affects the line characteristic impedance but the width increase compensates (as the width increase to around 0.5 mm); therefore, the line is still matched around 50 Ω. Notice that with almost all the ink antennas, the transmission lines were too narrow to connect the SMA connector to the antenna. We had to fix the lines by increasing their width manually with some ink. Therefore, the ink line characteristic impedance decreases much which affected the results.

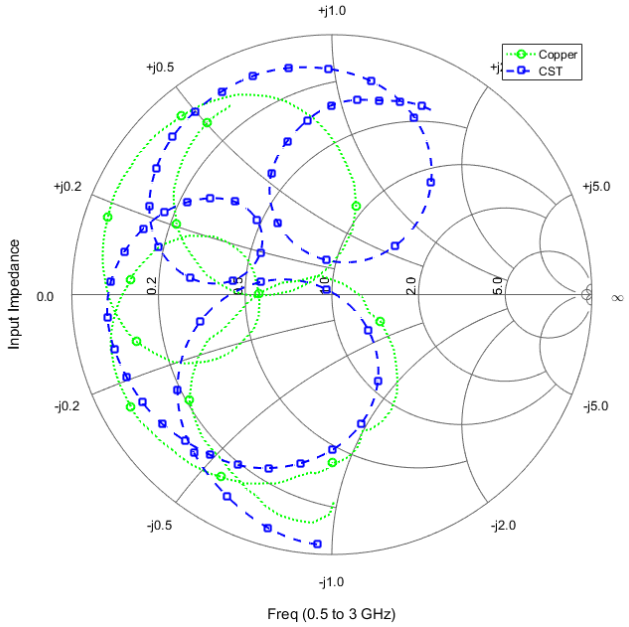

Figure 5-26. *Measured input impedance of the copper tape V2 antenna against CST time domain solver simulation results*

Figure 5-27 shows the measured efficiency of the constructed antennas with ink 3 and copper tape (measured with VNA) against ADS (frequency domain solver) and CST (time domain solver) simulation results. Simulated efficiency on CST (time domain solver) is calculated only at the three frequency of interest due to long simulation time. Simulated radiation efficiency on ADS and CST matches each other. However, due to the degraded return loss value on CST at the middle (1.8 GHz) and higher (2.6 GHz) bands, the simulated total efficiency is degraded. Both constructed antennas with ink 3 and copper tape keep the overall characteristics of the simulated ones with triple-band operation at 800 MHz, 1.8 GHz and 2.6 GHz. The copper tape antenna measured efficiency can be considered as a very good result. It agrees with the CST simulated results at the three bands. The ink 3 antenna measured efficiency is degraded from the copper tape results due to

the degradation in the return loss results. However, both antennas show a very good practical results which can be enhanced in further work.

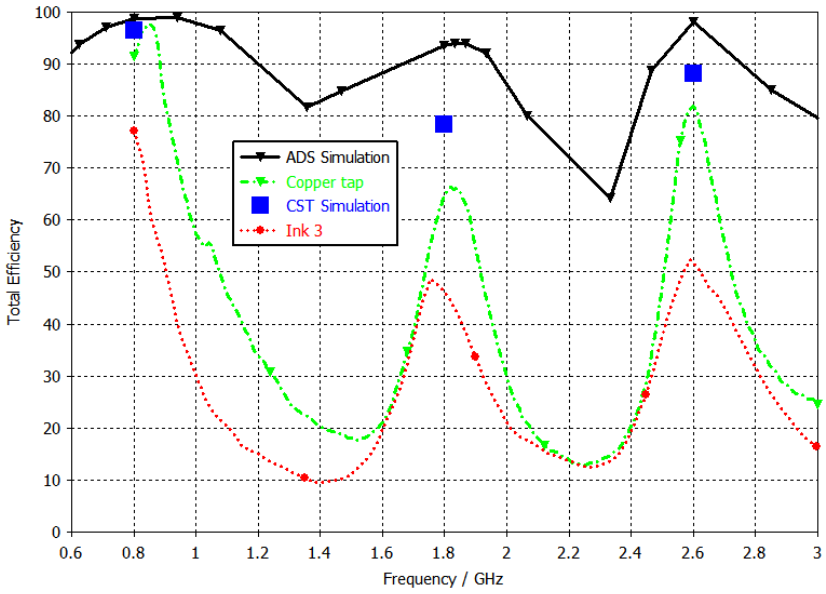

Figure 5-27. *Measured efficiency of the constructed V2 antenna with ink 3 and copper tape against ADS frequency domain simulation results*

Figure 5-28-Figure 5-29 show the measured 3D radiation pattern of the constructed V2 antennas with ink 3 and copper tape at 800 MHz. The measured results at 1.8 GHz and 2.6 GHz are available in Appendix 1. These measurements have been done using the Satimo antenna measurements anechoic chamber at Tampere university.

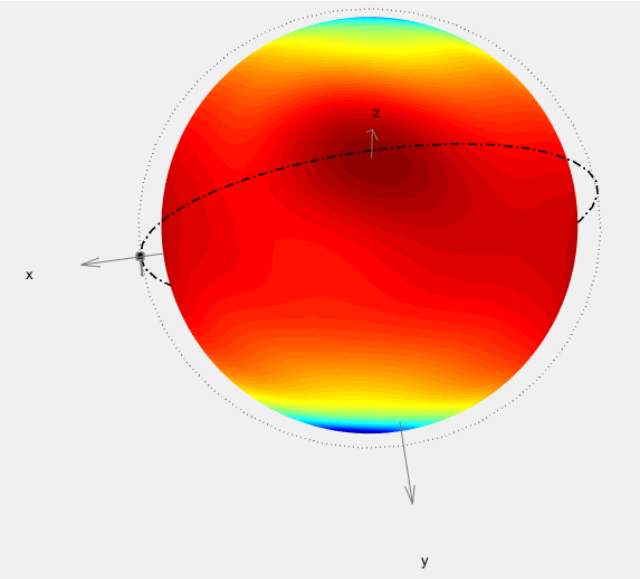

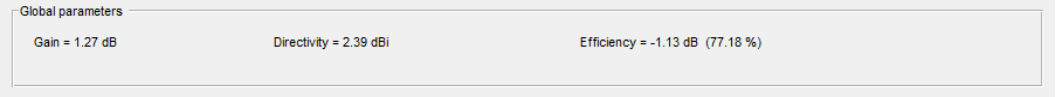

Figure 5-28 *Constructed ink 3 antenna V2 measured 3D radiation pattern at 800 MHz (measured by Satimo antenna anechoic chambers at Tampere university)*

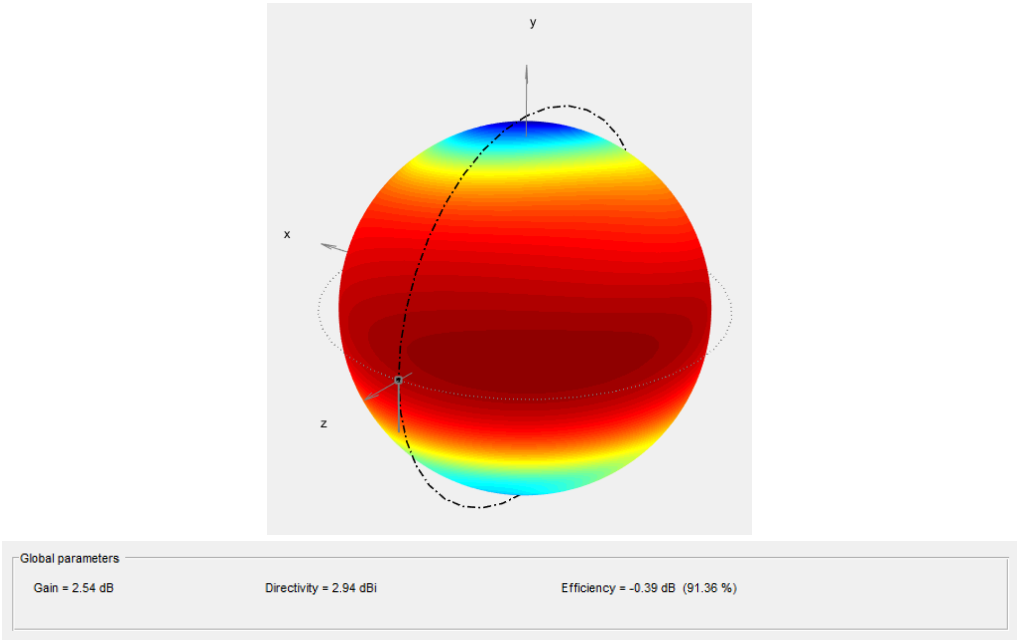

Figure 5-29. *Constructed copper tape antenna V2 measured 3D radiation pattern at 800 MHz (measured by Satimo antenna anechoic chambers at Tampere university*

Considering a 100 MHz of bandwidth at each band, Table 5-3 summarizes the main characteristics of the ink 3, and copper tape antennas measured results vs the ADS (frequency domain solver), and CST (time domain solver) simulation results.

Table 5-3. *Final version V2 antenna simulation vs measured results summery.*

Band (GHz)	Type	Max Gain (dBi)	100 MHz BW maximum return loss (dB)	100 MHz BW minimum total efficiency (%)
0,8	ADS	2,0	-10	97
	CST	1.87	-12	96
	Ink 3	1.27	-7	65
	Copper tape	2.54	-12	88
1,8	ADS	3.8	-10	91
	CST	2.47	-7	78
	Ink 3	1.31	-6	42
	Copper tape	2.14	-8	60
2,6	ADS	5,0	-10	95
	CST	4.1	-9	88
	Ink 3	3.48	-10.5	46
	Copper tape	4.38	--9.5	69

5.3 Version V3

The frequency domain solver is a good choice for strongly resonant structures because these are marked by long settling times of the time domain signals [10]. Figure 5-30 shows the areas of optimal operation for the different solvers [10].

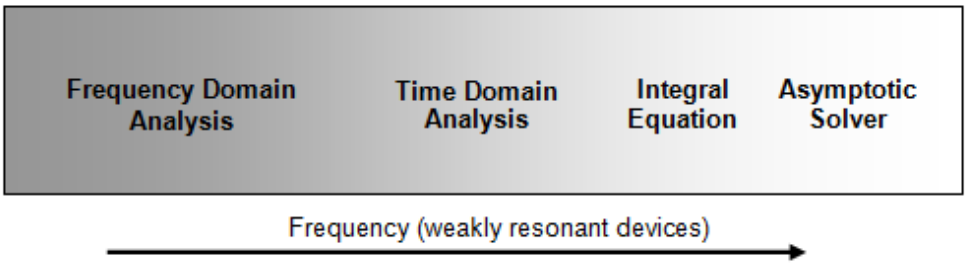

Figure 5-30. *Areas of optimal operation for the different solvers [10]*

The results of V1 and V2 antenna showed that the frequency domain solver ADS simulation results match the measured results at the lower band 800 MHz. This is probably because there is a clear single dominant mode at this lower band. On the other hand, measured results of V1 antenna showed that the resonance frequency of the higher band has shifted down to 2.4 GHz. This is probably due to the existence of four significant modes at the higher frequency band; thus, the frequency domain solver ADS simulation results were not accurate at that band. The results of V2 antenna, after adding the slit in ground plan, showed good agreement between the frequency domain solver ADS simulation results and measured results.

The resonance frequency of the mid-band 1.8 GHz of V1 showed good agreement between the frequency domain solver ADS simulation results and measured results. Although the return loss is degraded but this can be easily solved by utilizing the ideas of the simulation chapter 4. Figure 5-31 shows the third final version V3. This version has very few modifications from the dimensions of the final version V2 in Figure 5-9. First, the antenna width has been decreased from 11 mm to 6 mm. As mentioned in subchapter 4.2, increasing the antenna width makes circles on smith chart bigger which is desired for all bands as shown in the smith chart result of Figure 5-26. Second, the total antenna height decreased from 56 mm in antenna V2 to 54 mm in V3 which adjust the resonance frequency of the 800 MHz band (it decreased after decreasing the width to 6 mm) and enhanced its input impedance. Third, the 1.8 GHz arm has been shifted down by 4.5 mm (from 32.5 mm to 28 mm) which makes the circle bigger on smith chart and enhances the input impedance of the 1.8 GHz band. Fourth, the 2.6 GHz arm has been shifted down by 2 mm (from 14 mm to 12 mm) which makes the circle bigger on smith chart and enhances the input impedance of the 2.6 GHz band.

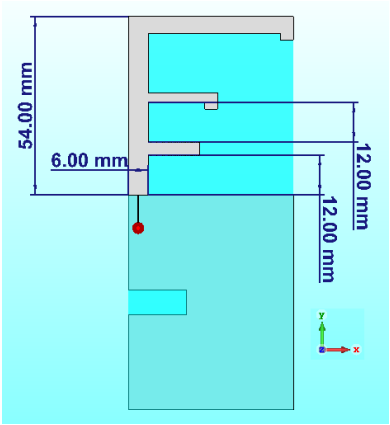

Figure 5-31. *Layout of three-band final version antenna V3*

Figure 5-32 shows the simulated return loss of the third final version V3 with CST time domain solver. Results show -10 dB return loss bandwidth of around 100 MHz at all the band, which meets the specifications.

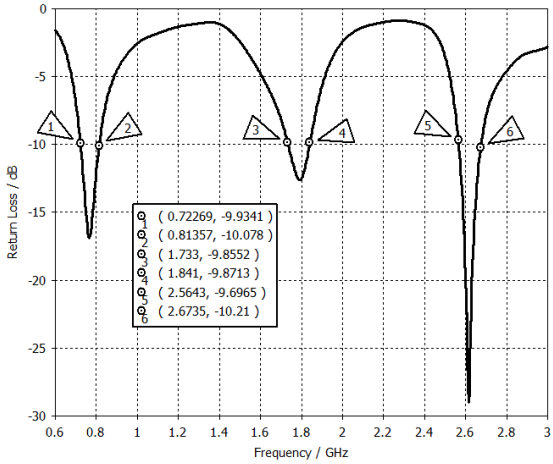

Figure 5-32. *CST time domain solver simulation results of V3 antenna*

Figure 5-33 shows CST time domain solver simulated total efficiency with noticeable enhancement at the 1.8 and 2.6 GHz bands (compared with the results of V2 antenna in Figure 5-27) due to enhancing the input impedance.

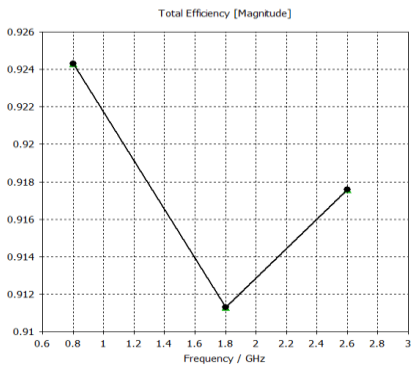

Figure 5-33. *CST time domain solver simulated total efficiency of V3 antenna*

5.4 Analysis of results

The deviation of the measured results could also be regarded to many other reasons. It could be due to the inaccuracies in the fabrication procces of the antenna. It should be noted that the constructed antennas are far from ideal. This could affect the dimensions of the constructed antennas and therefore the results. In addition, it turned out that the width of the 50 Ω microstrip feedline W = 250 μm was too narrow for screen printing technology. In most of the printed antennas, the microstrip feedline did not connect the SMA connector to the antenna. We had to fix microstrip feedline manually, which increased its width. For the copper tape version, the width of the line was around 500 μm. In both cases, increasing the line width will decrease its characteristic impedance from 50 Ω.

Three different types of ink were used to print the antennas. Table 5-4 shows different measurements of the sheet resistance of printed samples with different inks. The small number of ink 3 results is due to the significant surface roughness, which prevented measurement of some samples. All results of ink 3 are from one sample.

Table 5-4. *Measurements of the sheet resistance of printed samples with different inks.*

Ink name	Different measurements of sheet resistances (mΩ/square)	Mean value (mΩ/square)	Calculated conductivity (S/m)
1	30, 32, 37, 43, 41, 21, 20, 20, 16	29	3.5e6
2	77, 112, 212, 173, 134, 107, 167, 131, 146, 174	143	7e5
3	11, 16, 20, 17	16	6.25e6

These measurements were done at late stage of this thesis work after designing and constructing the antennas. The value of conductivity that has been used for simulating the antennas during the design phase was σ = 5e6 S/m. The mean value of the measured sheet resistance is around 120 mΩ/square. This means that the conductivity of the ink is around six times lower than the value used in the simulation (σ = 5e6 S/m), which increases the losses and affects the results. As mentioned, conductive glue is used to connect the SMA connector to the antenna and the ground plane. The conductivity of the glue is not well known which could also affect the results.

In addition, it turned out that the way we connect the VNA cable to the antenna may affect the results. This can be easily tested by touching the VNA cable and check if the measured results change. In our case, the results changed by touching the VNA cable. This happens as there is high coupling between the VNA cable and the antenna. Figure 5-34 shows the evaluation board of the comercial Fractus TRIO mXTENDTM chip antenna copied from its user manual [13]. They use a RF 50 Ω test probe; therefore, they can route the cable in the way that minimizes the coupling between the antenna and the test instrument cable (VNA or Satimo test device) [13].

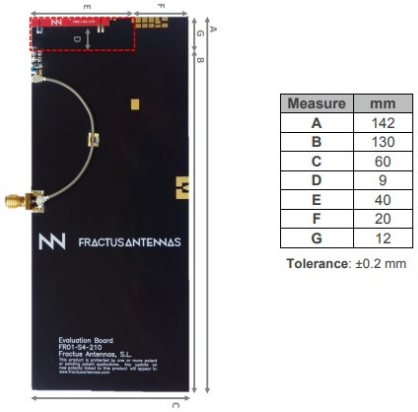

Measure	mm
A	142
B	130
C	60
D	9
E	40
F	20
G	12

Tolerance: ±0.2 mm

Figure 5-34. *Evaluation board of the commercial Fractus TRIO mXTENDTM chip antenna with RF test probe routed to minimize coupling [13]*

Finally, Figure 5-35 shows the simulated radiation efficiency of V2 antennas (where the substrate thickness is 0.275 mm) against another three-band antenna simulated on the same substrate material but with 1 mm thickness. The dimensions of other antenna (with thickness 1 mm) have been optimized to cover the same bands (0.8, 1.8, 2.6 GHz). Results show that radiation efficiency increases as the substrate thickness decreases. This could be a result of decreasing the antenna input capacitance (which agrees with our simulation results and the results reported in [38]). Consequently, the storing reactive power decreases. This could be considered as a good result as decreasing the substrate thickness increases the antenna flexibility.

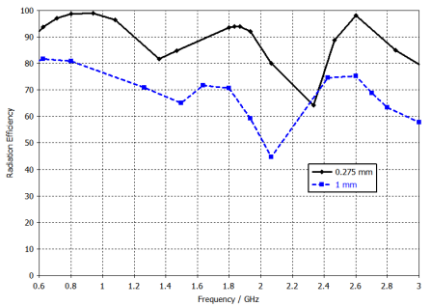

Figure 5-35. *ADS simulated radiation efficiency of V2 antenna with substrate thickness 0.275 mm against another optimized antenna with substrate thickness 1 mm*

6. CONCLUSIONS

Three-band operations of a novel compact printed monopole antenna with letter F–like shape have been demonstrated. The step-by-step analysis on how various geometrical features affect the antenna results allowed for a better understanding of the working principle of the proposed antenna. We have supported the ideas with both ADS (frequency domain solver) and CST (time domain solver) simulation results. The characteristic mode analysis CMA simulation results supported the results that we achieved through the hard optimization way. Also, it has explained and introduced many ideas to enhance the results.

We were able to design the first three-band final version antenna V1 and showed its working principle through the driven model and CMA simulation results. The main disadvantage of antenna V1 is that the direction of maximum radiation at 2.6 GHz was not perpendicular to the antenna-GND plane. Simulation and measured results showed that introducing the ground plane slit in the second final version antenna V2 has successfully fixed the radiation pattern of the 2.6 GHz band with minor impact on the bandwidth of the 1.8 GHz. The direction of peak gain at the 2.6 GHz of V2 antenna was fixed and became more perpendicular to the antenna-GND plane compared with the results of V1 antenna.

Both constructed antennas with ink and copper tape showed the overall characteristics of the simulated ones with triple-band operation at 800 MHz, 1.8 GHz and 2.6 GHz. The copper tape antenna showed a 100 MHz bandwidth with minimum measured total efficiency of 88, 60, 69 % at the 0.8, 1.8, 2.6 GHz respectively. The ink antenna showed a 100 MHz bandwidth with minimum measured total efficiency of 65, 42, 46 % at the 0.8, 1.8, 2.6 GHz respectively. The copper tape antenna measured efficiency can be considered as a very good result. It agrees with the simulated results at the three bands. The ink antenna measured efficiency is degraded from the copper tape results due to the degradation in the return loss results. However, both antennas show a very good practical results which can be enhanced in further work.

Simulation results showed that there is no single design parameter that tune only one frequency band. However, the step-by-step analysis on how various geometrical features affect the antenna results beside the characteristic mode analysis CMA simulation results allow for a systematic antenna design approach. We were able to develop V3

antenna with few modifications to enhance the return loss results of V2 antenna. Simulated return loss of the third final version V3 with CST time domain solver show -10 dB return loss bandwidth of around 100 MHz with minimum total efficiency of 90% at all the band.

Unfortunately, we were not able to experimentally study the flexibility attribute of the proposed antenna. As mentioned, it turned out that the width of the 50 Ω microstrip feedline W = 250 μm was too narrow for screen printing technology. In most of the printed antennas, the printed microstrip feedline did not connect the SMA connector to the antenna and we had to fix it manually which increased its width. For furthur versions, different feeding techniques (for example coplanar waveguide CPW feed) would be considered.

Although introducing the ground plane slit in the second final version antenna V2 has successfully fixed the radiation pattern of the 2.6 GHz band, it has decreased the bandwidth of the 1.8 GHz. For furthur versions, the characteristic mode analysis CMA would suggest different ideas to fixed the radiation pattern of the 2.6 GHz band without decreasing the bandwidth of the 1.8 GHz. Finally, an RF 50 Ω test probe is strongly recommended to be used for measurements purposes. The probe can be routed in the way that minimizes coupling between the antenna and the test instrument cable (VNA or Satimo test device). Consequently, the test instrument cable does not affect the measured results.

REFERENCES

[1] Abutarboush HF, Shamim A. Paper-based inkjet-printed tri-band U-slot monopole antenna for wireless applications. IEEE Antennas and Wireless Propagation Letters. 2012;11:1234-1237.

[2] Antenna Analysis and Design with Characteristic Mode Analysis, CST STUDIO SUITE, website, 2017. Available (accessed on 01.09.2019): https://www.cst.com

[3] Antenna Measurement Software EMQuest™ EMQ100 User's Manual, ETS-Lindgren, software, 2006. Available (accessed on 01.06.2019): http://www.ETS-Lindgren.com

[4] Balanis CA. Antenna theory: Analysis and design. Fourth ed. Hoboken, New Jersey: Wiley; 2015.

[5] Biegeleisen JI(I, 1910. The complete book of silk screen printing production. New York: Dover Publications; 1963.

[6] Cabedo-Fabres M, Antonino-Daviu E, Valero-Nogueira A, Bataller MF. The theory of characteristic modes revisited: A contribution to the design of antennas for modern applications. IEEE Antennas and Propagation Magazine. 2007;49(5):52-68.

[7] Chakravarthy S S, Sarveshwaran N, Sasi V, Sriharini S, Shanmugapriya M. A four-band antenna for wireless applications. 2016 IEEE Indian Antenna Week (IAW 2016). 2016:11-16.

[8] Chen H, Chen J, Cheng Y. Modified inverted-L monopole antenna for 2.4/5 GHZ dual-band operations. Electron Lett. 2003;39(22):1567-1569.

[9] Chen I-, Peng C. Microstrip-fed dual-U-shaped printed monopole antenna for dual-band wireless communication applications. Electron Lett. 2003;39(13):955-956.

[10] CST STUDIO SUITE 2018 help documentation, CST STUDIO SUITE, software, 2017. Available (accessed on 01.06.2019): https://www.cst.com

[11] DOBKIN, D. M. The RF in RFID : Passive UHF RFID in Practice. Amsterdam: Newnes, 2008.

[12] E. ANDY, The Anechoic Chamber Guide for EMC and RF (Wireless) Testing, website. Available (accessed on 15.09.2019): https://emcfastpass.com/anechoic-chamber-guide/

[13] Fractus TRIO mXTENDTM chip antenna user manual, Fractus Antennas, 2018. Available: https://www.fractusantennas.com/files/UM_FR01-S4-210.pdf

[14] Garbacz R, Turpin R. A generalized expansion for radiated and scattered fields. IEEE Transactions on Antennas and Propagation. 1971;19(3):348-358.

[15] Harrington R, Mautz J. Theory of characteristic modes for conducting bodies. IEEE Transactions on Antennas and Propagation. 1971;19(5):622-628.

[16] IEEE standard test procedures for antennas. ANSI/IEEE Std 149-1979. 1979:0_1.

[17] Jiwei H, Weiping D. A novel printed monopole antenna for dual-band WLAN application. 2009 International Conference on Wireless Communications & Signal Processing. 2009:1-3.

[18] Khaleel HR, Al-Rizzo HM, Rucker DG. Compact polyimide-based antennas for flexible displays. Journal of Display Technology. 2012;8(2):91-97.

[19] Kumar G, Ray KP. Broadband microstrip antennas. Boston: Artech House; 2002.

[20] Kuo Y, Wong K. Printed double-T monopole antenna for 2.4/5.2 GHz dual-band WLAN operations. IEEE Transactions on Antennas and Propagation. 2003;51(9):2187-2192.

[21] Kurian J, Upama Rajan MN, Sukumaran SK. Flexible microstrip patch antenna using rubber substrate for WBAN applications. 2014 International Conference on Contemporary Computing and Informatics (IC3I). 2014:983-986.

[22] Lee KF, Yang SLS, Kishk AA, Luk KM. The versatile U-slot patch antenna. IEEE Antennas and Propagation Magazine. 2010;52(1):71-88.

[23] Maci S, Gentili GB. Dual-frequency patch antennas. IEEE Antennas and Propagation Magazine. 1997;39(6):13-20.

[24] Miccoli I, Edler F, Pfnür H, Tegenkamp C. The 100th anniversary of the four-point probe technique: The role of probe geometries in isotropic and anisotropic systems. Journal of Physics Condensed Matter. 2015;27(22).

[25] Pan CY, Huang CH, Horng TS. A new printed G-shaped monopole antenna for dualband WLAN applications. Microwave Opt Technol Lett. 2005;45(4):295-297.

[26] Pozar DM. Microwave engineering. 2nd ed. New York: Wiley; 1998.

[27] Song Y, Jiao Y, Zhao H, Zhang Z, Weng Z, Zhang F. Compact printed monopole antenna for multiband WLAN applications. Microwave Opt Technol Lett. 2008;50(2):365-367.

[28] Stutzman WL, Thiele GA. Antenna theory and design. 2nd ed. New York: Wiley; 1998.

[29] Sultan Jasim KA, Mohammed Ali YE. Compact dual-band monopole antenna for WLAN/WiMAX applications. 2013 Annual International Conference on Emerging Research Areas and 2013 International Conference on Microelectronics, Communications and Renewable Energy. 2013:1-3.

[30] Tung H, Fang S, Wong K. Printed dual-band monopole antenna for 2.4/5.2 GHz WLAN access point. Microwave Opt Technol Lett. 2002;35(4):286-288.

[31] V D, Raj RK, Joseph M, M.N S, Mohanan P. Compact asymmetric coplanar strip fed monopole antenna for multiband applications. IEEE Transactions on Antennas and Propagation. 2007;55(8):2351-2357.

[32] Webinar: Intelligent Design with Characteristic Mode Analysis, Altair Feko, website, 2014. Available (accessed on 01.09.2019): www.feko.info

[33] Wulandari IY, Alaydrus M. Observation of multiband characteristics of microstrip antenna using defected ground structure. 2017 International Conference on Broadband Communication, Wireless Sensors and Powering (BCWSP). 2017:1-4.

[34] Yeh S, Wong K. Integrated f-shaped monopole antenna for 2.4/5.2 GHz dual-band operation. Microwave Opt Technol Lett. 2002;34(1):24-26.

[35] Young HD, Freedman RA, Ford AL. University physics with modern physics. 14. Global ed. Harlow: Pearson; 2016.

[36] Zhai H, Ma Z, Han Y, Liang C. A compact printed antenna for triple-band WLAN/WiMAX applications. IEEE Antennas and Wireless Propagation Letters. 2013;12:65-68.

[37] Zhang L, See KY, Zhang YP. Impact of PCB ground plane size on dual-band antenna performance. 2012 Asia-Pacific Symposium on Electromagnetic Compatibility. 2012:593-596.

[38] Zivkovic Z, Sarolic A, Roje V. Effects of effective dielectric constant of printed short dipoles in electric field probes. 10th International Symposium on Electromagnetic Compatibility. 2011:73-78.

APPENDIX 1:

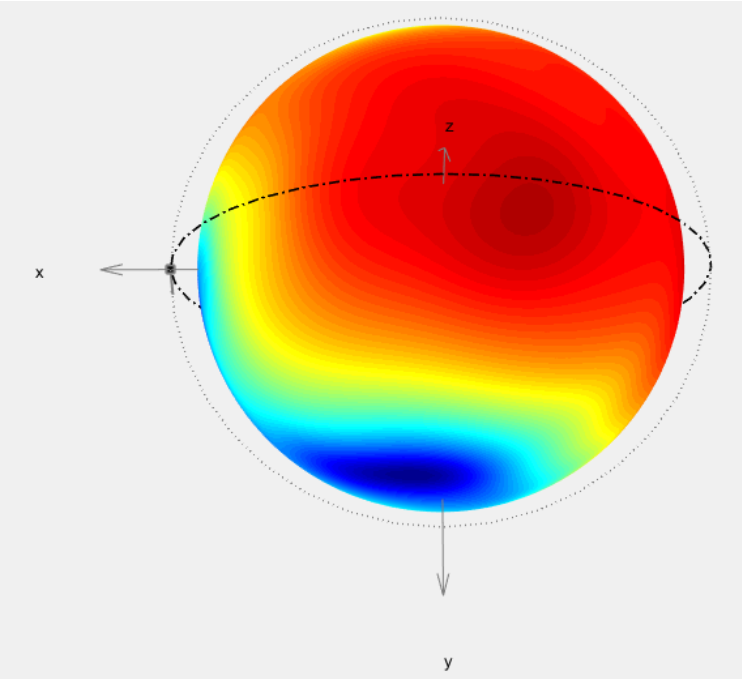

Global parameters

Gain = 1.31 dB | Directivity = 4.76 dBi | Efficiency = -3.45 dB (45.17 %)

Figure 1. *Constructed ink 3 antenna V2 measured 3D radiation pattern at 1.8 GHz (measured by Satimo antenna anechoic chambers at Tampere university)*

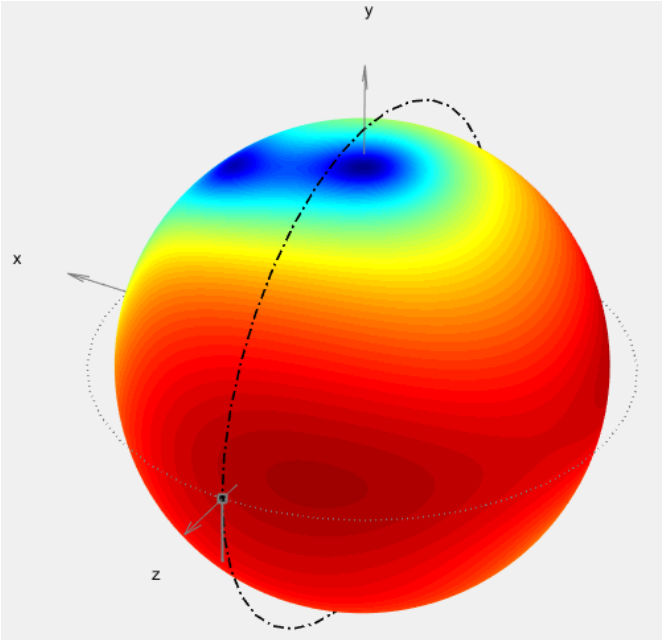

Global parameters

Gain = 2.14 dB | Directivity = 4.04 dBi | Efficiency = -1.90 dB (64.59 %)

Figure 2. *Constructed copper tape antenna V2 measured 3D radiation pattern at 1.8 GHz (measured by Satimo antenna anechoic chambers at Tampere university)*

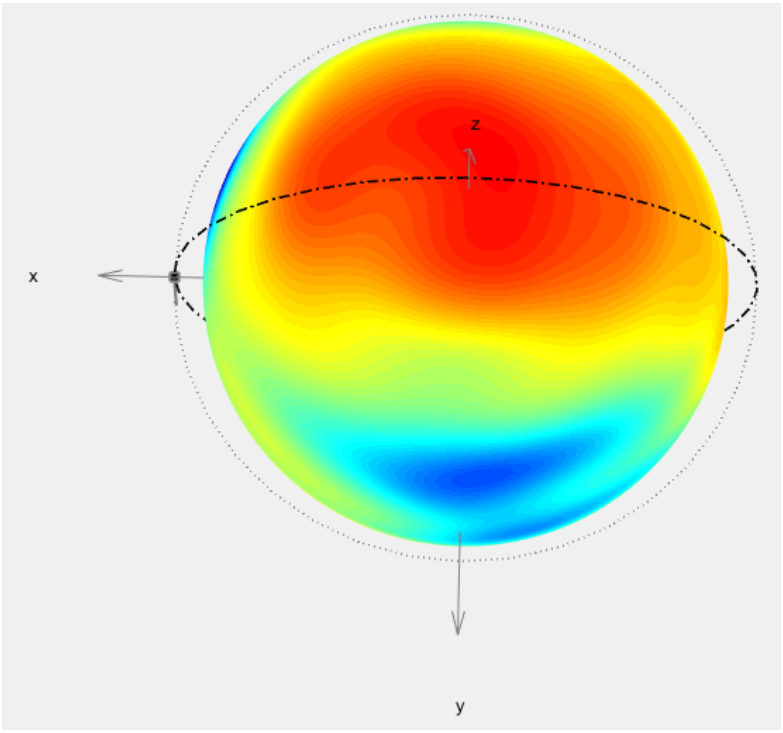

Figure 3. *Constructed ink 3 antenna V2 measured 3D radiation pattern at 2.6 GHz (measured by Satimo antenna anechoic chambers at Tampere university)*

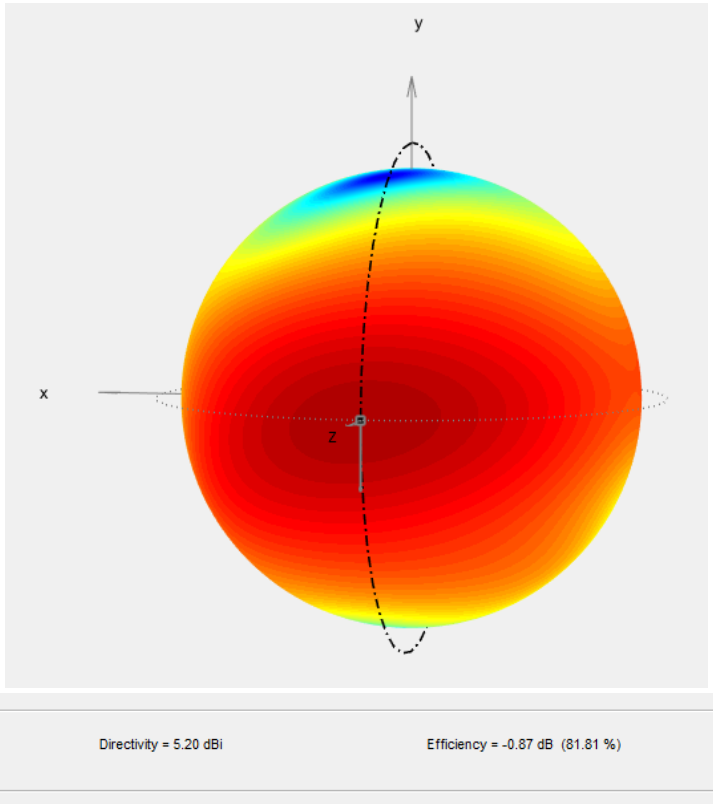

Figure 4. *Constructed copper tape antenna V2 measured 3D radiation pattern at 800 MHz (measured by Satimo antenna anechoic chambers at Tampere university)*